# Experimental and Numerical Analysis of Damage in CFRP Laminates under Static and Impact loading conditions

**by**

**George Tsigkourakos**

A doctoral thesis submitted in partial fulfilment of the requirements for the award of doctor of philosophy of Loughborough University

Wolfson School of Mechanical and Manufacturing Engineering


Loughborough University

# Certificate of Originality

This is to declare my responsibility of the work submitted in this thesis. All the original work is my own except as stated in the acknowledgment. Neither the thesis nor the original work included has been submitted to this or any other institution for a degree.

Signed

Date: 27/09/2013

# Abstract

Engineering composites and especially long fibre carbon composites have been in high demand not only in aerospace and automotive applications, but also in high end everyday applications. In aerospace, carbon composites are used predominantly for secondary structures attached by joints or fasteners to various alloys or even different composites, and are exposed to service loads and repetitive impacting. Impact fatigue (IF) is not studied adequately for long cycles and relevant literature is investigating mainly drop weight tests and high speed projectile experiments.

The main aim of this research was to investigate the behaviour long fibre CFRP'S exposed to repeated low-velocity, low energy impacts, and to observe the damage effects of this regime on the structural integrity of these materials.

Two types of specimen configurations using CFRPS's were used and exposed to loading conditions relevant to the Izod impact fatigue test (IIFT), and the tensile impact fatigue test (TIFT), in order to determine the fatigue behaviour of the specimens for each of these load conditions. For the IIFT, the fatigue life was investigated using IM7/8552 unidirectional specimens and T700/LTM45 cross-ply specimens were utilised for the TIFT. The specimen thicknesses were altered in both cases and parametric studies were carried out, where it was seen that IF results in high level of scatter and the apparent decrease in life was seen at relatively modest levels of maximum force after relatively few cycles. In the case of the IIFT, a durability limit was not apparent which increases the complications when designing against IF. In the case of the TIFT the stiffness deterioration was reflected as an increase of the loading time, in the force vs time graph, over the total fatigue life span.

Fatigue crack growth was investigated using fractography and X-ray micro-CT at the micro and macro level. It was seen, that IF had the potential to initiate cracks and to cause their propagation at low levels of loading. For the IIFT, a single crack was growing substantially in the fibre direction and across the sample width causing matrix cracking and probably breaking of some fibres, which acted as impact wave guides since matrix cracks were propagating initially along the length of the fibres. In the case of the TIFT multiple damage modes were presented (matrix cracks, axial splits and delaminations). Their sequence and progression was successfully

captured and contrasted against the number of impacts. Axial splits governed the damage scenario, with delaminations extending between them and the free edges.
For the TIFT, IF was studied using the force-life (F-Nf) and energy-life (E-Nf) curves. The tests undertaken showed that when halving the thickness of the laminates the fatigue life presented a 10-fold decrease as well as higher scatter.
Finite element modelling was undertaken to validate the experimental data of the TIFT test. Successful simulation of a single impact was carried out using a fully transient 3-D model of the actual experiment configuration which involved geometric non-linearities in addition to the multiple contact conditions. The analysis was undertaken using the Abaqus 6.11 explicit solver. Since the numerical single impact results (force vs time response) was in agreement with the experimental results, the crack modes, experimentally observed, were also incorporated in the model utilising the use of the cohesive zone elements (CZE).

**Keywords:** Impact fatigue; CFRP; CZM; tensile-impact; finite-element

# Symbols

| | |
|---|---|
| $\sigma_{11}$ | Longitudinal stress (MPa) |
| $\sigma_{22}$ | Transverse stress (MPa) |
| $\sigma_{33}$ | Radial stress (MPa) |
| $\sigma_m$ | Mean stress (MPa) |
| $\sigma_a$ | Stress amplitude (MPa) |
| $\sigma_{max}$ | Maximum stressamplitude (MPa) |
| $\sigma_{min}$ | Minimum stress amplitude(MPa) |
| $\sigma I_{max}$ | Interfacial strength under mode I(MPa) |
| $\sigma II_{max}$ | Interfacial strength under mode II(MPa) |
| $\sigma_{eff}$ | Effective stress(MPa) |
| $\sigma_{static}$ | Failure stress under static loading(MPa) |
| $\sigma_R$ | Residual strength(MPa) |
| $\varepsilon_{11}$ | Longitudinal strain |
| $\varepsilon_{22}$ | Transverse strain |
| $\varepsilon_{33}$ | Radial strain |
| $\gamma_{12}$ | Shear strain in longitudinal direction, 2, perpendicular to plane 1 |
| $\gamma_{13}$ | Shear strain in radial direction, 3, perpendicular to plane 1 |
| $\gamma_{23}$ | Shear strain in transverse direction, 2, perpendicular to plane 3 |
| $\gamma s$ | Surface energy (J) |
| $\Gamma$ | Path surrounding the crack tip (m) |
| $\Delta t$ | Time difference (s) |
| $\delta^c$ | Damage onset displacement (mm) |
| $\delta^f$ | Maximum opening displacement-absolute decohesion of surfaces (mm) |
| $\rho$ | Cured density (kg/m$^3$) |
| a | Crack size (mm) |
| C | Miners sum |
| d | Specimen displacement (mm) |
| D | Damage |
| E | Impact energy (J) |
| Eeff | Effective stifness(N/m) |
| $E_{11}^T$ | Longitudinal elastic modulus (GPa) |
| $E_{22}^T$ | Transverse elastic modulus (GPa) |
| $E_{33}^T$ | Radial elastic modulus (GPa) |
| F | Impact force (N) |
| $G_{12}$ | Shear modulus in longitudinal direction, 2, perpendicular to plane 1 (GPa) |
| $G_{23}$ | Shear modulus in radial direction 3, perpendicular to plane 2 (GPa) |
| $G_{13}$ | Shear modulus in longitudinal direction 3, perpendicular to plane 1 (GPa) |
| $G_c$ | Critical strain energy release (J/m$^2$) |
| $G_{I,II,III}$ | Strain energy release rate under mode I,II,III respectively (J/m$^2$) |
| J | Strain energy release rate in the case of the elastic-plastic behaviour(J/m$^2$) |
| k | function of crack speed |

| | |
|---|---|
| $K_{I,II,II}$ | Stress intensity factor for mode I,II,II $(MPa\sqrt{m})$ |
| K | Instantaneous stiffness (N/m) |
| $K_{10}$ | Normalised instantaneous stiffness |
| $l_{cz}$ | Length of cohesive zone (mm) |
| $l_e$ | Element size (mm) |
| n | Number of cycles |
| $N_d$ | Notch depth (mm) |
| Nf | Number of cycles to failure |
| P | Applied load (N) |
| rp | Radius of plasticity contour (m) |
| R | Load ratio |
| $S_e$ | Fatigue limit (MPa) |
| $S_D$ | Damaged area ($m^2$) |
| $S_f$ | Fatigue strength (MPa) |
| $S_{11}^T$ | Longitudinal tensile strength (GPa) |
| $S_{11}^C$ | Longitudinal compressive strength (GPa) |
| $S_{22}^T$ | Transverse tensile strength (GPa) |
| $S_{22}^C$ | Transverse compressive strength(GPa) |
| $T_F$ | Definition loading time in IF experiments (ms) |
| T | Loading time (s) |
| $T_{10}$ | Normalised loading time with respect to the tenth impact |
| Tg | Glass transition temperature (°C) |
| $u$ | Displacement vector |
| $\nu_{ij}$ | Poisson's ratio that corresponds to a contraction in the direction when an extension is applied in direction |
| $\nu_{12}$ | Ratio of strain in transverse direction, 2, to strain in longitudinal direction, 1 |
| $\nu_{23}$ | Ratio of strain in radial direction, 3, to strain in transverse direction, 2 |
| $\nu_{13}$ | Ratio of strain in radial direction, 3, to strain in longitudinal direction, 1 |
| V | Hammer velocity (m/s) |
| Vc | Wave speed (m/s) |
| W | Strain energy density (J) |

# Acronyms

| Abbreviation | Meaning |
|---|---|
| 2D | Two-dimensional |
| 3D | Three-dimensional |
| µXCT | X-ray micro-computed tomography |
| CA | Constant amplitude |
| CBM | Crack band model |
| CCT | Crack closure technique |
| CDM | Continuum damage mechanics |
| CFRP | Carbon fibre reinforced polymers |
| CT | Computed tomography |
| CZM | Cohesive zone modelling |
| CZP | Cohesive zone parameters |
| DCB | Double-cantilever beam |
| DFM | Dynamic fracture mechanics |
| FE | Finite-element |
| FEM | Finite-element modelling |
| FPZ | Fracture process zone |
| FRP | Fibre reinforced polymer |
| HCF | High cycle fatigue |
| IF | Impact fatigue |
| ILSS | Interlaminar shear strength |
| LCF | Low cycle fatigue |
| LEFM | Linear elastic fracture mechanics |
| NDT | Non destructive technique |
| NLEFM | Non linear elastic fracture mechanics |
| PMMA | Poly(methyl methacrylate) –transparent thermoplastic |
| ROI | Region of interest |
| SF | Standard fatigue |
| SHPB | Split-Hopkinson pressure bar |
| SIF | Stress intensity factor(s) |
| UD | Unidirectional |
| VAF | Variable amplitude fatigue |
| VCCT | Virtual crack-closure technique |

# Contents

# List of Figures

# List of Tables

## Acknowledgments

I would like to thank my supervisors Prof. Vadim Silberschmidt and Prof. Ian Ashcroft for their invaluable guidance, support, encouragement, knowledge, and patience throughout the different stages of this work. Their understanding, suggestions and constructive criticism helped me to tackle the milestones of this project. Both gave me the confidence to enrich my academic and personal life in so many various aspects.

The author is also grateful to Dr. Aamir Mubashar and Mr. Himayat Ullah for assisting with their vast experience in the field of numerical analysis.
Additionally, I am thankful to all the staff and especially the technicians of Wolfson school for being friendly and always available, making my life comfortable in the department. A special thanks to Mr. Andy Sandavar for his help with specimen preparation and experimental work.

Finally, special thanks to my friends Yannis, Apostolis, Maryam & Rubi as well as my family who have supported and encouraged me throughout this work.

***For Kelly, Veta, Dimitris and Teerak***
***Without your love and support***
***I would not be where I am now.***

Date: 27/09/2013 George Tsigkourakos

Loughborough/Leicester
UK

## Publications

### Journal Publications

George Tsigkourakos, Juan Pablo Casas-Rodriguez and Vadim V. Silberschmidt, “Analysis of Damage Propagation in Single Lap Joints in Impact Fatigue”, Vibro-Impact Dynamics of Ocean Systems and Related Problems, 2009, Vol 44, pg.247-257, DOI: 10.1007/978-3-642-00629-6_25.

George Tsigkourakos, Vadim.V.Silberschmidt and Ian.A.Ashcroft, “Damage Analysis of CFRP under Impact Fatigue”, Journal of Shock and Vibration, 2009, IOS press, DOI: 10.3233/SAV-2011-0651.

George Tsigkourakos, Vadim.V.Silberschmidt and Ian.A.Ashcroft, “Damage assessment in CFRP laminates exposed to impact fatigue loading”,Journal of Physics: Conference Series, 2011,Vol. 305, Number 1, DOI:10.1088/1742-6596/305/1/012047.

### Conference Publications

George Tsigkourakos, H .Ullah, Ian. A.Ashcroft and Vadim.V.Silberschmidt
Damage in fibre-reinforced composites subjected to dynamic loading in CFRP laminates exposed to impact fatigue loading. In: Proceedings of 18$^{th}$International Conference on Composite Materials ICC, 21-26August 2011, Jeju, Korea.

H. Ullah, G. Tsigkourakos, F. Vartzopoulos, I.A. Ashcroft, V.V. Silberschmidt, Dynamic loading of fibre-reinforced laminates: experiments and simulations. In: Proceedings of 15$^{th}$ European Conference on Composite Materials, 25-28 June 2012, Venice, Italy. Paper 157, pp. 1-8. ISBN 978-88-88785-33-2.

H. Ullah, G. Tsigkourakos, F. Vartzopoulos, I.A. Ashcroft, V.V. Silberschmidt, Damage in fibre-reinforced laminates under dynamic loading. In: Computational Mechanics 2012. Proceeding of 10th World Congress on Computational Mechanics, 8-13 July, 2012, Sao Paulo, Brazil. P.M. Pimenta, E.M.B. Capello (eds.) Paper 16649, p.p. 16.ISBN 978-85-86686-78-2.

**Conference contributions**

George Tsigkourakos, Vadim.V.Silberschmidt and Ian. A. Ashcroft ,
BSSM workshop on Advanced Structural Health Monitoring, NPL institute, UK, 25th May 2010.

George Tsigkourakos, Vadim.V.Silberschmidt and Ian. A. Ashcroft,The 20th International Workshop on Computational Mechanics of Materials (IWCMM 20), Loughborough University, UK, 8-10 September 2010.

George Tsigkourakos, Vadim.V.Silberschmidt and Ian. A. Ashcroft,The 21st International Workshop on Computational Mechanics of Materials (IWCMM 21), University of Limerick, Ireland, 21-24 August 2011.

# Chapter 1 Introduction

## 1.1 Project Background

Demand for advanced composites in the aerospace industry is continuously increasing. In recent years, carbon fibre reinforced polymers (CFRP) have become one of the most important structural materials in the aerospace industry due to their excellent stiffness and high strength-to-weight ratio. Fatigue is generally approximated as a sinusoidal loading, characterised by the stress ratio, frequency and maximum force. This type of loading can be termed standard fatigue (SF). However, real-life loading histories usually involve vibrating loads that can propagate in structural elements as cyclic impacts. This phenomenon is known as impact fatigue (IF). Cyclic loading causes various types of damage in laminate composites: matrix cracking, delamination, splits, de-bonding between fibres and matrix and fibre breakage, resulting in a reduction of residual stiffness and loss of functionality.

The effects of IF are of major importance due to its detrimental effect on the performance and reliability of components and structures after relatively few impacts at low force levels compared to those in SF loading. Loughborough University employs a unique testing system with the capability of subjecting specimens to uni-axial tensile dynamic loading, making feasible direct comparison with tensile SF.

The main aim of this thesis is to provide results illustrating the effect of IF on the damage behaviour of CFRP specimens and in order to do so microstructural,

detailed damage analysis is implemented utilising X-ray micro CT. The experimental part of the research is concentrated on the response of CFRP specimens to single and multiple impacts. The numerical part of this thesis involves the application of finite element analysis (FEA) to model damage development under both quasistatic and dynamic loading conditions.

A significant amount of work has been undertaken in the analysis of damage mechanisms in CFRP laminates. The effect of multiple impacts on the damage mechanisms in CFRP laminates is an area that has received little attention to date. Based on this, the aim and objectives of this PhD project were decided, and are presented in the following section.

## 1.2. Aim and objectives

This PhD project is aimed at experimentally investigating the behaviour of CFRP subjected to Impact Fatigue (IF) and the development of numerical techniques to model the observed behaviour. To accomplish this aim, the following objectives were identified:

1. Experimental testing of CFRP laminates under quasi-static and impact fatigue conditions.

2. Characterising damage development in the CFRP specimens as a function of sample type, loading method and time.

3. Develop finite element methods to accurately represent dynamic strain development in the CFRP samples under loading

4. Develop finite element methods to characterise damage initiation and propagation in the CFRP samples under quasistatic and impact fatigue loading conditions.

To the author's knowledge, the problem of damage initiation and propagation exhibited by CFRP laminates under uniaxial IF conditions utilising only cohesive zone methodology has not been previously addressed and this is being emphasised in section 2.6.4.

### 1.3. Thesis Layout and Research Methodology

A schematic of the overall layout of this thesis including the research methodology is given in Figure 1.1. The thesis covers five main areas: introduction, literature review, experimentation, simulations, conclusions and future work. A brief description of the chapters will be given in the following section. The rest of this section will be focusing on the interaction between the elements of research methodology. In fact, it is comprised of two main parts: experimentation and simulations. Experimentation was carried out to characterise fatigue life under IF conditions and analyse damage scenarios produced by the multiple impacts. Two types of IF tests were performed; Izod and modified Charpy which will be referred as izod impact fatigue test (IIFT) and tensile impact fatigue test (TIFT). In both cases detailed microstructural examination took place in between the tests in order to correlate the damage observed with the damage parameter identified in each case. In the case of IIFT a parametric study was undertaken investigating the effect of altering thickness and notch size on the fatigue life. In the case of the TIFT similarly two different thicknesses were investigated. It has to be noted, for this specific test a numerical model was also built. A fully transient explicit model using Abaqus served the purpose of validating the experimental results. Initially, for the validation of the non-damage scenario (single impact) the force response of a single impact was used as a correlation parameter. With the use of cohesive zone elements (CZE), introduction of damage was feasible in the numerical model. Partitions were made at predetermined experimentally damaged areas and CZE were inserted. For calibration of the boundary conditions and more specifically of the properties of CZE a quasistatic numerical model was also built and results were contrasted with the experiment. The validation of the quasistatic model gave confidence in the correct implementation of CZE and steps were undertaken to model the fatigue life using a cycle jump strategy

## 1.4 Chapter Structure

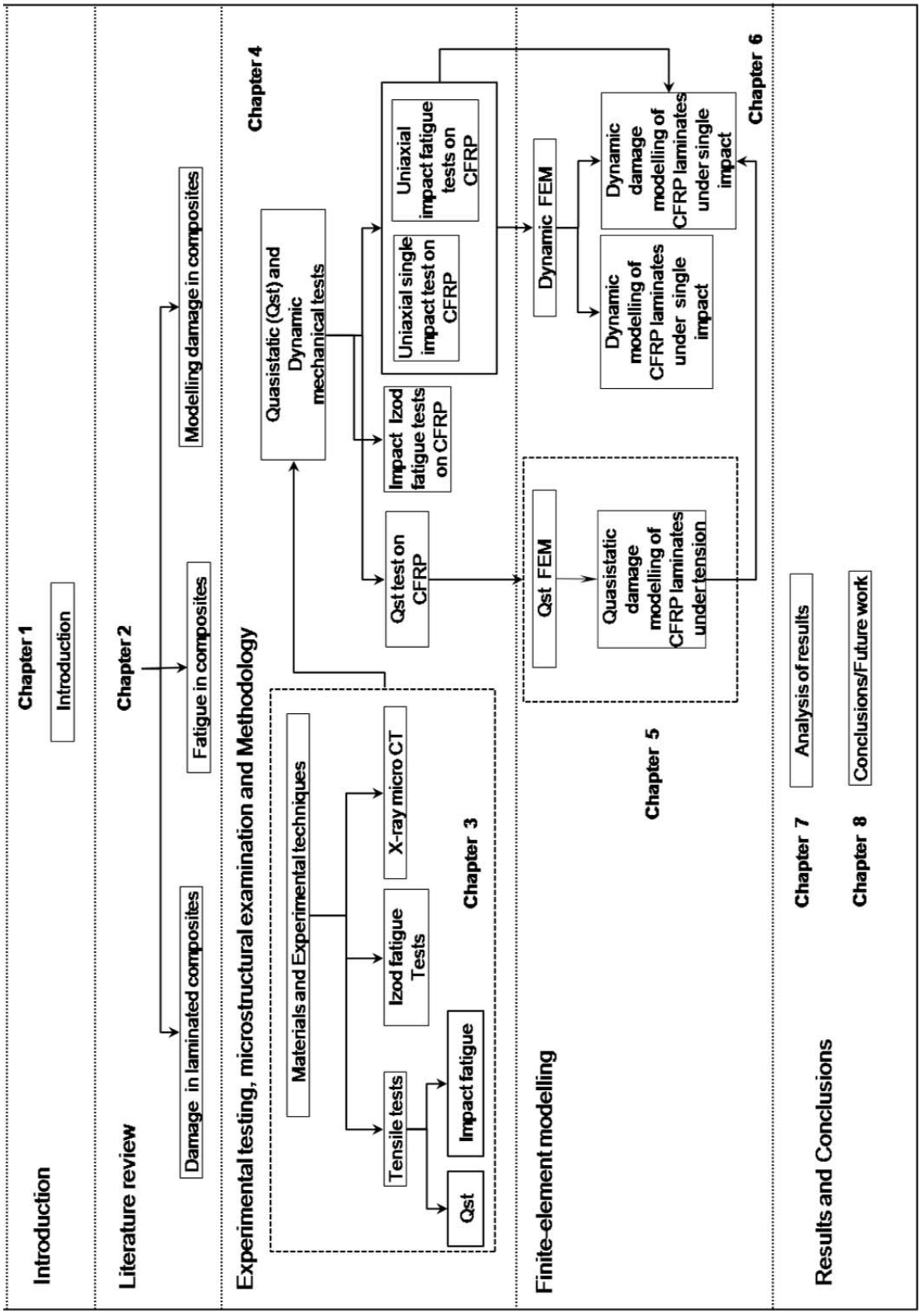


Figure 1.1 Overall thesis layout and research methodology

A brief description of the remaining Chapters of this thesis is given below:

**Chapter 2 Literature Review**

This chapter is divided into 4 parts. In the first part, a description of the significance of composites in aerospace and their advantages compared with other commonly used materials is presented. In the second part, the composite damage mechanisms are investigated in a) the ply level, b) the laminate level. Emphasis is being given in the crossply laminates and the main damage scenarios governing them such as the matrix cracks and delaminations. Their effect on the structural integrity is being also discussed together with various models and simulation approaches that have been developed to study these damage mechanisms as well as the link between them. The third part is an overview of different types of fatigue that exist in nature. Emphasis is being given on impact fatigue and especially impact fatigue of composites. Finally, the fourth part describes fracture and damage mechanics principles highlighting their importance when modelling composite systems.

**Chapter 3 Materials and Experimental techniques**

A review of the experimental techniques utilised in this work, as well as the different types of materials used in each test are described. Two mechanical low rate impact tests were employed to simulate the effects of impact fatigue (IF).

The first part of experimentation involved an Izod impact fatigue test (IIFT) of unidirectional (UD) long fibre composite IM7/8552.The impact toughness over the fatigue life was evaluated for various energy levels and two specimen thicknesses for reproducibility reasons. The second part of experimentation was undertaken using a modification of the Charpy test otherwise known as the tensile impact fatigue test (TIFT). It allows specimens to be subjected to tensile IF and so comparison with standard fatigue (SF) could be possible. The specimens used were crossply T700/LTM45 containing a centrally located hole which would act a stress concentrator.

Finally, in both tests crack initiation and propagation scenarios were investigated by means of fractography and Xray-micro-Ct

## Chapter 4 Experimental Results

This chapter is a brief presentation of the results obtained for a) IIFT, b) TIFT. For the IIFT, the effect of altering specimen thicknesses and impact energy levels on the fatigue life of the composite is thoroughly investigated. Additionally, detailed x-ray studies, undertaken at intervals of fatigue life were carried out on a specially designed specimen which allowed the maximum possible Xray-resolution of 3μm to be possible. The crack growth scenarios when then correlated with the percentage of cycles to failure.

For the TIFT, the same methodology was followed with the only difference that the impact energy levels did not alter. The preferred energy level of 1Joule was proven to be ideal for investigating fatigue life of two thicknesses. 2mm and 1mm thickness of crossply specimens were under investigation for reproducibility reasons. Common result was the increase in the loading time which hindered stiffness deterioration. X-ray studies were undertaken at intervals of fatigue life for both configurations, however emphasis was given in the 2mm configuration since results seemed more stable.

## Chapter 5 Finite Element Modelling of Single Impacts

In this chapter the numerical model considerations are explained explicitly. More specifically, the hammer specimen interaction, identical with the experimental TIFT, is explained in numerical terms. The numerical built up considerations involve geometry and boundary assumptions, material data input details, reasons for element choices as well as selection process for solvers.

In addition, the calibration process using an aluminium specimen before the successful modelling of the composite layup is explained. Validation of numerical and experimental data was done using two parameters: Force and strain.

**Chapter 6 Finite element modelling of Damage**

The main focus of this chapter is the correct implementation of the cohesive zone elements in the model that was previously created. This was partially achieved by contrasting the cohesive zone properties with a quasistatic case. For that aim, a quasistatic experiment was carried out and the global stiffness was used as the validation parameter between numerical and experimental work. Furthermore, literature review revealed that for low dynamic range and for epoxy matrices the static cohesive zone parameters can be used. Finally it was shown that the stiffness response remained unaltered even after manipulating significantly the cohesive zone parameters.

**Chapter 7 Discussion of results**

Chapter 7 presents a detailed discussion of the main experimental and numerical results. The experimental results are divided between the IIFT and TIFT tests while the numerical are concentrated solely on the IIFT. In the experimental results the main focus was the fatigue life assessment in the two fatigue tests as well as the damage characterization. In the numerical work, the step towards the modeling of the damage behavior in the TIFT was the subject.

**Chapter 8 Conclusions/Future work**

Chapter 8 provides the main conclusions obtained in this research, presenting also the suggested areas for the future work.

# Chapter 2 Literature Review

## 2.1 Introduction

The scope of the literature review is based on the main aspects of the project. These were:

Material, test configuration, type of test, rate of loading, computational modelling and damage modelling approach. The structure of the literature review was built around the above milestones.

Regarding the material, the use of fibre reinforced composites (FRC's) has increased considerably in last few decades. Automotive, aerospace and sport industries display a considerable interest in these materials. FRC's exhibit a combination of properties such as ease of fabrication (according to application) and a high strength to weight ratio. More specifically carbon fibre reinforced polymer (CFRP) composites, which is the material under investigation here, are used in areas were high strength is required and weight restriction is important. CFRP's are usually supplied in the form of plies, with the fibres already embedded in the matrix in a specific parallel orientation, which makes them easy to manufacture in a specific orientation.

Composites, behave differently to ductile materials when subjected to loading. Their quasi-brittle, non-homogeneous and anisotropic nature dictates complex damage scenarios, including matrix cracks, delaminations, axial splits, fibre fracture etc. The crossply orientation was selected for this work and the literature review is focused on

this orientation and the associated damage mechanisms at ply and laminate level. The type of test, as well as the rate of loading was determined early in the project. The specimens would be subjected to uniaxial tensile impacts at velocities less than 10m/s. In the literature review undertaken it was revealed that the majority of impact fatigue testing was performed for very few cycles and with tests such as dropweight, Izod or split Hopkinson bar.

The repetition of low energy low velocity impacts, with each impact being insufficient to cause the complete fracture of a specimen, could be defined as Impact Fatigue (IF). IF is present in many everyday problems. The impact of a car tyre on a bump, the wind gusts on a plane during flight, the tennis racquet or a runner's shoe are everyday examples of IF in composite materials. It has been proven that IF is more dangerous than Standard Fatigue (SF) in terms of resulting in higher crack growth rates and presenting more brittle behaviours. For the same energy levels when compared with SF the fatigue life is lower. The different types of fatigue as well as the reponse of different types of materials to fatigue conditions are presented in Section 2.5.

In section 2.6 the effect of IF on metals, polymers and finally CFRPs is presented. In an attempt to standardise IF, researchers have tried to implement the same principles as in SF. However this is not straightforward since in IF the stress magnitude that is used in stress controlled SF can not be used solely as the same level of this parameter can correspond to different levels of the applied energy, depending on the loading conditions, especially impact velocity. Also, it has been shown that the effects of IF vary between different materials and tests. For example, in metals high velocity repetitive impacting (shot peening) seems to increase the fatigue life while in composites subjected to dropweight test there is a possibility that the damage is distributed away from the impact area due to delamination resulting again in an increase in the fatigue life.

In terms of modelling, IF can be analysed with analytical and numerical methods Fatigue can be characterised, broadly, by 3 main methods, namely Fatigue life models, phenomenological models and progressive damage models.

A detailed description is given in Section 2.6.4. Fatigue can be numerically modelled with methods implementing fracture mechanics (linear, nonlinear and dynamic) or

damage mechanics principles, as discussed in Section 2.8. The main difference between fracture mechanics methods and damage mechanics methods is that the first is based explicitly on evaluating the conditions necessary for the propagation of a macro crack while the second is based on the progressive degradation of material properties prior to macro-crack formation. The literature review is mainly focused on the application of the cohesive zone elements to model progressive damage in composites since it was decided that cohesive zone elements allow the potential simulation of the multiple damage mechanisms seen in the fatigue tests of cross-ply CFRP samples.

## 2.2 Engineering Composites in Industry

As previously mentioned, CFRP have become one of the most important structural materials in the aerospace industry due to their excellent stiffness and high strength-to-weight ratio. Other advantages of engineering composites include the fact that their properties can be tailored. Composites also exhibit much better resistance to fatigue than aluminium, which can be critical in aircraft structures where cyclic loading is a major design consideration [3].

Furthermore polymer composites have:

- Good corrosion resistance
- Cost effective fabrication
- Low density
- Insulating properties

Figure 2.1 presents a schematic of the use of CFRP in the Airbus A380 passenger aircraft.

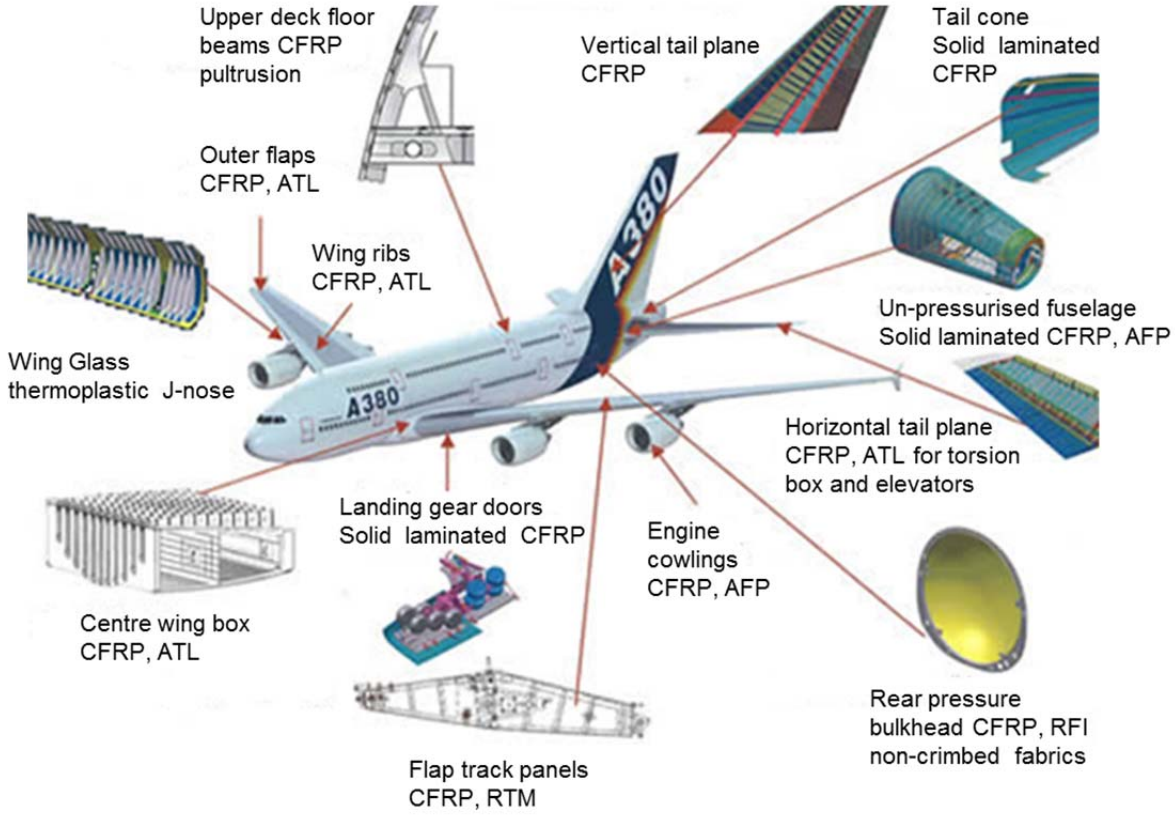


Figure 2.1 CFRP application in Airbus A380 [1]

Composites make up the majority of nature's structural materials and can be categorised according to the function and dimensions of their reinforcement, as shown in Figure 2.2. The reinforcement largely determines the structural properties and in general the greater the percentage of reinforcement the better the structural properties will be [4]. FIbre reinforced composites (FRPC) are the most used type of polymeric composite with fibres such as glass, carbon and kevlar and matrix materials including both thermosets, such as epoxies, and thermoplastic, such as polyester [5].

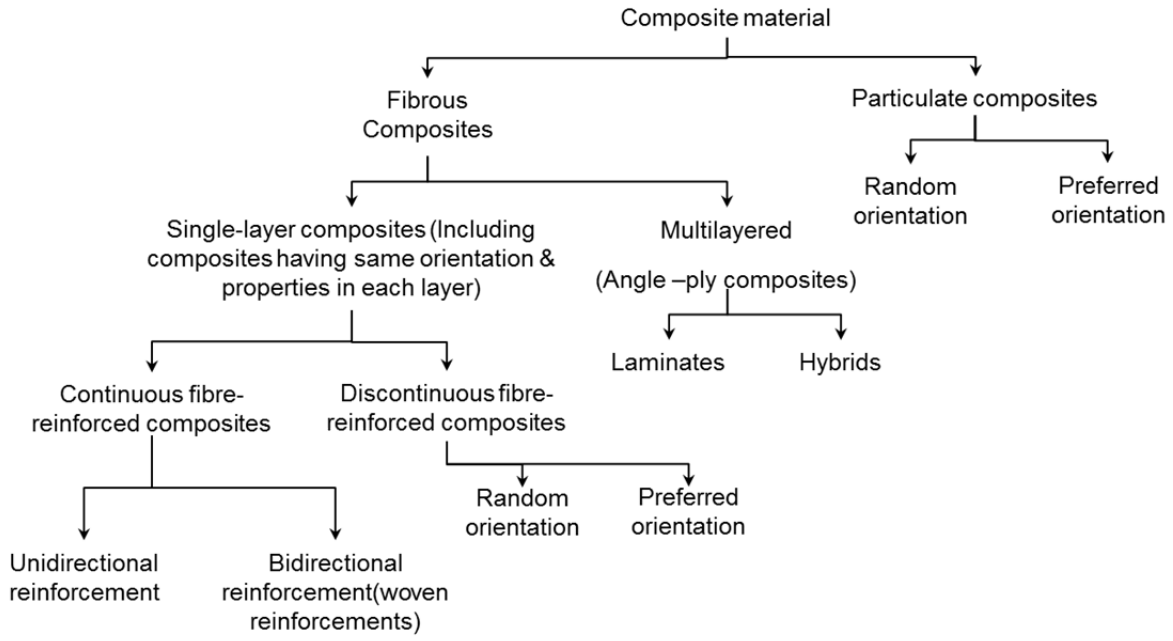


Figure 2.2 Classification of composite materials [4]

## 2.3 Damage Mechanisms in Laminated Long Fibre Composites

### 2.3.1 Ply Level

Analysing fibre reinforced composites with conventional fracture mechanics can prove to be difficult. For the case of delamination, a fracture mechanics approach can be appropriate; however, the origin of this method was based on homogeneous materials. Conventional fracture mechanics methods are based on the propagation of a single macro-crack through a homogeneous media, maintaining the same shape and orientation. When dealing with fibre reinforced composites, fracture is controlled by a number of various failure mechanisms as seen in Figure 2.3. Failure is a progressive process in composites and progressive damage mechanisms are of great interest in the study of failure in composite materials. A simple model to represent the crack growth stages in fibrous composites can be seen in Figure 2.4.

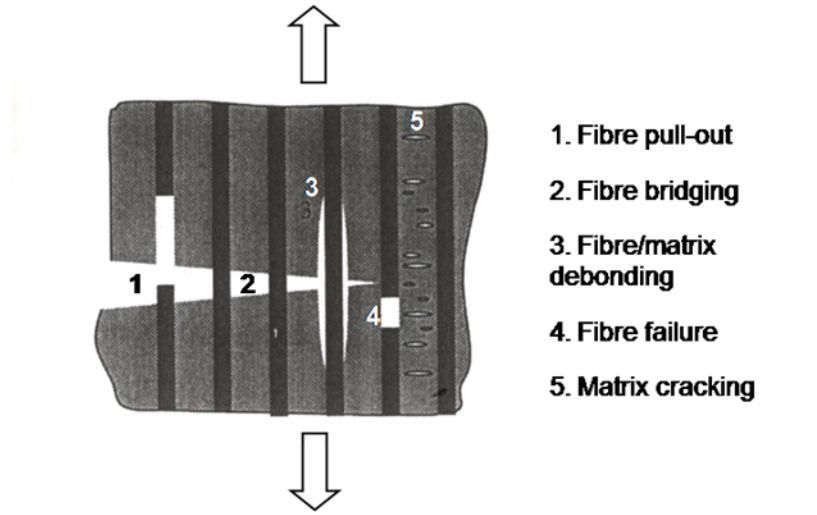


Figure 2.3 Damage mechanisms in fibre reinforced composites under tension at ply level [4]

A crack propagating through the matrix reaches a fibre. Increasing the load results in high localised stress at the fibre. The tensile stress normal to the fibre creates fibre /matrix debonding, as seen in Figure 2.4(c).The shear stress resulting from the modulus difference between the matrix and the fibre cause extension of the debond in both directions normal to the crack. The process is then repeated at the following fibre, whilst opening of the crack leads to fibre brake and fibre pull-out, as seen in Fig 2.4(d) and (e).

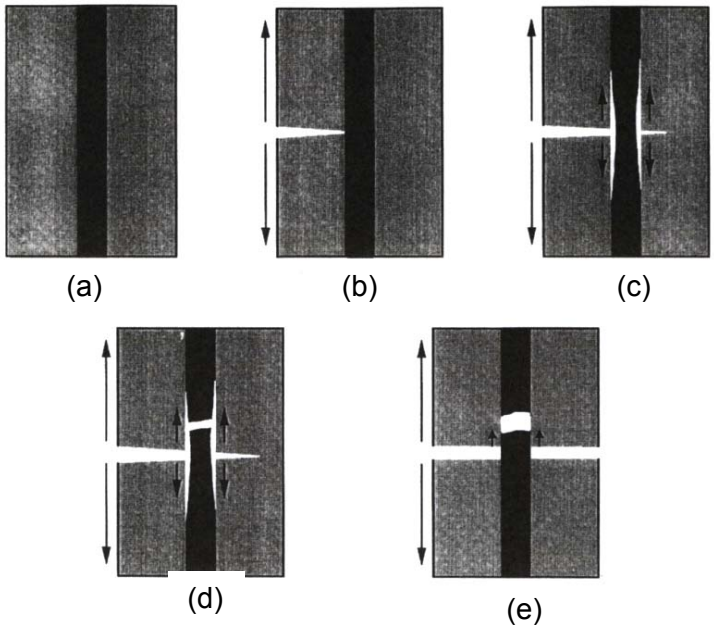


Figure 2.4 Crack growth representations in fibrous composites [4]

It can be seen that the general response of laminated composites subjected to tensile stress is much more complex than is for isotropic materials. Additionally, during loading other deformation processes can occur, such as bending, twisting and in plane shear deformations. In the following section the damage development in a cross-ply specimen is presented.

### 2.3.2 Laminate Level

When carbon fibre-reinforced cross-ply laminates are subjected to mechanical loading, several damage scenarios can occur, such as transverse matrix cracking in $90^0$ plies, delamination at the interface between $0^0$ and $90^0$ plies, axial splits in the $0^0$ plies in the direction of the loading and fibre fracture in the $0^0$ plies, as seen in Figure 2.5. Three out of these four major damage modes are primarily in-plane damage events, because they occur in individual plies and are associated mostly with in-plane stresses [6].

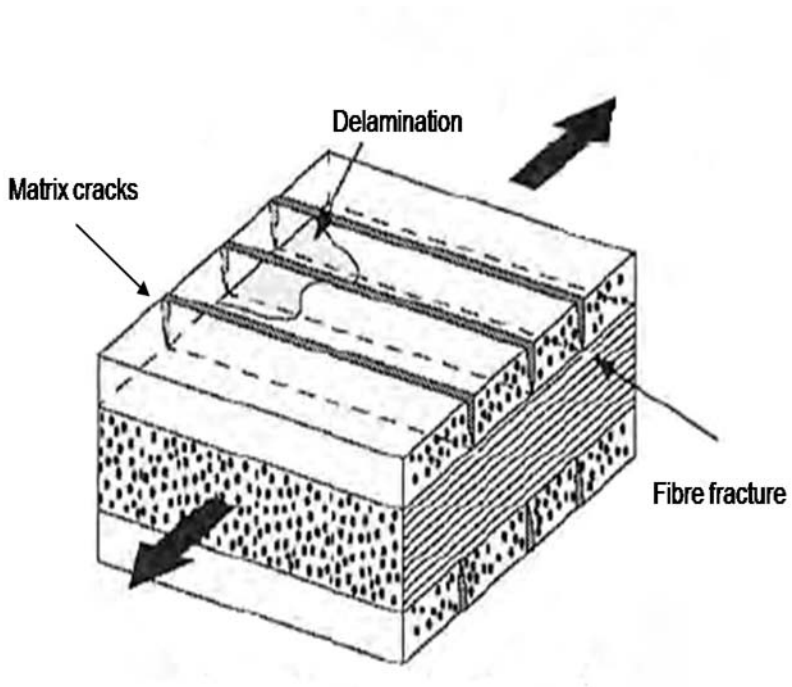


Figure 2.5 Common damage types in composite laminates [8]

Delamination, however is an out-of-plane damage mode and is a result of interlaminar stresses [7].

In case of uniaxial loading, the early stage of damage is dominated by transverse matrix cracking in $90^0$ plies. Matrix cracks develop across the width of the specimen starting from the free edges. The analysis of transverse matrix cracking is important

since it reduces the effective strength and stiffness of the laminate. According to [8], in tensile loaded crossply laminates after delamination, the decrease in the Young modulus is not significant, however the decrease in Poisson's ratio is. This is because in the direction of loading, the majority of the load is taken by the $0^0$ fibres.

**Matrix cracking**

Matrix cracks are the starting point of subcritical damage development that eventually can lead to failure. Matrix cracking is an intra-laminar failure mode, which means that it occurs within a ply. Matrix cracking results in the redistribution of interface stresses and can induce delaminations between the layers. In [9], cross-ply glass-reinforced polyester specimens were subjected to tensile loading. Various transverse-ply thicknesses were used and crack spacing was investigated in relation to the applied stress. It was shown that the density of crack spacing was proportional to the ply thickness and inversely proportional to the applied stress. The initiation, as well as the evolution, phases of cracking were analysed in notched and unnotched specimens, with thin and thick transverse plies, in [10].

Numerous analytical models have been proposed to predict accumulated matrix cracking in laminated composites based on shear lag analysis and its modifications. A shear-lag analysis was developed in [11] for predicting stiffness deterioration in cross-ply laminates due to matrix cracking. In [12], the shear-lag analysis incorporates an energy criterion to predict matrix cracking as well as the stiffness reduction. Based on that work, [13] developed a two-dimensional shear lag analysis. Hashin [14] proposed an analytical model based on the complementary energy principle to predict stiffness degradation due to matrix cracking in cross-ply laminates. Based on Continuum Damage Mechanics (CDM), Talreja [15] first proposed a continuum model describing the internal damage in composites with the use of internal state variables.

**Delamination**

Delamination occurs between the plies of a laminated composite due to mismatch of Poisson's ratio and in plane shear stiffness between plies. Hence, plies with greater difference in the in-plane properties are more prone to this damage mechanism. The

overall result of delamination can be a reduction of stiffness and strength [16]. However, although in-plane properties are not affected as much, the compressive strength as well as the Poison's ratio are seriously affected [8].

For laminated composites, research into damage is dominated by the matrix cracking and delamination types of damage. Various models and simulation approaches have been developed to study the link between matrix cracking and delamination [17-18]. A three-dimensional finite-element analysis of CFRP cross-ply laminates was carried out by [17] in order to calculate the strain energy release rate as a function of the progressive delamination. This study revealed the significance of the interaction of transverse cracks and delamination in evaluation of the degraded Young's modulus and strain induced by the damage development. In [19] a cross-ply laminate with a centrally located slit was examined under monotonic loading. Experimental results revealed a triangular delamination zone which could be related to the progressive formation of axial split starting at the edges of the slit. The author successfully simulated this phenomenon employing a finite-element method and interface elements. A similar approach incorporating interface elements was followed by [20] where quasi-isotropic laminates where tested. Matrix cracks were introduced at the locations observed in experiments, which acted as notches, while interface elements were embedded at potential locations of delamination development. Additional work done by the same author [18] extended this approach to CFRP laminates containing circular holes. The hole size effect on the tensile strength was investigated for sub-laminate level and ply-level specimens, demonstrating a large effect, both in damage mechanisms and failure stress. The crucial damage event observed in both cases was localised delamination at the hole edge. For ply-level specimens, delamination was the ultimate failure mechanism while for sub laminate level specimens fibre fracture occurred.

Concluding, it can be said that matrix cracking and delamination are the dominant damage mechanisms in CFRP laminates. They interact with each other and can cause early failures of laminates. Matrix cracks are the origin of delamination initiation, and such interaction can be modelled and simulated using progressive damage models.

## 2.4 Failure Criteria in Laminated Long Fibre Composites

Broadly speaking, strength based failure criteria for lamina can be categorised into two types: maximum stress and maximum strain. In the case of a laminate, failure prediction can be obtained by applying failure criteria on a lamina-by-lamina basis. Both maximum stress and strain criteria incorporate five sub-criteria each one of which describes a different failure state. If one of those criteria is exceeded then failure occurs. The following equation describes the maximum stress case.

$$\sigma_{11} \geq \sigma_{11}^{*}t; \sigma_{11} \geq \sigma_{11}^{*}c;$$

$$\sigma_{22} \geq \sigma_{22}^{*}t; \sigma_{22} \geq \sigma_{22}^{*}c; \qquad (2.2.1)$$

$$\tau_{12} \geq \tau_{12}^{*}$$

where t and c represent for tension and compression respectively while σ* is the ultimate stress. The maximum strain failure criteria are similar to the maximum stress failure criteria. A number of failure criteria have been proposed that consider stress and strain interactions present in intermediate angle laminates, such as: Tsai-Hill, Tsai-wu, and Hashin [22]. One of the most widely used is Tsai-Hill which is defined as:

$$\left(\frac{\sigma_{11}}{\sigma_{11}*}\right)^2 + \left(\frac{\sigma_{22}}{\sigma_{22}*}\right)^2 + \left(\frac{\tau_{12}}{\tau_{12}*}\right)^2 \geq 1 \qquad (2.2.2)$$

This criterion is an extension of the von Mises criterion as a yield criterion for orthotropic materials and is illustrated in Figure 2.6(c).

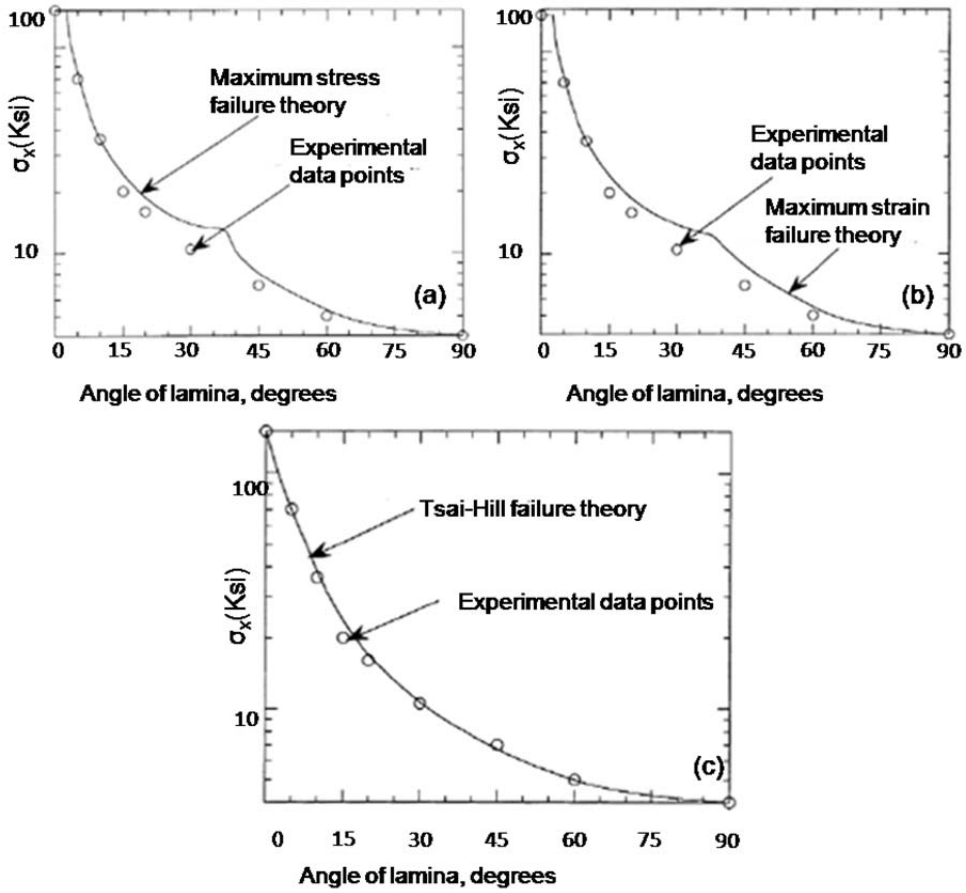


Figure 2.6 Failure criteria of stress in x-direction as a function of angle of lamina using: a) maximum stress criteria, b) maximum strain criteria, c) Tsai-Hill criterion [22]

The Tsai-Wu failure criterion [21] is a phenomenological failure criterion which is widely used for anisotropic composite materials. The Hashin's failure criterion [22] was specifically proposed for transversely isotropic composites, e.g. UD composites. From the above it can be stated that the interactive criteria are phenomenological models which predict failure in laminates with non-orthogonal plies better than the single maximum stress and strain criteria.

## 2.5 Fatigue in Engineering Materials

Fatigue failures in metallic structures were observed in the 19$^{th}$ century. August Wohler is considered the pioneer in the field of fatigue. He concluded that a single load application far below the static strength of a structure is incapable of damaging the structure, however, when it is applied several times can lead to crack generation, crack growth and ultimately, catastrophic failure [23]. Although fatigue failures in metallic structures share a lot of characteristics with fatigue failures in polymers and composites, the latter employs mechanisms of fatigue that differ significantly from those in metals. Polymers and polymer composites tend to be more sensitive to environmental conditions, such as moisture and temperature. Furthermore, due to their viscoelastic nature at relatively low temperatures, their response to cyclic stresses can also be frequency dependent [24].

In the following sections, basic concepts of fatigue and fatigue models are presented that will give to the reader a deeper understanding of the fatigue phenomenon. The main purpose of this chapter is to highlight the significance of accounting for impact fatigue when designing for service life. The following objectives are suggested

- Review types of fatigue
- Review the effects of impact fatigue on metals, polymers and composites
- Review predominant ways of analysing fatigue and fatigue damage

Fatigue can be categorized in 3 types:

- Standard fatigue (SF);
- Variable Amplitude fatigue (VAF);
- Impact fatigue (IF).

### 2.5.1 Standard Fatigue

In SF, commonly a sinusoidal waveform is used with constant amplitude loading (or displacement) being characterized by a number of parameters, such as; maximum stress ($\sigma_{max}$), minimum stress ($\sigma_{min}$) and frequency. These parameters are used to identify the following parameters which are shown in Figure 2.7:

- Stress amplitude ($\sigma_a = (\sigma_{max} - \sigma_{min}/2)$);
- Mean stress ($\sigma_m = (\sigma_{max} + \sigma_{min})/2$);
- Load ratio R ($\sigma_{min}/\sigma_{max}$).

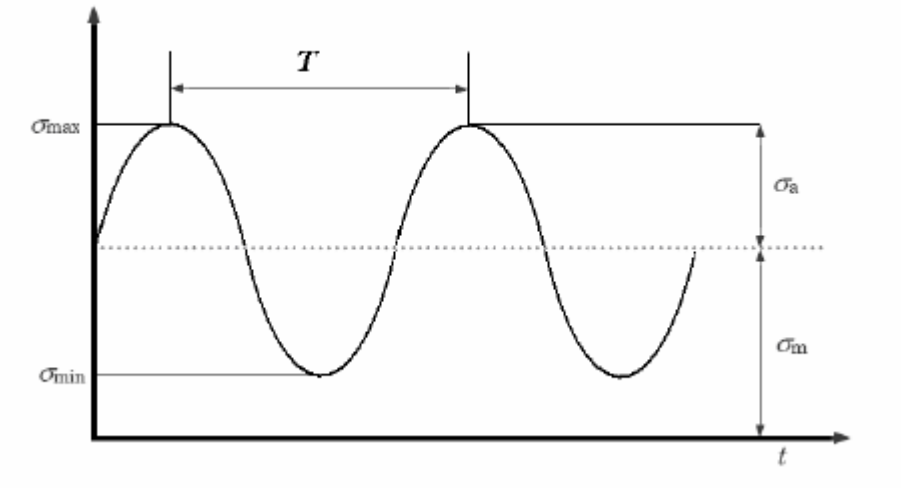


Figure 2.7 Sinusoidal, constant amplitude waveform [27]

.

Fatigue data are commonly represented in S – N curves that relate a stress (or load) parameter to the number of cycles to failure (Nf) as illustrated inFigure 2.8.

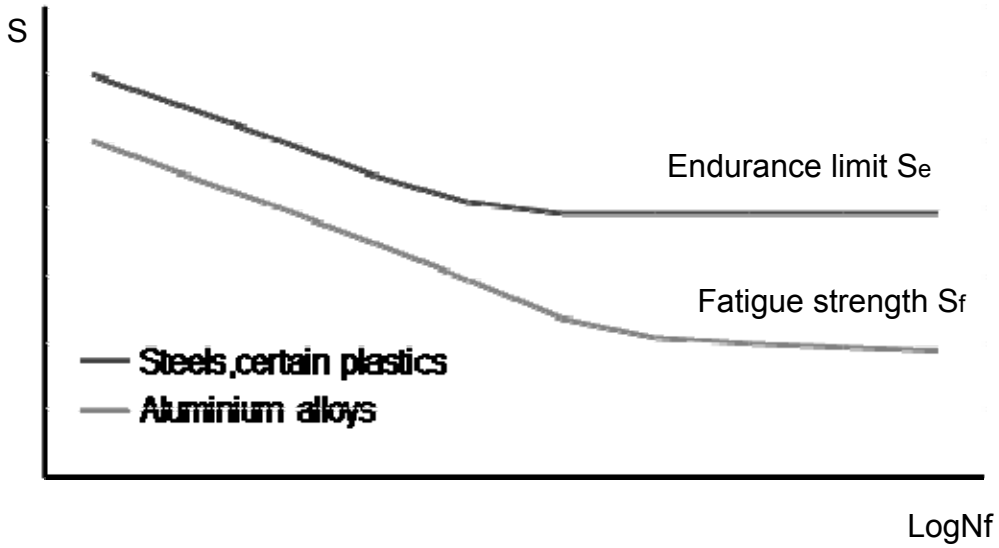


Figure 2.8 S-N diagram

On the S-N diagram three important features are:

- The fatigue life increases as the stress amplitude decreases.
- Due to the logarithmic scale, a small decrease in the stress amplitude results in a great increase of the fatigue life.
- At high cycles the curve is asymptotic to an infinite life at a stress amplitude of $S_e$. For certain materials this is called the fatigue or endurance limit and it can be seen in most steels and certain plastics. However, $S_e$ does not exist for aluminium alloys. This means that failure will occur, regardless of the stress level, if fatigued for long enough. In this case a fatigue strength, $S_f$, can be defined for a practically infinite life relative to the number of cycles experienced during a parts life [24, 25]. This is typically $10^6$-$10^7$ cycles.

### 2.5.2 Variable Amplitude Fatigue

Variable amplitude fatigue (VAF) is the typical example of service loads. Sinusoidal loading which is present in laboratory conditions is not the case for applications such as suspension loading or transmission loading etc. In order to design accurately for VAF a simplified approach of the spectrum is required. For that reason, VAF is frequently simulated as blocks of constant amplitude (CA) fatigue loads, as shown in Figure 2.9. This method enables the analysis of VAF using similar techniques as those used in CA tests. These techniques utilise mostly linear damage laws using the S-N graph as inputs. However, in the case of VAF some of the difficulties imposing these laws are that the sequence or interaction of events might lead to a wrong estimation of life. For example, fatigue life can be affected by the change in mean stress when transferring from one CA block to other.

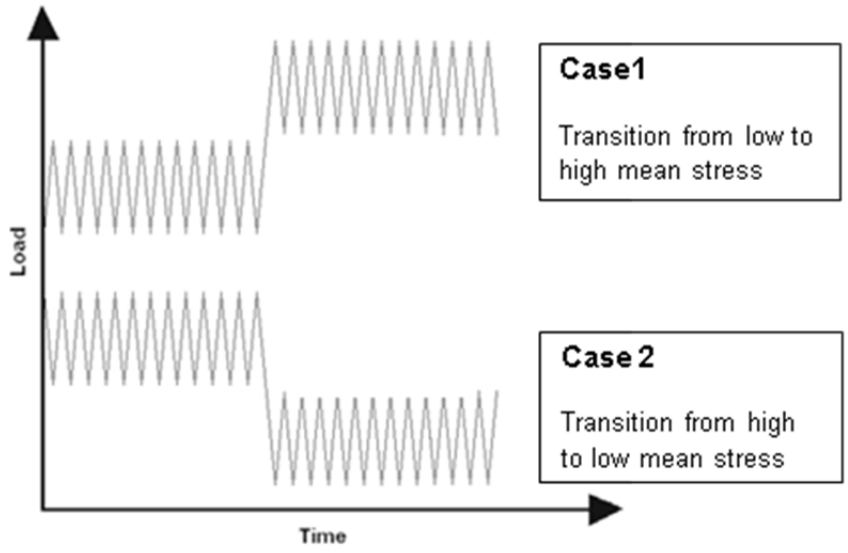


Figure 2.9 CA fatigue loads representing VAF [26]

It was found in [26] that case 1 was more harmful than case 2 in terms of overall fatigue durability. However, this tendency depends strongly on the number of transitions. Other authors have developed a model for combinations of transitions, otherwise known as the cycle mix effect model [27].

## 2.6 Impact Fatigue

The repetition of cyclic low energy impacts, with each impact being insufficient to cause the total failure of a structure or component can be defined as impact fatigue IF [28]. Research into impact fatigue started a similar time as standard fatigue SF i.e. in the middle of the 19$^{th}$ century. More than a century ago, a 'shock-fatigue' test, that involved a large number of relatively small blows, was used to study the response of steels to this type of loading and was compared with a static test and a single impact. Differences between the effects of impact fatigue and both single-impact loading and standard fatigue were noted in this work as well as the absence of a durability limit [28]. However, more than a hundred years after those conclusions, the area of IF is considerably less studied than that of SF. There are several reasons, as discussed below:

a) **Ambiguity in the choice of the loading parameter**. For SF, an obvious parameter is the stress in stress-controlled fatigue. In impact fatigue, a maximum stress magnitude can hardly be used as a sole parameter as the same level of this parameter can correspond to different levels of the applied energy, depending on the loading conditions, especially impact velocity [28].

b) **Controversy of impact fatigue results in different types of materials**. Brittle specimens experience significant endurance when subjected to lighter impacts. Some authors even mention a higher resistance to IF than standard fatigue. An extreme example is shot peening, which is repetitive impacting with tiny particles. This results in improved fatigue performance as a state of compression is induced in a near-surface layer. Another example is repetitive impacting of laminated composites in drop-weight test systems, where the most affected zone is situated below the contact area, resulting in delamination initiation (in this part of the laminate) and its subsequent spreading to other parts of tested specimens. The controversy lies in the fact that in only few cases the residual strength is increasing. It can be seen, therefore, that there are many interacting factors, such as material type, impact speed as well as absorbing capability, affecting the behaviour of components and structures under repetitive low-energy impacting [28].

### 2.6.1 Impact FatigueTests

Several tests can be employed to simulate IF in the laboratory but the literature review will concentrate at the most common, which are:

- Charpy, Izod test (Pendulum impact testers),
- Drop weight test
- Split Hopkinson pressure bar

These tests involve different rates of loading. Pendulum impact testers are in the range of less than 5m/s. Drop weight tests involve rates greater than 10m/s while Split Hopksinson pressure bar involves rates around 100m/s or greater.

In the experimental work undertaken in this thesis a modification of Charpy and the Izod tests were employed.

### 2.6.2 Impact Fatigue in Metals

The most extended work on the IF behaviour of metals subjected to light blows, especially irons and steels, was carried out by Stanton and Bairstow [29]. Other authors [30-31] used Stanton and Bairstow's results to develop phenomenological models for bot low cycle impact fatigue (LCIF) and high cycle impact fatigue (HCIF) of plain carbon steels. It was found that for HCF the IF limit increases linearly with the square root of silicon content while for LCF depends on the carbon, manganese and silicon content [31].

Most of the literature involves split Hopkinson pressure bar tests and the results are compared with SF in terms of fatigue strength, material deformation and fractographical features. In terms of fatigue strength the general trend notes that the IF strength is lower than the non-impact fatigue strength with the exception of few cases [32,34]. This phenomenon can be explained due to the fact that the IF loading time is very short (0.1-1% of SF). Short loading produces high strain rates which in turn raise the yield strength of the material. This means that plasticity deformation is

not as apparent as in SF. Propagation distance of the impact strain wave is short meaning that the resulting plastic deformation under IF concentrates very close to the Impact loading point. Since plastic deformation is more difficult than in SF, the deformation under IF is more non-homogeneous and shows signs of brittle fracture.The crack growth rates are also higher in the case of IF [32-34], again with some exceptions [35-36].

When examining the effect of the loading time of the impact the findings can be divided between notched and un-notched specimens. For notched specimen the longer the loading time the greater the impact fatigue life, which is due to increased plastic deformation that occurs with higher loading times. For un-notched specimens, the opposite trend is observed [32,37].The reason for this difference is that the crack initiation life is longer in IF for smooth specimens but shorter in notched specimens when compared with non-impact fatigue. It is also noted that the crack initiation life increases with increasing loading time. In both cases microstructural defects have a greater effect in IF than in SF [32].

### 2.6.3 Impact Fatigue in Polymers

Compared with metals, the literature on the effect of IF on polymers is quite limited. Due to the rate dependency exhibited by these materials, IF, as a general rule, is causing brittle failure due to high strain rates. Differences in the behaviour of brittle and ductile polymers subjected to IF were investigated by [38] using a drop weight test. For brittle polymers the absorbed energy remained constant during the fatigue life while for ductile polymers the maximum force increased or displacement increased.

The properties and fracture behaviour of epoxy resins filled with $S_iO_2$ particles under IF and SF were investigated by [36, 39]. It was found that the crack propagation under IF was unstable and occured at a higher rate, reaching final fracture almost immediately. For SF, a lower crack propagation rate was observed and the crack grew in a more stable manner.

Others authors [40], have examined subcritical crack propagation in PMMA specimens in four point bend configurations struck with an incident bar at a rate of $1s^{-1}$. The notched specimens were more resistant to crack propagation under IF than under SF. The stable crack propagation was larger under IF due to the fact that the elastic energy stored in the specimen, within the duration of each impulse, was dissipated in craze formation at the tip of the advancing front.

According to [41], when a fracture mechanics approach was employed to evaluate the effects of impact fatigue damage on a rubber-modified epoxy-material in a 3 point bend configuration, it was observed that there was no threshold value of the applied energy below which impact fatigue would not be observed. Furthermore, the crack-growth rate could be described by a power-law equation. Another observation that was drawn from this work was that the damage accumulation mechanism involved the growth of the initial crack until the crack length was such that the energy level required for the material to fail was the same as that required for the material to fail subjected to a single impact.

In conclusion, it can be said that the majority of the authors above report that crack growth rates are higher under IF than SF and that cracks propagate in a more unstable fashion.

### 2.6.4 Impact Fatigue in Composites

Evaluating the mechanical properties and failure modes in composites can be challenging because of the non-isotropic, non-homogeneous nature of these materials and the complexity of failure mechanisms. In [41] a review of the testing methods for composites is presented. According to the author, tensile strength depends mainly on the fibres while compressive strength mainly on the matrix. It was also shown, that a material is more prone to failure under an impact blow in comparison to the same force applied more slowly. A number of authors have shown that low energy impacts, although insufficient to leave visible damage to a FRP surface, could create internal damage that could grow under cyclic loading [41-42].

This contradicts previous research which proposed a threshold energy below which no delamination signs are observed [43-45].

Impact testing of UD CFRP specimens using an Izod system was carried out by [43,46-47].It was demonstrated, that the impact response depends on the impact velocity, fibre and matrix architecture, interfacial bonding and volume fraction of the fibres. More specifically, in [46] quasi-isotropic laminates were shown to posses superior impact resistance to cross-ply laminates. In [47] it was revealed that the higher the interval impact time the higher the damage recovery (confining the damage zone to a small area).

Interlaminar shear strength (ILSS) of CFRP has several characteristics under impact loading [48-52]. It Increases with increasing strain rate, varies during loading and unloading and decreases with an increase in temperature and impact energy.

The effect of different ply stacking sequence on impact performance of CFRP has been investigated by [53-56] with a drop weight test. Non-woven composites proved to be less impact resistant than woven while replacing the 45degree plies with a woven fabric resulted in an improved impact performance. The order of stacking in laminates does not influence the impact strength [54]. However, in [55] 45degree plies found to increase the residual properties since the load carrying 0degree fibres were being protected. In [56] two fibre geometries $[\pm 45°]_4$ and $[0/90°]_{2s}$ stitch bonded glass fibre reinforced polyester resin composites have been investigated using a drop weight test. The $[\pm 45°]_4$ composite was found to be really sensitive at even low impact energies meaning that both strength and stiffness were significantly reduced. On the other hand, the [0/90°] geometry required higher impact energies for degrading its tensile properties. It was found that impact damage is influencing fatigue life and the fatigue performance is related to the post-impact residual tensile strength. This means that prediction of the fatigue life of impact damage composites maybe feasible by knowing the residual strength of the impact damaged composite and the S-N curve for the undamaged material.

The damage induced by impacts can be investigated by the measurement of residual strength and fracture energy of impacted specimens [42-43, 57-61]. In [58] where plane weave CFRP specimens were tested using a drop weight test, it was demonstrated that damage may not be visible but the strength of the laminate can

still be decreased. Furthermore, it was shown that in tension the reduction in strength depends on the extend of fibre breakage and the difference between the response in tension and compression is due to delamination being less extensive in compression. In [43, 59-60] pre-impacted specimens were tested using a commercial CFRP and an instrumented Izod machine, to cause complete failure. The results showed that the energy necessary to break specimens could be divided into three ranges; initiation of micro cracks, debonding, and fracture. This division into various damage regions was also seen in curves of local damage *vs*. number of impacts for IF [60]. Finally the latest work on the impact experimentation involves impact response and energy absorption characterization of more advanced lay-ups and matrix, reinforcements such as woven twill, thermoplastic matrices and particle infused matrices [68-70].

More specifically, in [68] the impact behaviour of carbon woven (twill 2x2, T300) specimens reinforced with standard epoxy matrix was examined under low velocity impact load. Specimens were subjected to drop-weight tests with energy values between 1.5J and 10J corresponding to velocities in the range of 1.5-3.3m/s. Four different stacking sequences were examined $[0]_8$, $[0]_4$, $[0_2/45_2]_s$, $[0/45]_s$ corresponding to nominal thicknesses of 2.4mm, 1.25mm, 2.4mm and 1.25mm respectively. The main results were presented with respect to contact load, absorbed energy as well as delamination formation/propagation. The magnitude of the contact load was increasing with increasing impact energy, as expected, but it was shown that there is an apparent 3-fold decrease with increasing laminate thickness. In other words the increase solely depends on the thickness and not the lay-up/configuration of the laminate. In terms of the absorbed energy, it was shown that there is a linear increase with level of impact energy and that the absorption percentage increases with thickness but also depends on stacking sequence. More specifically [0/45] interfaces improved the energy absorption. Lastly, the damage events prior perforation, such as damage initiation and delamination, are independent of impact energy levels and laminate lay-up but solely depend on the laminate thickness (2 times higher threshold for higher thickness). In others words, it was shown that the damage initiation, in this particular case, is mainly controlled by the matrix.

In conformity with [69], in a similar low velocity drop weight impact study, the author compares the response of epoxy based laminate thermosets with thermoplastics such as PEEK laminates. Quasi-isotropic configuration of T300 3K5HS 2.5 mm thick specimens reinforced with thermoset and thermoplastic matrices were subjected to impacts utilizing a drop weight tower with energies ranging from 2-25 Joules. The scope of this study was to prove if PEEK thermoplastic resin offers a promising alternative for TS resins. According to the author, the TS matrix has been used for over 40 years and presents drawbacks in the sense that needs low-temperature storage, difficult to control curing process as well as long curing time. Alternatively, thermoplastics possess high degree of chemical resistance, are more flexible in wider range of temperatures and obtain better damage, impact resistance.

The main findings are presented below with respect to absorbing capability and damage threshold. According to the experimental results deducted from the F-d graph, C/epoxy had the least absorbing capability at all the energy levels. Also, the after impact indentation threshold was reached at 11J in C/epoxy while in C/PEEK at 16J. Epoxy always displayed larger delaminated areas than thermoplastic counterparts reaching twice as large delaminations for low energies and 70% for higher energies. The better performance was attributed to various interacting factors. According to the author, the initial matrix damage, which does not influence significantly overall stiffness, is an initiation point for delamination and fibre breakages. This damage depends on the out of plane and in-plane shear strengths of the matrix. In PEEK the out of plane strength is 54% higher that epoxy while the in plane is 30% higher. These cracks furthermore propagate in modes I, II interacting with the matrix regions and the structures. In other words, modes I, II interlaminar fracture toughness parameters are as important as the neat resin. The GIc of the C/PEEK is 6 times higher than the C/epoxy while the GIIc is 3 times higher. Also the neat resin is 40 times stronger in PEEK than epoxy.

Lastly, in [70] the shear strength of the fibre matrix interface proved to be important in the impact behavior and damage tolerance of Kevlar composites. The results obtained in [70] are discussed in terms of load-time, load displacement, energy time and evaluation of damage. The author analyzed and contrasted the impact behavior of woven, bidirectional kevlar filled with epoxy and epoxy with nanoclays. The two sets of 3mm thick specimens were subjected to experimentation with a dropweight

testing device at 6, 12 and 21 J. In terms of average peak force in the F-t graph for 6, 12J no significant difference was observed but at 21J a 16, 1% increase was observed for the nanoclay case. The largest displacement was obtained in specimens containing only epoxy. In terms of elastic recuperation, i.e energy at peak load minus the absorbed energy a 40.1% higher elastic recuperation was observed when nanoclays were added for the maximum impact energy of 21J.Similarly for the same impact energy nanoclays improved the residual strength by 27.1%.

In addition to the material presented above, numerous researches have concentrated on the numerical aspects of IF in composites utilising modelling softwares. This section a description of the major published work on modelling of impacts in FRPCs. The main strategies to do this can be divided in three categories. Stress or strain based continuum damage approaches, fracture mechanics and cohesive zone approaches

In the first category, normally, a failure criterion is imposed at the ply level of the composite and damage parameters are used to represent the damage scenarios. For example, in [62] two damage parameters were used to represent fibre-matrix debonding and transverse cracks effects. An attempt to implement failure criteria for laminated composite structures into LS-DYNA3D was carried out by [63]. Out-of-plane stresses were considered for damage initiation. It was suggested that delamination is restricted by through-thickness compression and interlaminar shear stress. Interactions between various damage mechanisms have been considered and damage predictions were in conformity with experimental data. Impact damage was also investigated by [64] on graphite/epoxy laminated composites. A model was developed for predicting the initiation and propagation of damage as a function of material properties, laminate configuration and the impactor's mass.

Fracture mechanics approaches [65], such as the (CCT), which although really popular couple of years ago have been replaced by cohesive zone modelling approaches because of some limitations such as preliminary assumption of a pre-crack in the material and adaptive remeshing [66,67]. Most of the differences will be discussed in Section 2.9

For the cohesive zone approaches the following section will inform the reader about the development of these techniques and the links with this work.

Damage in composite structures can be categorised in two main groups. Intralaminar failure and interlaminar failure. Intralaminar failure occurs at the ply level, and includes damage scenarios such as fibre tensile and compressive failure, matrix tensile and compressive failure as well as damage interaction between the fibre and the matrix interface. Interlaminar failure occurs between the adjacent plies. The intralaminar damage mechanisms are normally predicted using ply-based strength/strain failure criteria coupled with continuum damage mechanics (CDM) [71, 72]. Delamination is mostly analysed with interface modelling techniques such as cohesive-zone models (CZMs) [73, 74]. Numerous studies applied the CZE successfully for delamination analysis in composites under tensile quasi-static loading regime such as [145, 146, 147-148,149-150].

The interface damage behaviour of composite structures subjected to dynamic loads was recently studied in [151-155]. In the above work, inter-ply delamination was analyzed with interface modelling techniques such as cohesive-zone models (CZMs) whereas the intra-ply damage mechanisms was mostly predicted using CDM models that incorporated a stiffness degradation parameter for each of the existing damage modes. More explicitly, in two of the papers that are more relevant to this work the authors established a large part of our methodology.

In [154], a 3D FEM was built to examine behaviour of crossply carbon fibre composites under low velocity impact. 2mm thick laminates $[0/90]_{2s}$ were subjected to increasing levels of drop weight impact energy at 7.35J, 11.03J and 14.7J.The experimental results were kept in order to contrast with the FE model built. In the sequent work, the author used cohesive elements for the delamination mode, with the appropriate bilinear cohesive law, while Hashin and Puck criteria were used for the intralaminar damage. For the intralaminar damage evolution, the author imposed a stiffness degradation rule for each of the modes. Discrepancies between experimental and numerical results in the energy absorption parameters kept decreasing with increasing impact energy and at the highest level very good agreement of reaction forces and area / location of delamination area were achieved.

In [155], low velocity drop weight impact experiments and the numerical verification was carried out on glass/epoxy laminates containing no hole, one hole and two holes. The specimens possessed a 2mm quasisotropic sequence and hole diameters of 4mm. A 3D FE model was built with mixed-mode bilinear cohesive law

implemented at the interfaces. The results were discussed in terms of load time, load displacement, energy time and profile of damage. The model represented adequately the experimentation and no large differences were observed in the load time relation or load displacement data. However, the absorbed energy as well as the damage size and outline were increased with the presence of holes.

Despite the above work, several recent studies, such as [156, 157] showed that computational models based on CDM are incapable of accurately representing the discrete cracks in a composite laminate. In composite structures both interlaminar and intralaminar damage scenarios are interacting in the damage evolution acting as damage dissipation mechanisms. Due to the homogenisation process that the CDM models possess these discrete interactions are not being captured. This leads to loss of critical information regarding the coupling/interaction of multiple damage modes at the macro scale. A typical example is the false estimation of the crack path resulting to a mistaken estimation of the global stiffness of the structure. According to [157] to accurately predict multiple damage mode interactions, an explicit kinematic representation of all damage mechanisms in global models of composite structures is required. Furthermore the same author suggested that the above drawback could be resolved by representing all major damage modes in FE models by cohesive-zone elements. Advanced CZM procedures are able to couple directly the bulk with the interface damage scenarios. In others words, damage initiation and evolution by accurately predicting the crack path scenarios is feasible.

Recently, this interactive damage modelling approach was studied in [158-160]. In [158, 159] the author simulated fracture of quasi-isotropic laminate specimens in tension tests using CZMs accounting for both inter-ply delamination and intra-ply splitting damage mechanisms and their interaction. Okabe et al. [160] applied CZEs to model transverse cracks and delamination in cross-ply GFRP laminates loaded in tension. The FE models simulated complex progressive damage mechanisms in the laminates very well.

At this point we need to reiterate on the basics of impact and also the dynamic tension. An important difference between static and impact loadings is that statically loaded components are designed to carry loads while components subjected to impacts are designed for energy absorption mainly. Dynamic response of composite structures can be categorized into high, intermediate and low-velocity impact. In our

case low velocity (large mass) scenarios occur. Low-velocity impact is associated with an impact, which is long enough for the entire specimen to respond to the impactor by absorbing energy elastically and through damage. Deformation of the entire structure is established in low-velocity impact. Response to low-velocity impacts can be treated almost as quasi-static because deflection and load would have similar relation as in a static loading. The velocity range of these events can vary from 1 to 10 m/s, depending on the target's stiffness, material properties and the impactor's mass and stiffness. When the impact velocities are below 5 m/s, the response type is controlled by the impactor/target (laminate) mass ratio rather the impact velocity [161]. Cantwell and Morton [162] has classified low velocity as up to 10 m/s, by considering the test techniques, which are generally employed in simulating the impact events such as Charpy, Izod and drop-weight impact tests. In our case a modification of Charpy has been used with velocities up to 7m/s.

In conclusion, it can be said that since low velocity impact can be treated almost as quasistatic phenomenon and there is a background of work with quasistatic tensile modelling by [158-160] it is a valid starting point to use the above information to built a dynamic tensile FE model that utilises cohesive zone modelling not only for the intralaminar cases but for all the interactive damage scenarios. To the author's knowledge most of the literature related to damage modelling of composites under impact is relevant to drop weight or modification of drop weight scenarios.

At this point work on the analytical modelling will be presented. Broadly speaking, there are 3 ways of analysing fatigue life and damage analytically. This can be done with:

- Fatigue life models
- Phenomenological models
- Progressive damage models

This section is concentrated on analysis methods applied to SF regime and composite materials as there is little in the literature review on the analysis of IF. However, similar models can be implemented and applied to IF. The following sub-

sections will describe the various different methods that have been used to analyse and characterise fatigue in composites.

**Fatigue Life Models**

Fatigue life models use S-N curves and Goodman-type constant life diagrams. The most common method to analyse fatigue life is the Palmgren-Miner (P-M) method. For a CA load, the Miner's rule is defined as:

$$C=\frac{n}{Nf} \qquad (2.2.3)$$

where $n$ is the number of cycles at a given stress amplitude $\Delta\sigma$ and $Nf$ is the number of cycles to failure at $\Delta\sigma$. C is called the Miner's sum and is theoretically equal to one at the point of complete rupture [25]. An extension of the P-M rule is the Marco-Starkey model where damage can be defined as

$$D=\left(\frac{n}{N}\right)^{a}, \qquad (2.2.4)$$

In the Howe-Owen model [75] the cumulative non-linear damage in glass reinforced composites is given by:

$$D=\sum_{i=1}^{j}\left[A\left(\frac{ni}{Ni}\right)+B\left(\frac{ni}{Ni}\right)^{2}\right]. \qquad (2.2.5)$$

where A and B are material's parameters while i and j are the initial number for the cycles and the last respectively.

Other models, experimentally characterising the fatigue life of using CFRP specimens, are the Adams and Harris's model [76] and the Jen and Lee's model [77].

An alternative to the fatigue life approach are the phenomenological models which can be categorised as residual stiffness or residual strength models. Residual stiffness models have an advantage over residual strength models because the residual stiffness data are not as highly sensitive to damage progression. In addition, this method can be used as a non-destructive measure. These models are discussed below.

**Residual Stiffness Models**

The Sidoroff & Sugadio's model suggests that damage results from the degradation of elastic properties and can be defined as

$$D=1-\frac{E}{E_{initial}} \qquad (2.2.6)$$

According to [78] the stiffness of elastic materials ( E ) decreases as a function of numbers of cycles ( n/Nf ). This reduction is carried out in three stages, formation, propagation and final failure, as seen in Figure 2.10.

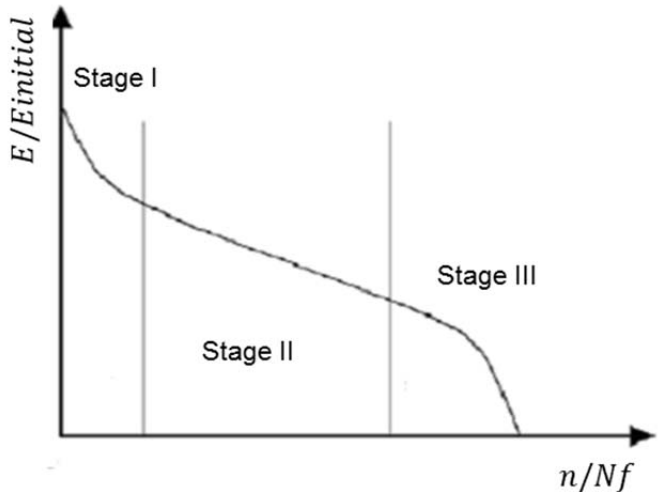

Figure 2.10 Stiffness degradation curve over life [78]

Damage growth in tension is described in Sidoroff &Sugadio's model as:

$$\frac{\partial D}{\partial n} = \frac{A(\Delta\varepsilon)^c}{(1-D)^b}, \qquad (2.2.7)$$

where $c,b$ are material constants and $\Delta\varepsilon$ is the applied strain amplitude.

According Whitworth's model the residual stiffness is monotonically decreasing with increasing fatigue cycles [79].

The degradation law is defined as:

$$\frac{\partial E^{aff}(n)}{\partial n} = \frac{-a}{(n+1)E^{aff}(n)^{m-1}} \qquad (2.2.8)$$

where $E^{aff}(n)=E(n)/E(Nf)$ is the ratio between the residual and the failure stiffness. Also, $a,m$ are parameters dependent upon stress, loading frequency and environmental conditions. Integrating the above equation and assuming that failure occurs when fatigue strain equals ultimate strain, the residual modulus is given by:

$$E(n)=E_0\left(\frac{\sigma_{max}}{c_1\sigma^{static}}\right)^{1/C2}\left[-h\ln(n+1)+\left(c_1\frac{\sigma^{static}}{\sigma_{max}}\right)^{m/c2}\right]^{1/m}, \qquad (2.2.9)$$

where: $c1,c2$ are constants, $\sigma^{static}$ is failure stress under static loading [79].

**Residual Strength Models**

The Yao-Himmel's model considers that the experimental data follows a sinusoidal pattern on a residual strength $\sigma_R$ vs fatigue life ($(Nf)$ graph [25,80].

$$\sigma_R=\sigma^{static}-(\sigma^{static}-\sigma_{max})\frac{\sin(\beta\frac{n}{Nf})\cos(\beta-a)}{\sin(\beta)\cos\left(\beta\frac{n}{Nf}-a\right)} \qquad (2.2.10)$$

where $\beta,a$ are parameters defined empirically [80].

The Schaff and Davidson's model was proposed to account for the damage evolution in composites under VA fatigue [27,81]. The model assumes that the initial residual strength is equal to $\sigma^{static}$ (static strength) and it decreases with increasing number of cycles. Failure occurs after $\sigma_R(n)$ reaches the same value that has the maximum stress from the sinusoidal spectrum $\sigma_{max}$ which happens after N cycles. The model assumes that the residual strength $\sigma_R(n)$ for a block satisfies the following function:

$$\sigma_R(n)=\sigma^{static}-(\sigma^{static}-\sigma_{max})(\frac{n}{N})^v \qquad (2.2.11)$$

where $v$ is a degradation parameter [81].

Additionally in the case of VA fatigue, the way the two-stress loading sequence is handled by the model is shown at Figure 2.11.

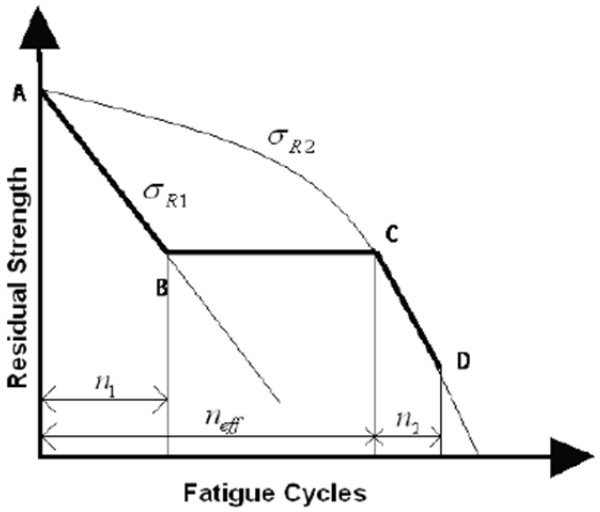


Figure 2.11Schaff & Davidson's method [27]

The curve ABCD represents the residual strength before completing two load blocks. Curve AB presents the strength degradation for specimens subjected to constant amplitude loading at stress level $\sigma_{R1}$. Curve ACD presents the strength degradation of specimens subjected to constant amplitude loading at stress level $\sigma_{R2}$.

This model assumes that the specimen will be at point B when loaded at $\sigma_{1max}$ by n1 cycles and the strength will be defined by Equation 2.2.11 However, when the second load block appears, the system will follow ACD and point C represents an equivalent strength that a specimen has before being loaded $\sigma_{2max}$ value.

In other words, the specimens that reached point B following the AB path have the same residual strength and therefore damage as the specimen that reached point C following the AC curve. To achieve the shift from point B to point C, an effective number of cycles $n_{eff}$ has to be introduced assuming that the specimen has the same strength between these two points. The $n_{eff}$ value is defined as the equivalent number of cycles required to produce the same strength loss in the second segment as that predicted to occur within the first segment [25,27].

**Progressive Damage Models**

These models use one or more damage variables related to manifestations of damage (transverse matrix cracks, delamination size). The graph in Figure 2.12 shows, the algorithm plot of propagation rate against strain energy release rate (G) energy required to open the same crack. This graph is used to predict crack growth in a sample subjected to a defined fatigue load. It has to be noted that $G$ is usually used as a fracture mechanics parameter for adhesives and composites rather than $K$ which is used for metals [27]. Also $G_{max}$ is used over $\Delta G$ because the cracked surface can be affected in the unloading process which results in an increase of the real value of $G_{min}$ [24].

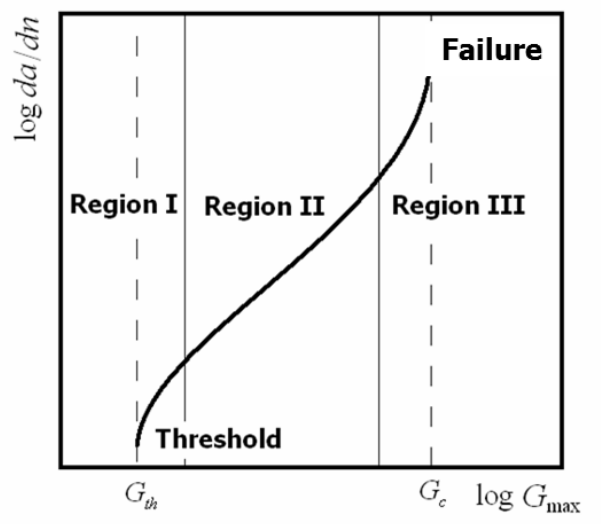


Figure 2.12 Typical fatigue crack growth law and regions [27]

Commenting on the graph it can be said that at region II (intermediate $G_{max}$ values) the curve is linear, but the crack growth rate deviates from that trend at high and low $G_{max}$ values. The crack growth rate accelerates as $G_{max}$ approaches $G_c$ which is the fracture toughness of the material. On the other hand the crack growth approaches zero at the threshold $G_{th}$.Region II of the graph can be described by an empirical relation commonly referred to as Pari's law [82].

$$\frac{\partial a}{\partial N} = C\Delta G^{m} \qquad (2.2.12)$$

where $C,_{m}$ are material constants determined experimentally and $\Delta G(G_{max}\text{-}G_{min})$ is the fracture toughness values

## 2.7 Fracture Mechanics

In nature, there are two types of fractures. These can be categorised in crack dominated and yield dominated. Fracture mechanics approaches are employed for characterising crack dominant failures.

Crack propagation is a product of stress distributions near the crack tip. There are three types of crack opening which are shown in Figure 2.13. Mode I denotes crack opening with the crack faces separated in direction normal to the crack plane. Mode II is characterized by an antisymmetric separation of the crack surfaces due to relative displacements in the direction of the crack front propagation. Finally, Mode III describes a separation due to relative displacements in z-direction. Fracture mechanics can be divided into linear elastic fracture mechanics (LEFM) approaches and non linear (NLEFM). LEFM treats a cracked body as linear elastic and the possible inelastic/plastic processes within or outside the process zone surrounding the crack tip must be restricted to a small region [83].

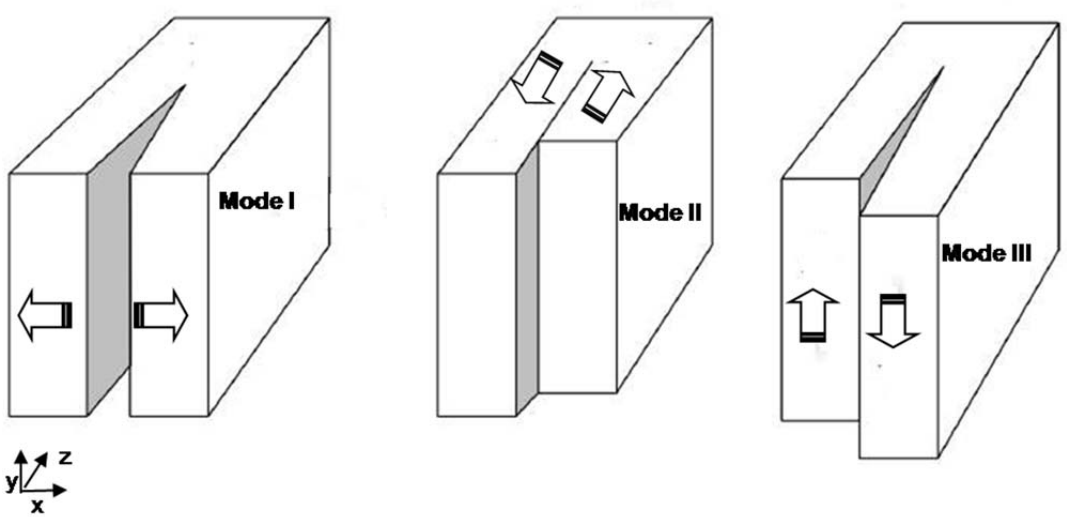


Figure 2.13 Crack propagation modes

NLEFM deals with materials that are loaded above the yield stress and therefore accounts for plasticity.

### 2.7.1 Linear Elastic Fracture Mechanics (LEFM)

Fracture mechanics theory was initiated by Griffith and developed by Irwin based on measurements that were carried out on glass rods [84,85]. Griffin proposed the energy balance approach while Irvin developed the stress field approach.

- **Energy balance approach**

Griffith accounted for crack growth in brittle solid materials and defined the concept of strain energy release rate $G$ which is defined as the energy dissipated during fracture per unit of newly created fracture surface area. This quantity is fundamental because the energy that must be supplied to a crack tip for it to grow must be balanced by the amount of energy dissipated due to the formation of new surfaces and other processes such as plasticity.

For a crack length 2a resulted from tensile stress the energy release rate is given by

$$G=\frac{\pi\sigma^2 a}{E} \qquad (2.2.13)$$

where $\sigma$,$E$ is the fracture stress and elastic modulus respectively .

Additionally $G$ can be expressed as:

$$G=\frac{P^2}{2B}\frac{\delta C}{\delta a} \qquad (2.2.14)$$

Where P,B,C are the load, the width of the specimen and material's compliance, respectively.

Furthermore the critical stresses required for fracture initiation can be described as :

$$\sigma=\sqrt{\frac{2E\gamma_s}{\pi a}} \qquad (2.2.15)$$

where $\gamma_s$,a,σ,E are the surface energy , the crack length , the applied stress and the elastic modulus in case of plane stress , respectively.

- **Stress field approach**

The amplitude of the stress distribution in the area near to the tip can be expressed in terms of a scalar quantity called stress intensity factor (K). It was proposed that the stress field around a crack tip at mode I of loading at a position with coordinates rand θ (using polar co-ordinates)

can expressed as:

$$\begin{aligned}
\sigma_{xx}&=\frac{K_I}{\sqrt{2\pi r}}\cos\frac{\theta}{2}\left(1-\sin\frac{\theta}{2}\sin\frac{3\theta}{2}\right);\\
\sigma_{yy}&=\frac{K_I}{\sqrt{2\pi r}}\cos\frac{\theta}{2}\left(1+\sin\frac{\theta}{2}\sin\frac{3\theta}{2}\right);\\
\tau_{xy}&=\frac{K_I}{\sqrt{2\pi r}}\sin\frac{\theta}{2}\cos\frac{\theta}{2}\cos\frac{3\theta}{2}.
\end{aligned} \qquad (2.2.16)$$

where $K_I$ depends on geometry, the crack size, load level and load mode [65]. A useful relation, also defined by Irwin, was developed, correlating K with G using the Young´s modulus:

$$G=\frac{K^2}{E'} \qquad (2.2.17)$$

where $E'=\frac{E}{(1-v^2)}$ for a plane strain rate and $E'=E$ for a plane stress one;

Moreover $\nu$ is the Poison's ratio.

If the body is exposed to more than one load mode, then a superposition expression for the total energy release rate ($G_T$) can be used:

$$G_T=G_I+G_{II}+G_{III}=\frac{K_I^2}{E}+\frac{K_{II}^2}{E}+(1+v)\frac{K^2_{III}}{E}, \qquad (2.2.18)$$

where the sub-indices denote each of the loading modes.

Stresses at the crack tip in real life are finite because the crack tip radius can not be infinitely small. However linear elastic stress analysis of sharp cracks predicts infinite stresses at the crack tip.

Simple corrections to LEFM are available from small crack tip yielding problems. For extreme cases of yielding a non linear approach should be used (NLEFM) that utilises alternative crack parameters. The size of the crack tip yielding zone can be estimated by the Irwin method [86]. Assuming the contour of the plastic zone is circular with a radius $r_p$, using Equation 2.16 at $\theta=0$ and considering the stresses in y direction the radius of plastic zone $r_p$ in mode I is:

$$r_p=\left(\frac{K_I}{\sigma_Y}\right)^2\frac{1}{3\pi} \qquad (2.2.19)$$

for plane strain

$$r_p=\left(\frac{K_I}{\sigma_Y}\right)^2\frac{1}{\pi} \qquad (2.2.20)$$

for plane stress

### 2.7.2 Non Linear Elastic Fracture Mechanics (NLEFM)

As it was discussed above LEFM methods do not account for crack tip plasticity.
In the case of crack tip plasticity $G$ cannot be determined since is affected from the plastic zone [25, 87,88].
The $J$ integral gives a way of determining the strain energy release rate in the case of the elastic-plastic behaviour.

$$J=\int_{\Gamma}\left(W dy-T\frac{\partial u}{\partial x}ds\right) \qquad (2.2.21)$$

where $\Gamma$ is any path surrounding the crack tip, $W$ is the strain energy density $T$ is the tension vector perpendicular to $\Gamma$, $u$ is the displacement vector and $s$ is the distance along the path $\Gamma$.
It has to be noted that $J$ cannot be evaluated in unloading conditions. According to [88] the $J$ integral is the change in potential energy with respect to the crack extension for nonlinear elastic materials and can be reduced to the strain energy release rate for linear elastic solids: $J=G$.

### 2.7.3 Dynamic Fracture Mechanics

Structures are often loaded under dynamic conditions, yet this type of loading is neglected. Dynamic fracture mechanics (DFM) can be used to analyse dynamic problems. Dynamic problems can involve load oscillations in addition to inertia effects. What differentiates LEFM, NLFM to DFM is the stress wave propagation. The wave can travel in a material with wave velocity $Vc$ and therefore the strain in

different segments of the material depends on the load rate, $Vc$ and the boundary conditions [89]. Noting that $Vc$ is a function of E and material density. The governing equation for Mode I crack propagation under elastodynamic conditions is based on the conventional static stress intensity formula and can be written as

$$K_I(t)=K_{ID}(V) \tag{2.2.22}$$

where $K_I$ is the instantaneous stress intensity and $K_{ID}$ is the dynamic fracture toughness.

According to [89−92] the dynamic stress intensity is given by the following equation.

$$K_I(t)=k(V)K_I(0) \tag{2.2.23}$$

where $k$ is function of crack speed and $K_I(0)$ is the static stress intensity factor. In conformity with [93]:

$$K(V) \approx \left(1-\frac{V}{cr}\right)\sqrt{1-hV} \tag{2.2.24}$$

where $h$ is a function of the elastic wave speeds and is given by

$$h \approx \frac{2}{c_1}\left(\frac{c_2}{cr}\right)^2\left[1-\left(\frac{c_2}{c_1}\right)\right]^2 \tag{2.2.25}$$

where $c_1, c_2$ are the longitudinal and shear wave speeds, respectively while *cr* is the Ralyeigh wave speed.

### 2.7.4 Numerical Methods for Fracture Mechanics

Fracture resistance can be assessed by a number of methods which are used to compute the strain energy release rate based on the results from FEA.

The virtual closure technique [84−86,94−96] is ideal for determining energy release rates due to the fact that fracture mode separation is determined explicitly. It is based on the assumption that the energy released during crack extension equals the work required to close the crack back to its original position. Based on this assumption the energy release rate is computed from the nodal forces and displacements. Crack growth is predicted when the components of the energy release rate are equal to a critical value. This method can be easily applied to the finite element method as shown in Figure 2.14

In this method the crack is extended, or closed during two steps. The change in strain energy $\Delta E$, when the crack is extended from $\alpha$ and $(\alpha+\Delta\alpha)$ is assumed to be equal to the energy required for the crack to close between b and c Figure 2.14, Figure 2.15.

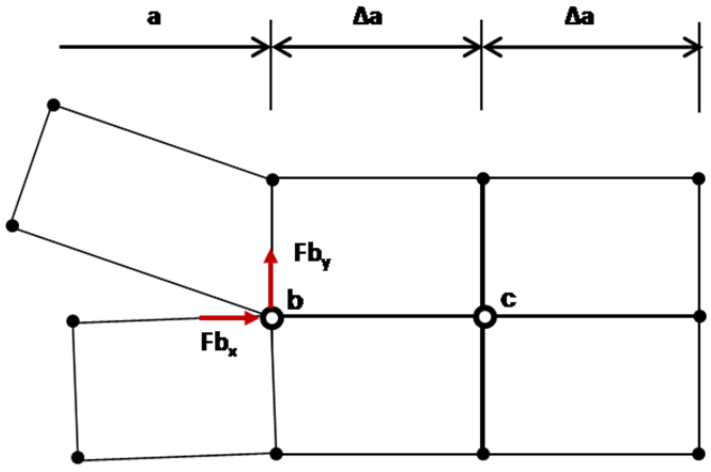


Figure 2.14 Crack Closure Method-Step 1 [65]

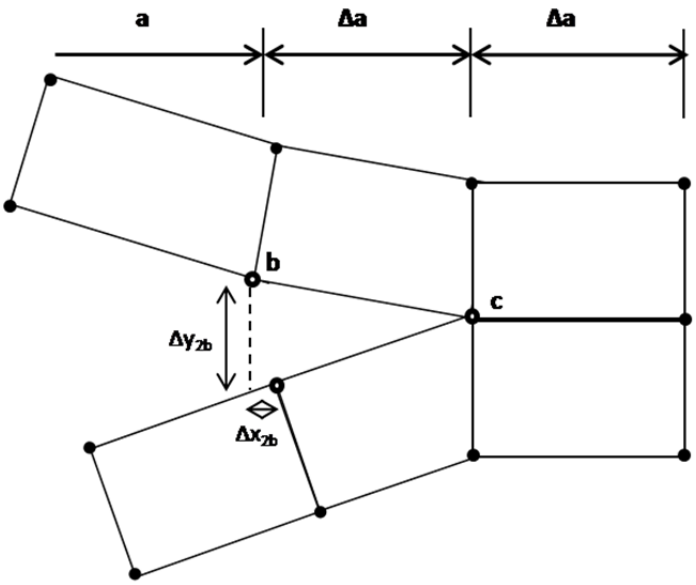


Figure 2.15 Crack Closure Method-Step 2 [65]

**Virtual Crack Closure**

The virtual crack closure differs from the crack closure methods only in that the assumption that a crack extension of $\Delta a$ from $a+\Delta a$ (node i) to $a+2\Delta a$ (node k) does not alter the crack tip state. It is a technique applied to evaluate strain energy release rate for crack propagation moded I and II.It is based on the evaluation of the crack closure integral. For a crack model with 2-D, four noded elements the energy required to close the crack along one element side is given by the following equation.

$$\Delta E=\frac{1}{2}\left[(Fc_x\times\Delta x_b)+(Fc_y\times\Delta y_b)\right], \qquad (2.2.26)$$

Where $Fc_x, Fc_y$ are direct and shear forces at point c and $\Delta x_b, \Delta y_b$ are the x and y displacements at node b, as seen in Figure 2.16.

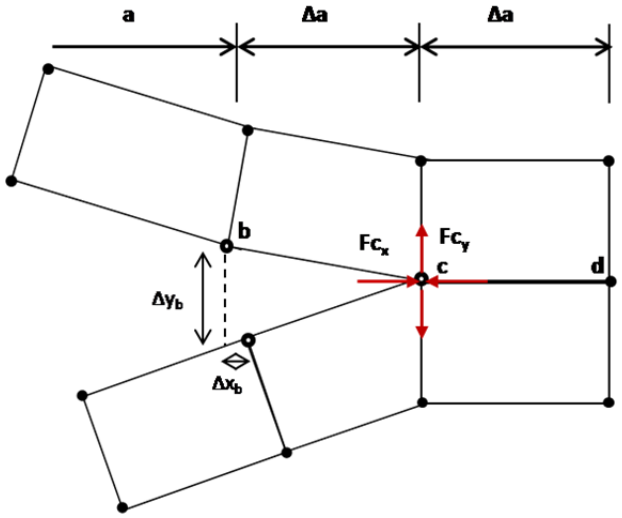


Figure 2.16 Modified Crack Closure Method [65]

From the above it can be deducted that the energy $\Delta E$ required to close the crack can be obtained from a single finite element analysis.

## 2.8 Damage Mechanics

A failure criterion utilizing a damage mechanics approach can provide several advantages over the fracture mechanics approach, which will be discussed. The fundamental difference between fracture mechanics and damage mechanics is that fracture mechanics deals with a crack in the macro scale with a given shape and position, while damage mechanics addresses the change in macro stress and macro strain (material degradation) due to the initiation and growth of micro-defects and the energy dissipated through plasticity around the crack tip in a 'real-life' material element under monotonic, cyclic or impact or loading. The general advantage, compared with classical fracture mechanics, is that, in principle, the parameters of the respective models do not necessarily need an initial crack for the analysis and take into account multiple cracks [97]. Damage models can be categorized according to their scale in 4 categories

- Atomic scale

- Microscale
- Meso-scale
- Macroscale

Regarding the atomic scale it can be said that damage at that level involves a reference to irreversible distributed configuration changes resulting from energy dissipation mechanisms such as rupture of atomic bonds.

On the microscale, damage is determined by the number of microcracks, microvoids as well as their size and configuration.

Damage on a micro level in a one-dimensional case loading case can be introduced as

$$D=\frac{S_D}{S}, \qquad (2.2.27)$$

where $S,S_D$ are the cross sectional area and the micro crack area as seen in Figure 2.17.

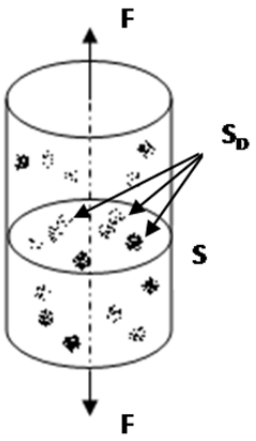


Figure 2.17 Damaged element [5].

Failure occurs when D=1, while in the fully undamaged case D=0. However, through a process of instability the material is most likely to fail before damage reaches the critical value of 1. Assuming that no forces act on the surfaces of microcracks we

can introduce the effective stress parameter $\sigma_{eff}$ which is related to the surface resisting the load

$$\sigma_{eff} = \frac{F}{S-S_D} = \frac{F}{S\left(1-\frac{S_D}{S}\right)} = \frac{\sigma}{1-D} \qquad (2.2.28)$$

On the macroscale in order to describe damage the use of effective state variables is common (scalars, vectors and tensors) as well as the use of the effective stiffness principle where damage evolution is related to the change in elastic properties. Using the elasticity law we can quantify damage by observing the variation in the elastic modulus.

| **Undamaged material** | **Damaged material** |
|---|---|
| D=0 | 0<D<1 |
| $\varepsilon=\sigma/E$ | $\varepsilon=\frac{\sigma}{E(1-D)}$ |

The elasticity modulus of the damaged material is

$$E_{eff}=E(1-D) \qquad (2.2.29)$$

For composites, when dealing with macro-scale the whole structure is regarded as a homogeneous continuum, and an anisotropic constitutive law is used to describe the structural behaviour. On the other hand, in the micro scale, the fibres, the matrix and, the fibre–matrix interaction are considered. In the meso scale which is a stage between micro and macro the plies are analysed. The failure prediction of a laminated composite is treated on a ply-by-ply basis. The behaviour of the ply, which is considered as homogeneous, is supposed to be orthotropic. Physical degradation generally appears inside the plies (splitting, matrix cracks, fibre breakage, or in the case of delamination between the plies.

Progressive damage models mainly arise when dealing with the micro level. Initiation of fractures involves growth of microcracks, creation of newly fractured surfaces and plasticity around the crack tip. All the above processes result in energy dissipation which can be modelled by progressive damage models. These models can be divided into continuum and discrete.

**Continuum Approaches**

Continuum approaches involve damage models such as the crack band model (CBM) and non-local continuum damage models.

In the CBM the fracture process zone is modelled using a single layer of continuum elements placed on a predefined crack path where the material properties are altered according to the element width. In other words the area under the stress strain curve is adjusted according to the width of the elements. The crack then evolves when the stress value goes to zero and as a result the element cells are removed.

Although this approach is successful for mode I fractures it is difficult to implement in mixed mode problems because is very computationally expensive. More specifically, the width and length of the fracture process zone (FPZ) must be explicitly modelled with a very fine mesh. The same problem occurs in non-local continuum approaches [97].

**Discrete Approaches**

Discrete approaches involve LEFM and CZM. Dugdale and Barenblatt [98,99] are considered to be the pioneers of the CZM methods. The method involves the representation of a nonlinear crack tip process zone. This idea is applicable in quasi-brittle fibre matrix composites where the fracture process is related to the development of a very narrow band, named the cohesive zone as shown in Figure 2.18.

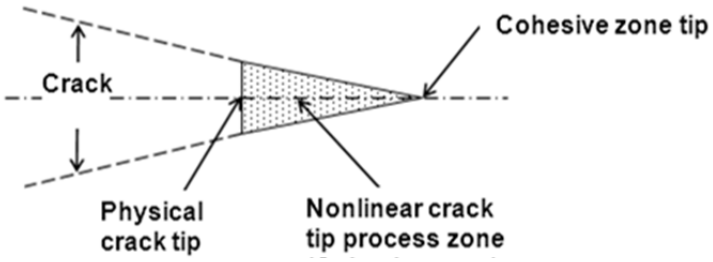


Figure 2.18 Schematic representation of a cohesive zone

The cohesive zone is created before the ultimate fracture, which is a more realistic approach for laminated composites as the onset of damage does not lead to ultimate failure [7,100]. The non-linear mechanisms can dissipate a considerable amount of energy so that additional external work is required for growth of the macro-crack which results in an increase of fracture toughness of the material [101].

In the CZM approach the cohezive zone is reduced to a line or plane of displacement discontinuity and the degrading mechanisms in the FPZ are characterized by a stress–displacement relationship across this line or plane. The crack grows when the separation of the starting point of the cohesive zone increases to a critical value. Until that critical displacement the, crack nucleation, propagation, and arrest have been accounted for.

In the finite element method cohesive elements are placed at the separation interface between continuum elements. The constitutive properties of these cohesive elements describe the evolution of cohesive traction (stress) as the interface is being opened (opening displacement). Hence, the cohesive zone elements describe the cohesive forces which occur when material elements are being pulled. On the occurrence of damage growth these cohesive elements open to simulate the crack nucleation and growth.

The constitutive behaviour of the cohesive elements is given by a traction-separation law or cohesive law. Cohesive elements serve the purpose of bridging the adjacent surfaces and direct the cracking in accordance with this traction-separation law.

The traction is a function of opening displacement, i.e.

$$\sigma=f(\delta) \qquad (2.2.30)$$

where $\sigma$ is the stress and $\delta$ is the opening displacement.

A vast range of different traction-separation laws can be found in the literature [98, 99, 102-107] which are extensions, developments of Dugdale and Barenbatt, some of which are illustrated in Figure 2.19. All of these laws exhibit the same global behaviour, i.e., the value of cohesive traction first increases as the cohesive surfaces separate until a maximum value of traction is reached, and subsequently the traction decreases to zero which results in complete (local) separation. This process applies to tractions in both normal and shear directions.

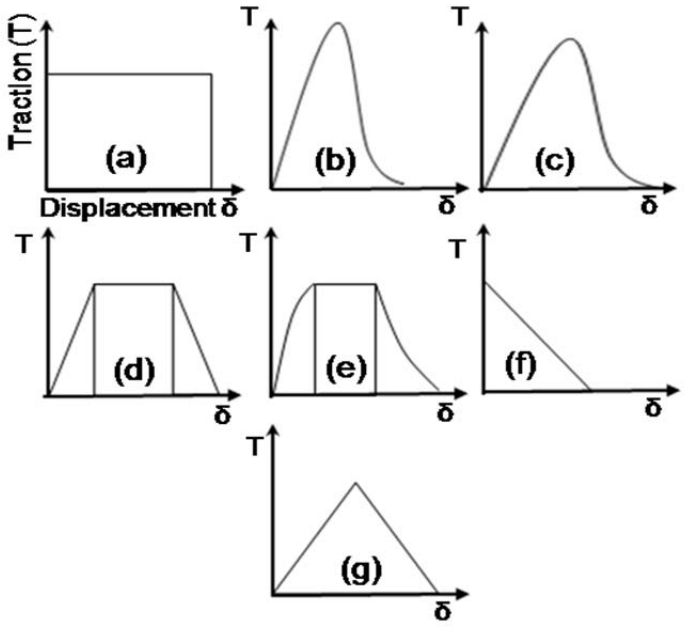


Figure 2.19Various cohesive laws proposed by different authors; (a) Dugdale; (b) Barenblatt; (c) Needleman; (d) Tvergaard & Hutchinson; (e) Scheider; (f) Camacho & Ortiz; (g) Geubelle

In all the cohesive laws except (a) and (f) the traction across the interface reaches a maximum, then decreases and eventually vanishes, allowing complete decohesion. The main difference among all the cohesive models lies in the shape of the traction-separation, and the constants that are used to describe the shape.

Dugdale [98] assumed the finite stress at the crack tip of steel sheets to be the yield stress Figure 2.19(a). Barenblatt [99] investigated the equilibrium of cracks in brittle materials by defining the traction along the crack path as a function of the crack tip distance along the crack front Figure 2.19(b). Application to other material systems such as biomaterial interfaces, elastoplastic materials was performed by [102,103] Figure 2.19(c), and [104] Figure 2.19(d) respectively. Extension of model (c) was performed by [105] to account for mixed-mode loading. The curve is shown in Figure 2.19(e). Camacho and Ortiz [106] employed a linear cohesive fracture mode to account for multiple cracks during impact damage in brittle materials. This model predicts failure by both shear and normal separation in tension and by shear separation in compression; its typical curve is plotted in Figure 2.19(f).

Cohesive zone models have been used to analyse composite delamination problems. Geubelle and Baylor [107] utilized a bi-linear cohesive model to simulate spontaneous initiation and propagation of cracks in thin composite plates subjected to low-velocity impact. The traction-separation curves for this model are shown in Figure 2.19(g). Other authors also have studied problems of delamination in concentration free specimens [89-94], [108-113]. Authors [18,19] have studied damage is composites that contain notches such as slits and holes. For furher analysis refer to section 2.6.4.

**Advantages and limitations of cohesive-zone model**

Cohesive-zone models use both damage and fracture mechanics approaches to define the behaviour of an interface. They are good compromise between computational efficiency and physical reality. Using cohesive models, we can have the following main advantages:

- A pre-existing crack region or propagation direction is not required for the application of the cohesive-zone model;
- In the CZM approach, there is no energy dissipation at the crack tip (no stress singularities) and material failure is quantifiable by means of displacements and stresses;
- No need for adaptive remeshing to monitor crack progression which requires a fine mesh around the crack front (happens as in the crack closure technique)
- Not dependent on the shape of the crack front. Fracture mechanics methods are particularly dependant on this for the determination of the correct mix-mode ratio
- Even though the physical separation occurs, mathematically the continuity conditions are maintained by the cohesive model ;
- It can also be perceived at the meso-scale as the effect of energy dissipation mechanisms, energy dissipated both in the forward and the wake regions of the crack tip;

**Limitations**

- Cohesive elements require a very fine mesh to remain accurate and this is a drawback when dealing with large structures
- Cannot account for random crack front shape meaning that differentiation between shear damage in mode II and III is not feasible

## 2.9 Summary

Presented in this chapter is a review of available research work addressing the damage in CFRP laminated composites under dynamic conditions. The main areas related to this topic were reviewed and important conclusions are summarized below. The basic principles of available experimental methods and their implementation to the analysis of damage in laminated composites were discussed. The modelling methods that are suitable for analysing the various damage mechanisms in such laminates were also presented.

Damage mechanics-based models have shown significant success in modelling stiffness degradation in laminated composites. Cohesive zone models were found to be capable of investigating damage initiation and propagation under static and dynamic conditions. To the author's knowledge, modelling of crossply composite damage under tensile uniaxial dynamic conditions using only cohesive zone elements has not been investigated in the past and this was emphasized in section 2.6.4.

# Chapter 3 Materials and Experimental techniques

## 3.1 Introduction

The main aim of this chapter is to describe the materials, specimens and procedures used in the experimental programme. This chapter contains the following:

- A description of the materials used in this research.
- A description of the specimen geometric configurations used.
- A description of the machines used for static and impact tests.
- A description of the cyclic impact tests performed and test parameter used
- A description of the apparatus used to analyse the damage in the samples post-impact.
- A description of the techniques used to measure damage.

## 3.2 Materials

Two carbon fibre reinforced polymer (CFRP) composites were used in this research. These are described below.

### 3.2.1 IM7/8552

The Izod impact fatigue test (IIFT) specimens used in this work were made from IM7/8552 unidirectional (UD) CFRP, supplied by Hexcel Corp., Duxford, UK. This material is commonly used in aerospace applications. The matrix, HexPly 8552, is an amine cured toughened epoxy material, the properties of which are shown in Table 3.1. The carbon fibre used as reinforcement in the composite is the intermediate modulus fibre HexTow IM7. UD pre-preg material with a nominal fibre volume fraction of 0.6 and thickness of 0.125mm was laid up in a 8-ply and 32-ply stacking arrangement since 2 thicknesses were studied. The final plate dimensions were 250mm x 200mm and the thicknesses of the cured plates were approximately 1mm and 4mm respectively. The plates were cured for 2 hours at 182ºC, with an initial autoclave pressure of approximately 700 kPa. Material data for UD IM7/8552 from the Hexcel product datasheet is shown in

Table 3.2.

Table 3.1 Properties of 8552 matrix at room temperature [114]

| | |
|---|---|
| Glass transition temperature Tg (°C) | 200 |
| Cured density ρ (g/cm$^3$) | 1.3 |
| Tensile strength (MPa) | 121 |
| Tensile modulus (GPa) | 4.67 |
| Elongation at failure (%) | 1.7 |

Table 3.2 Properties of IM7/8552 composite at room temperature [114]

| $E_{11}^T$ (GPa) | $E_{22}^T$ (GPa) | $E_{33}^T$ (GPa) | $G_{12}$ (GPa) | $G_{23}$ (GPa) | $G_{13}$ (GPa) | $\nu_{12}$ | $\nu_{23}$ | $\nu_{13}$ |
|---|---|---|---|---|---|---|---|---|
| 165 | 11.38 | 11.38 | 5.12 | 5.12 | 3.92 | 0.3 | 0.49 | 0.3 |

| $S_{11}^T$ (GPa) | $S_{11}^C$ (MPa) | $S_{22}^T$ (MPa) | $S_{22}^C$ (MPa) |
|---|---|---|---|
| 2.6 | 1.5 | 60 | 290 |

### 3.2.2 T700/LTM45

The tensile impact fatigue test (TIFT) samples were made using UD carbon/epoxy T700/LTM45 prepreg with a nominal ply thickness of 0.128 mm. The T700 fibre is used in the wings and the fuselage of airplanes and is due to its high strength. LTM45 is a toughened, low temperature curing epoxy resin capable of high temperature end use. The composite system T700/LTM45 (From Advanced composite Group ACG), was selected because it can be easily cured at low temperature and its mechanical properties have been characterised in Loughborough University. Its UD mechanical properties are displayed in Table 3.3 and were measured in Loughborough University. Two cross-ply lay-ups of $0_2/90_4/0_2$ and $0_4/90_8/0_4$ were selected, as this enables a number of failure mechanisms to be investigated in a relatively simple system and investigate the effect of thickness on the fatigue life. Laminates of 100 mm × 150 mm were laid up in 8-ply and 16-ply stacking arrangements and cured in an autoclave at 60°C under a pressure of 0.62 MPa for 18 hours. The thickness of the cured plates were approximately 1mm and 2mm respectively. Each sandwich panel was then cut into four 25 mm × 150 mm specimens using a water jet cutting procedure.

Table 3.3 Properties of T700/LTM45 composite at room temperature

| $E_{11}^T$ (GPa) | $E_{22}^T$ (GPa) | $E_{33}^T$ (GPa) | $G_{12}$ (GPa) | $G_{23}$ (GPa) | $G_{13}$ (GPa) | $\nu_{12}$ | $\nu_{23}$ | $\nu_{13}$ |
|---|---|---|---|---|---|---|---|---|
| 127 | 9.1 | 9.1 | 5.6 | 5.6 | 4 | 0.31 | 0.4 | 0.31 |

### 3.2.3 Adhesive/Surface Preparation

For the uniaxial impact specimens end tabs were introduced at the stress areas. Aluminium end tabs were fitted using the adhesive/primer combination FM 73M/BR

127 from Cytec Industries Inc. FM 73M is a general purpose aerospace adhesive designed to provide structural performance in the temperature range -55°C to 82°C, giving good durability for metals and composite bonds. This adhesive is supplied in films of 0.12 mm nominal thickness. BR 127 is a modified epoxy-phenolic primer that contains 10% solids, of which 2% is a strontium chromate corrosion inhibitor. The remaining 90% of the solution is methylethyl ketone (MEK) solvent. The surfaces of the joining areas were subject to a surface treatment prior to bonding in order to improve adhesion and increase repeatability in the tests. Initially, grit blasting of the surface of both aluminium and composite specimens was carried out, employing alumina particles with dimensions of approximately 400 μm under a pressure 55 kPa with a working distance of 15-20 cm. The grid blasting procedure was carried out utilising a Guyson 300/200AD blast cleaner .This kind of pre-treatment increases the contact area between the adhesives and the adherends resulting in a better interaction between these two components [28].

The next stage was a degreasing process with acetone; aluminium tabs and composite specimens were placed into a Pyrex vessel filled with acetone and exposed to ultrasound for 10 minutes. The ultrasonic bath used was a Decon FS200b. This process was repeated twice in order to fully remove any particulates from the surfaces before the priming stage. At this stage, a thin film of BR127 primer was applied to the bond area and dried for 30 min at room temperature. Following drying, the plates were placed in a Gallenkamp oven and cured at 120°C for 1 hour. A sheet of FM 73M adhesive supplied by Cytec Ltd was cut into pieces 12.5mm x 15mm. One piece of adhesive was placed to overlap between the adherends for each sample, and any excess adhesive was cut off. The bonding procedure was achieved by fixing the adherends using clamps and curing for 60 min at 120°C.

## 3.3 Specimen Manufacture

Two different types of configurations were used:

- Izod impact fatigue test (IIFT) specimens
- Tensile impact fatigue test (TIFT) specimens

### 3.3.1 Izod Impact Fatigue Test Specimens

The IIFT specimens used in this research served the purpose of evaluating the impact toughness of CFRP under fatigue conditions and the effect of specimen thickness on fatigue life. The two sets of samples were manufactured in conformity with British standard (BS EN ISO 180:1996) and were termed Group A and B, as shown in

Table 3.4.The samples, shown schematically, in Figure 3.1, were notched using a single-tooth carbide cutter with a slow cutter speed, fast feed rate and the use of coolant in order to avoid thermal damage to the sample. Notches of 2 and 6mm depth were cut into the 1mm thick specimens (8 in total) and 4mm thick (16 in total) specimens respectively. In the Izod test samples must have a 45° V notch in the middle of the sample length and the hammer must strike 22 mm above the notch.

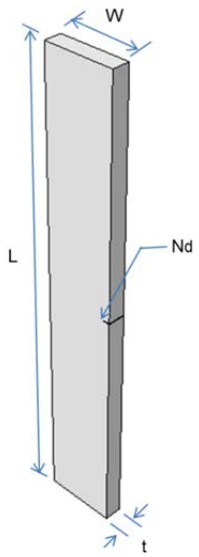


Figure 3.1 Schematic of the IIFT specimen where L is the length, W is the width and t is the thickness.

Table 3.4 IIFT specimen configurations all dimensions in mm

| | Width (W) | Length(L) | Thickness (t) | Notch depth ($N_d$) |
|---|---|---|---|---|
| **GROUP A** | 10 | 80 | 1 | 2 |
| **GROUP B** | 10 | 80 | 4 | 6 |

### 3.3.2 Tensile Impact Fatigue Test Specimens

The TIFT specimens were used in this research to analyse fatigue crack growth. The specimen configuration, as shown in Figure 3.2, was adopted in conformity with BS EN ISO8256:2004, with modification to fit the tensile impact machine shown in Figure 3.7.

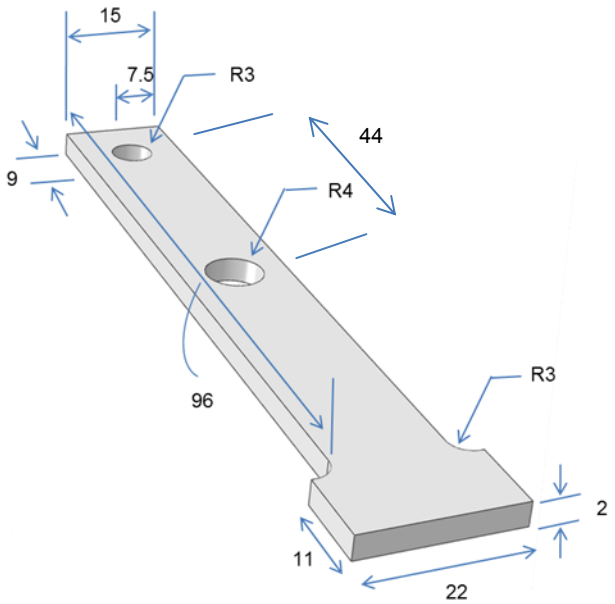


Figure 3.2 Schematic and dimensions of TIFT specimens, units in mm

Initially the specimens did not contain a centrally located hole and evaluation of fatigue life was impossible as the specimen remained relatively undamaged up to 100,000 cycles when impacted with 1J. The decision to introduce a hole rather than

a notch or a slit, was because this is a more controllable parameter and has a more direct industrial significance, e.g. in bolted CFRP structures. The reason for the diameter selected was 2-fold. First, in industry a common range for drilling in composites is 2-12 mm. Secondly, the specimen should be more prone to damage than the end tab area, which contains a hole of 6mm. Holes were drilled using a carbide tip tool at feed rates of 100mm/min and spindle speed of 3000 RPM which results in the lowest thrust force for drilling, minimising damage around the drilled hole [115]. The specimen was clamped during drilling to avoid oscillations that could lead to the generation of further damage in the CFRP around the hole.

## 3.4 Experimental Test Procedures

The following sections describe the mechanical tests conducted on the CFRP specimens. The tests can be divided as follows:

- Impact fatigue tests
  - Izod test (IIFT)
  - Tensile test (TIFT)

### 3.4.2 Izod Impact Fatigue Test

The Izod test is a single impact test used to measure the impact resistance of a material. In that test the reduction in kinetic energy of a swinging pendulum is equated to the energy required to completely break a notched sample of standard dimensions. The notch in the Izod specimen serves to concentrate the stress, attenuate plastic deformation, and direct the fracture behind the notch. Scatter in energy-to-break is thus reduced. Izod impact strength is expressed in $kJ/m^2$or kJ/m depending on the standards followed. For example if the ISO standards are used then the results are reported in terms of energy absorbed per unit cross-sectional area under the notch while if the ASTM standards are used the energy absorbed per unit of specimen width is utilised. In either case, the higher the resulting number, the tougher the material. Brittle materials such as composites tend to exhibit low impact energy due to their relatively low energy absorption capabilities. The Izod impact fatigue test utilises the same principles as the Izod with the difference that is concentrating on the fatigue response and progressive damage accumulation rather than the energy absorbing capability during a single impact. Testing involves a specimen clamped into the test fixture with the notched side facing the striking edge of the pendulum, as shown in

Figure 3.3.

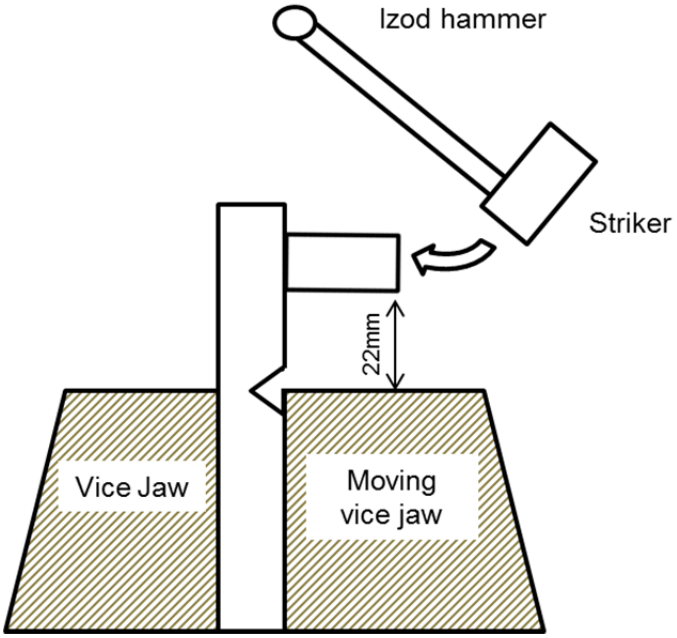


Figure 3.3 Impact test set-up indicating the position of the specimen in the vice, the motion of the Izod hammer and the impact point

In this work a calibrated impact hammer with mass of 0.334 kg and nominal length of 0.3268 m was used. The pendulum hammer was released from a pre-selected initial angle in the range of 0-150° which corresponds to a potential energy in the range of 0-2J and velocity between 0-3.46m/s. The IIFT were carried out using a modified CEAST Resil impactor, which is shown in

Figure 3.4. The specimen is supported at one end by an instrumented vice and its opposite end is struck repeatedly by a controlled pendulum hammer, with the hammer being caught and returned to the same starting position after each impact. The impact of the pendulum hammer in the specimen produces a flexural loading over a period of 6-7 ms and the period between the impacts is approximately 15s.

The evolution of force, displacement and the energy during each impact can be monitored at 5μs intervals and up to 8000 points can be stored for each impact. In order to decrease the data noise a 1 KHz filter can be used. The amplified and filtered data is downloaded to a computer as magnitudes of force and time and this data is then used to calculate velocity, V, displacement, d, and absorbed energy, E, for each impact, as indicated in Figure 3.5.

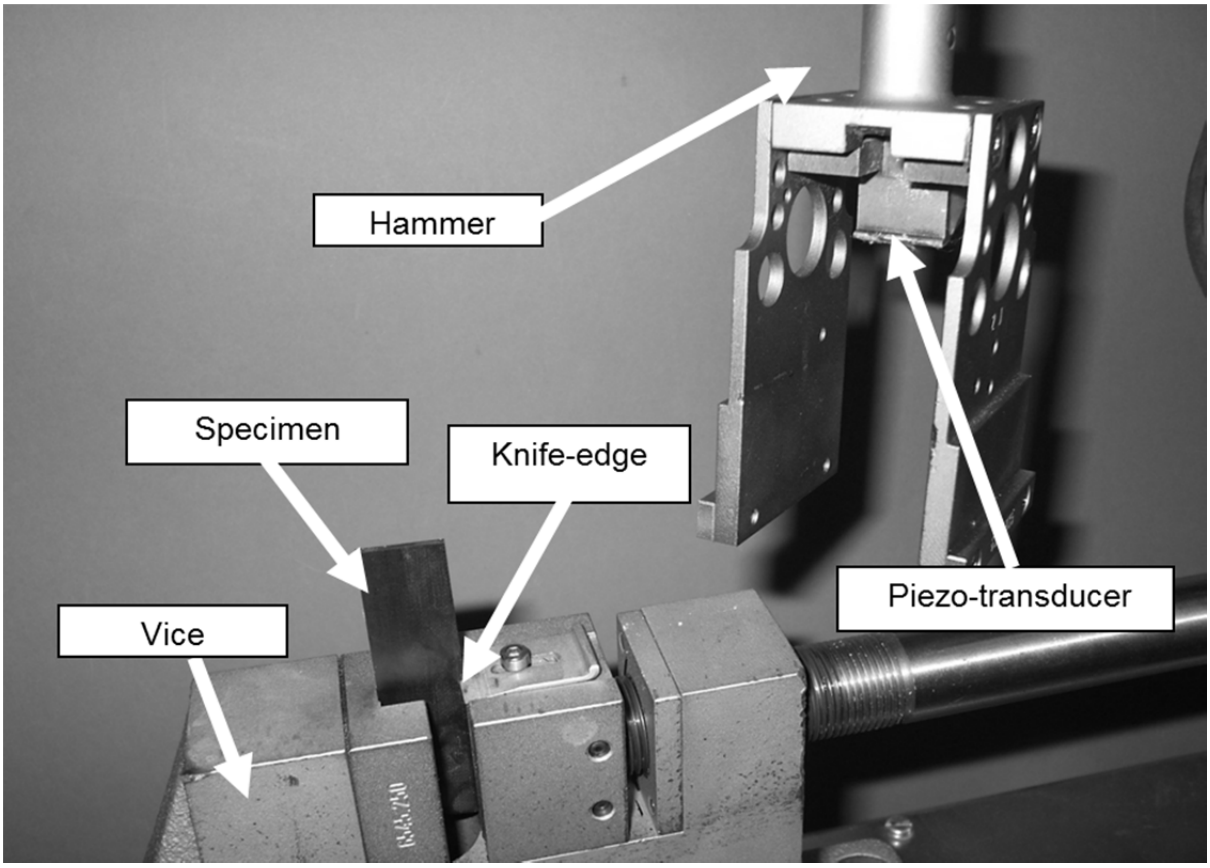


Figure 3.4 Izod test configuration during testing

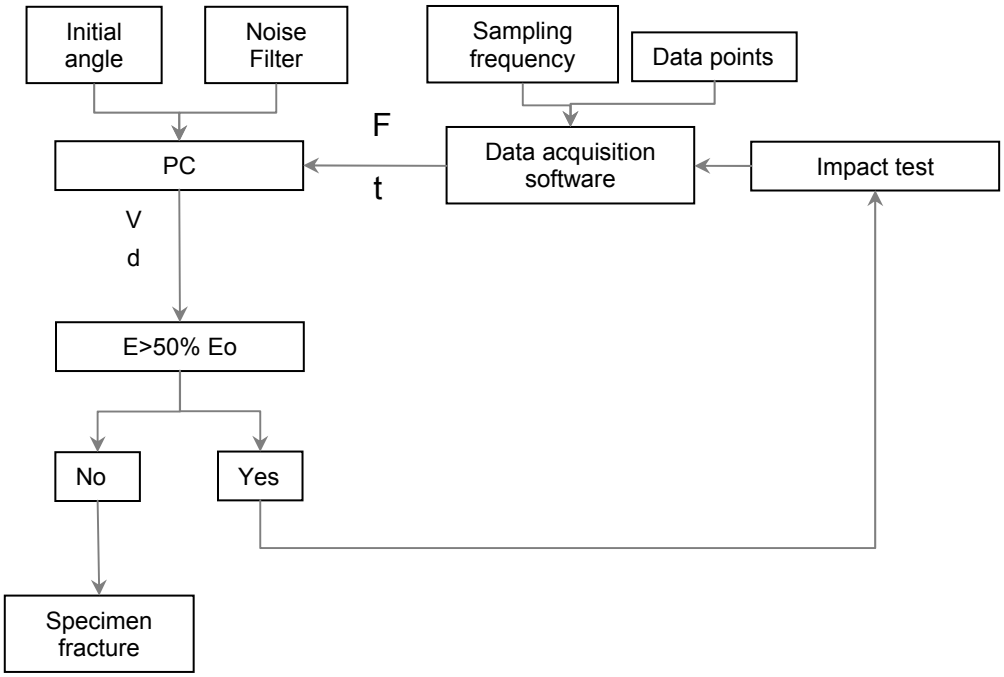


Figure 3.5 Data acquisition procedure during testing

Initially, the velocity (V) is calculated based on the initial/previous velocity, time difference $\Delta t$, the mass of the pendulum (m) and the acceleration of gravity (g).
The relation that describes the above is:

$$V_i=V_{i-1}-\Delta t\left(\frac{F_{i-1}+F_i}{2m}-g\right) \quad (3.1)$$

where F in the impact force which the pendulum strikes the specimen.
Similarly, displacement of the specimen during impact (d) and impact energy (E) are given by:

$$d_i=d_{i-1}+\frac{\Delta t}{2}(V_{i-1}+V_i) \quad (3.2)$$

$$E_i=E_{i-1}+\frac{\Delta t}{2}[(FV)_{i-1}+(FV)_i] \quad (3.3)$$

where i is the surrent state of measurement and i-1 corresponds to the previous measurement.

### 3.4.3 Tensile Impact Fatigue Test

The TIFT used for our experiments utilises a CEAST RESIL impactor which differs from the Izod impactor by having 2 impact points. The basis of this method is that a specimen is supported at one end in a vice and its opposite end is struck repeatedly by a controlled pendulum hammer, resulting in a dynamic uniaxial tensile load. The specimen is clamped at one end to a specimen support using bolts. A load cell is also rigidly fixed to this support. At the free end of the specimen a special impact block is fixed. This block consists of a two plates held together by bolts. A firm connection between the specimen and impact block is obtained by compression of the plates. The impact block is struck by a pendulum hammer at the location indicated in Figure 3.6. The experimental set up can be seen in Figure 3.7.

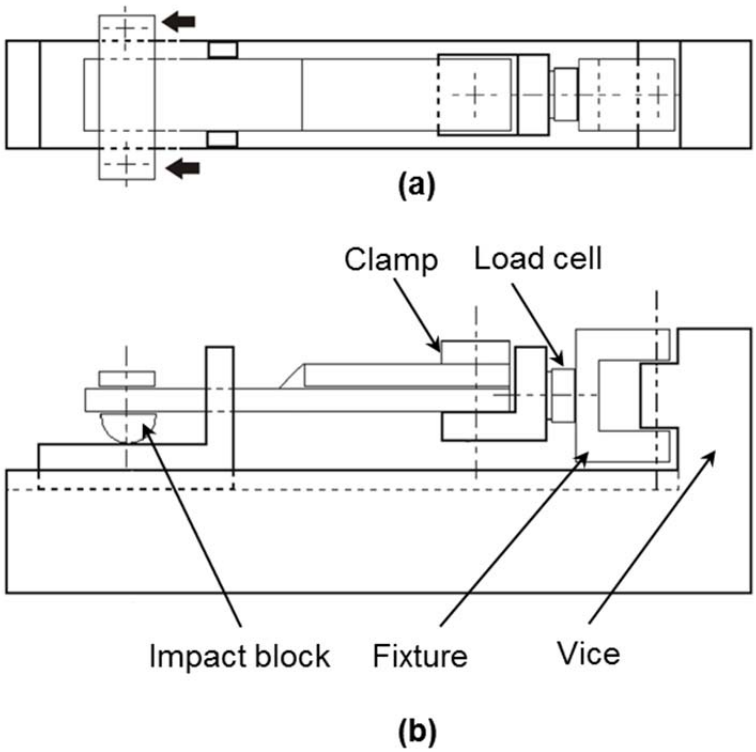


Figure 3.6 Schematic of specimen fixture for impact fatigue. (a) Top view, arrows denote impact loading direction, (b) Side view

The pendulum hammer is released from a pre-selected initial angle in the range of 0-150° which corresponds to a potential energy in the range of 0-4 J and velocity between 0-3.7 m/s. The impact of the pendulum hammer produces a tensile load in the specimen over a period of 6-7ms. The period between the impacts is approximately 15 s. The evolution of force during each impact can be monitored for 9 ms with up to 8000 data points for each impact. The amplified and filtered data are then downloaded to a computer as magnitudes of force and time and this data is then used to calculate velocity V, displacement, d, and energy E, for each impact. In our experiments the specimens were impacted at 1J, which corresponds to a hammer velocity of 1.48m/s.

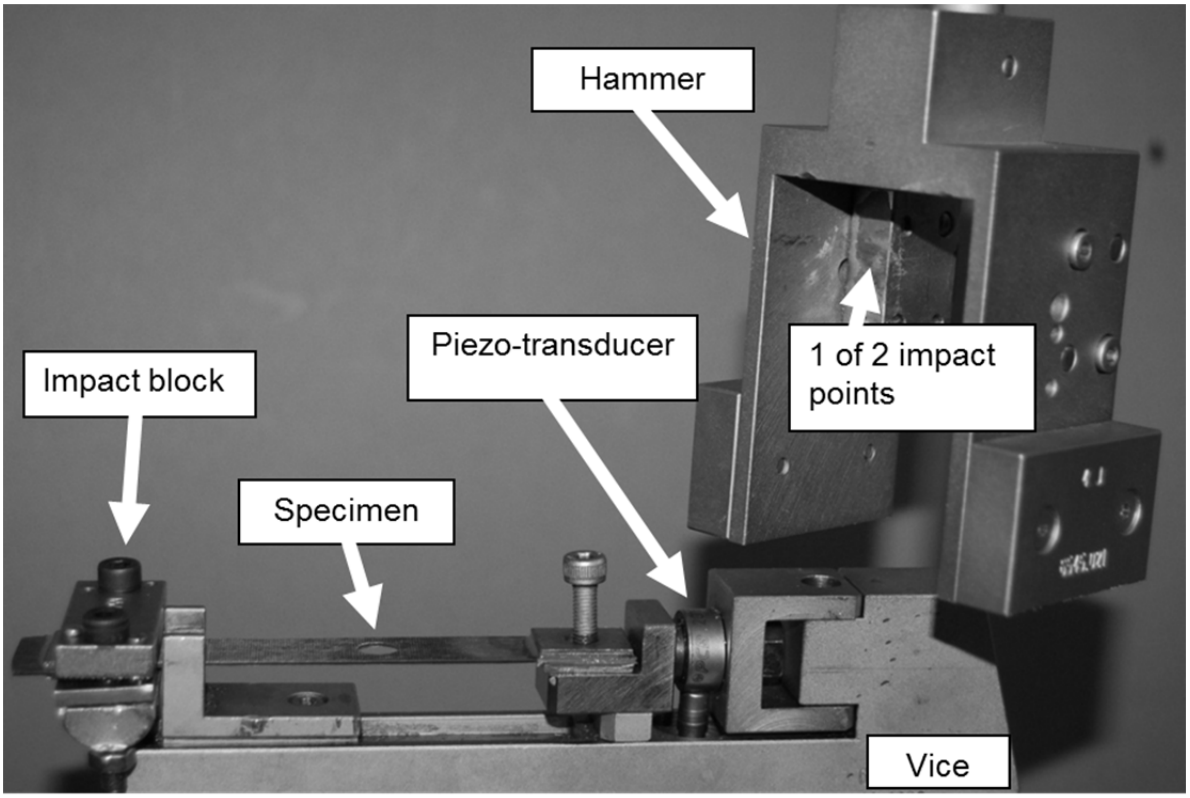


Figure 3.7 Experimental set-up highlighting the impact points and impact block

### 3.4.4 X-ray Micro-Computer Tomography

Non-destructive testing (NDT) is conducted both throughout the production process and the ultimate use of the composite for quality control purposes. Techniques such as ultrasounds, acoustic emission, resonant frequency, piezoelectric paint sensors

and light microscopy are amongst those that can be used to identify fibre pull-out, delamination and other damage modes.

X-ray micro-computer tomography (MCT) is a useful tool for the characterisation of internal flaws. It allows full insight into the inside of materials and structures. The principle of the technique is fundamentally very straightforward and is illustrated in Figure 3.8.

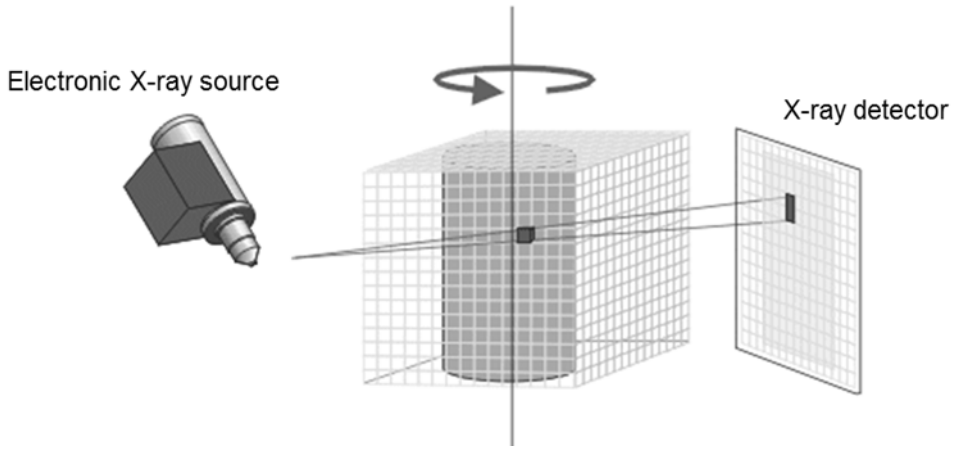


Figure 3.8 Schematic of MCT procedure [116]

The object is placed on a rotary stage between the X-ray source and detector. A high-precision microfocus source generates the X-ray radiation which is focused at a point within the sample. A digital flat panel detector captures a 2D image of the X-rays patterns that have passed through the specimen, showing different shades of gray depending on material and geometry. Thicker of denser material translate into darker areas than thin or light materials [5].

X-ray has been applied to date, mostly to metal-matrix and ceramic-matrix composites under drop-weight tests [117-123]. Some work has been carried with polymer matrix composites to characterise impact damage; investigating the fibre fracture and delamination associated with penetration tests [124-127].

In the most recent and relevant work of [124] unotched CFRP thermoplastic composites were subjected to repeated Izod impact testing and damage progression was evaluated by means of NDT. The NDT radiographs revealed successfully the

damage evolution, at frequent intervals, against the number impacts to fracture. Three distinct zones were identified: fibre micro buckling and shear fracture of fibres (1st zone), development of delaminations and matrix deformations (2nd zone), further development of delaminations and fibre rupture especially in tensile area (zone).

In our X-ray micro-CT measurements were performed using an XT H 225 X-ray and CT inspection system supplied from Nikon metrology instruments**.** The system consists of a 1-dimensional x-ray detector that captures the 2-dimensional cross-sections of the object projected from an electronic x-ray source as shown in Figure 3.8. The source is a sealed X-ray tube operating at 25–220 kV with 3 µm spot size. Data were collected at 70kV and 80µA. An object manipulator with two translations and one rotation facilitates rotating the sample for acquisition of tomographic data, raising/lowering the sample to select a region of interest, and translating along the optical axis to adjust the magnification. For 3-D reconstruction, transmission X-ray images were acquired from 3600 rotation views over 360° of rotation (0.1° rotation step). Following acquisition, a software program builds a 3D volume dataset by 'stacking' the individual slices one on top of the other.

The quantification of damage required the use of add on modules in the post processing procedure. The crack detection module is based on an existing region of interest (ROI).This selection mode requires an existing ROI describing one or more (small) “seed areas” inside the crack to be detected. Based upon this region, the crack detection will use one of the specialized region growing methods. The region growing is always three-dimensional and consists of two steps.

• Checking if each individual voxel is part of a defect and then create groups of connected defect points.

• Checking if each group of defect points fits the parameters specified by the user such as the following algorithms.

- Only threshold

  Only defects that match the size specifications and values below a specified gray value threshold are considered

- Default

Accounting for gray value variations

- Custom

Defect analysis that is based on a manually defined ROI

When crack detection is active analysis information on each defect may contain information like position, size, surface and volume of each individual defect as well as minimum, maximum and mean gray value within the defect. Figure 3.9 illustrates the acquisition of quantitative data.

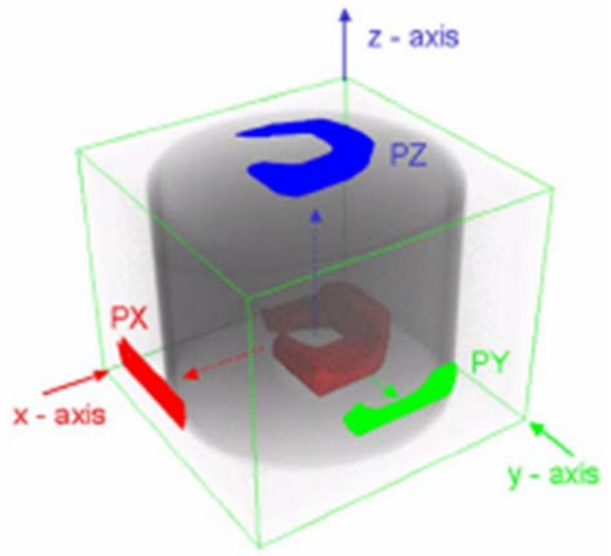


Figure 3.9 Surface area of the defect‘s shape projected along the axes o the currently selected coordinate system [116]

## 3.5 Summary

This chapter has described the experimental materials and techniques used to prepare and test CFRP specimens under various loading conditions and characterised the ensuing damage in tested samples.

# Chapter 4 Experimental results

## 4.1 Introduction

The main aim of this chapter is to characterise and quantify the response of CFRP specimens when exposed to IF. The chapter deals with a detailed experimental analysis of the behaviour of the Izod and tensile impact fatigue tests. The following sections present the experimental work carried out to obtain the impact fatigue life behaviour for the two different tests. The experimentation was based on the following objectives:

- To study the fatigue life of specimens subjected to IIFT;
- To study the fatigue life of specimens subjected to TIFT;
- To study the stiffness deterioration of specimens under TIFT;
- To determine the repeatability of the fatigue life for both tests;

- To perform a detailed M-XCT study of damage for specimens subjected to IF conditions.

## 4.2 Fatigue Life of Specimens Subjected to Impact Izod Fatigue Test.

The following subsections present the results obtained from subjecting specimens to IIFT. Additionally, the methods that are used to analyse the fatigue life and fatigue damage in the specimens are discussed.

### 4.2.1 Test Results

Izod impact fatigue (IIF) tests were carried out using the modified CEAST RESIL impactor described in Section 3.4. A pendulum hammer that transmits a maximum energy of 2 J was used. Different energy levels were used, in the range from 0.02 J to 2 J. This corresponds to impact speeds varying from 0.31 m/s to 3.46 m/s, respectively. Variations in the initial impact energy and velocity were achieved by changing the initial angle of the hammer. Impact tests were conducted in energy control which means that the applied force is not a directly controllable variable. Impact damage can be characterised by a decrease in impact energy (E) with number of cycles required to failure Nf [25]. The type of failure that defined the end of the test was a complete break through the specimen that separated the specimen into two. An E vs Nf plot for both 4mm and 1mm thick samples is presented in Figure 4.1. The energy lost by the pendulum during the complete rupture of the specimen is mainly the sum of a) the energy to initiate fracture of the specimen, b) the energy to propagate the fracture across the specimen and c) the energy necessary to

completely toss the free end. Unfortunately, the force sensor attached to the Izod hammer returned accurate F vs time data only for very low energies and for few impacts. In others words, for this test the energy absorption history could not be recorded. However, the figure demonstrates a similar trend in the data for the first and second groups of specimens in that there is an approximately linear relationship between E and log Nf. These graphs show that as the impact energy decreases, the number of cycles to failure will increase in a quasi-linear fashion. Additionally it is important to note that in both cases a fatigue limit is not clearly observable. The level of scatter in the results does not vary significantly with different energy levels.

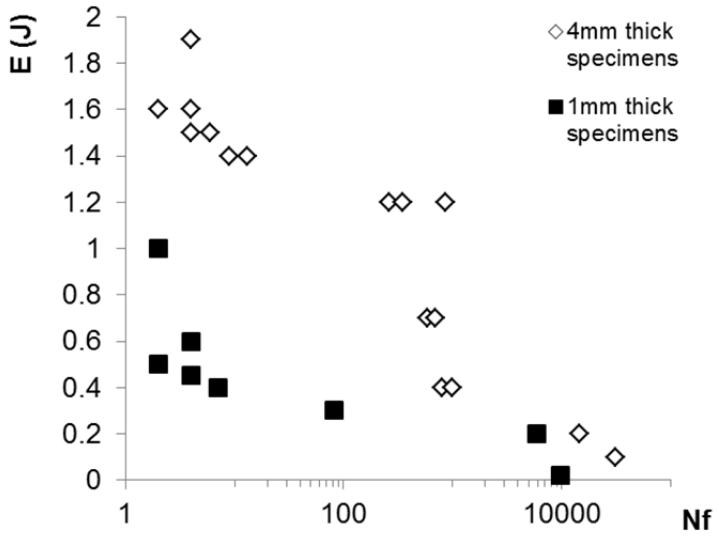


Figure 4.1 Impact energy (E) vs number of of impacts to failure (Nf) during IF in semi logarithmic coordinates

As it has been said two different thicknesses were tried, 4mm and 1mm, with 6mm and 2mm notch radius respectively. Of course, the impact energy associated with a given Nf is significantly lower for the 1mm thick samples than for the 4mm thick samples with the ratio in impact energy being approximately the same as the thickness ratio. However, analysis of the notch sensitivity between the two groups requires normalising the 4mm thick data. This is illustrated in Figure 4.2

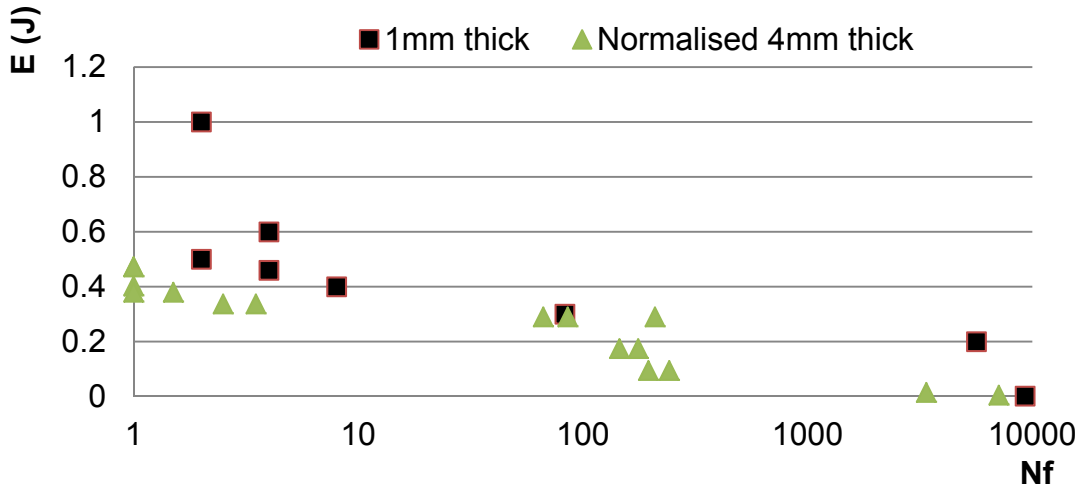


Figure 4.2 Effect of notch sensitivity on the impact life

Although, ideally more points are required, the above graph could be used to describe the effect of the notch sensitivity on impact life, i.e. the variation of absorbed energy as a function of notch radius.

Additionally, the experimental results acquired are re-illustrated and contrasted with the works of [59] in Figure 4.3. In [59] low velocity repeated impacting was carried out on thermoplastic matrix composites up to fracture. An analytical model (Coban model) was fitted describing the IF behaviour of unnotched unidirectional carbon fibre reinforced Polyetherimide (PEI) composites. As seen, up to 0.57 J, the impact numbers up to fracture show a parabolic variation. Lower than this impact energy value, the impact number up to fracture increased. The equation of the impact-fatigue life curve for the Coban model can be expressed as:

$y= 1.2226.10^{12}[e^{(x/-0.02737)}] +90.66.$

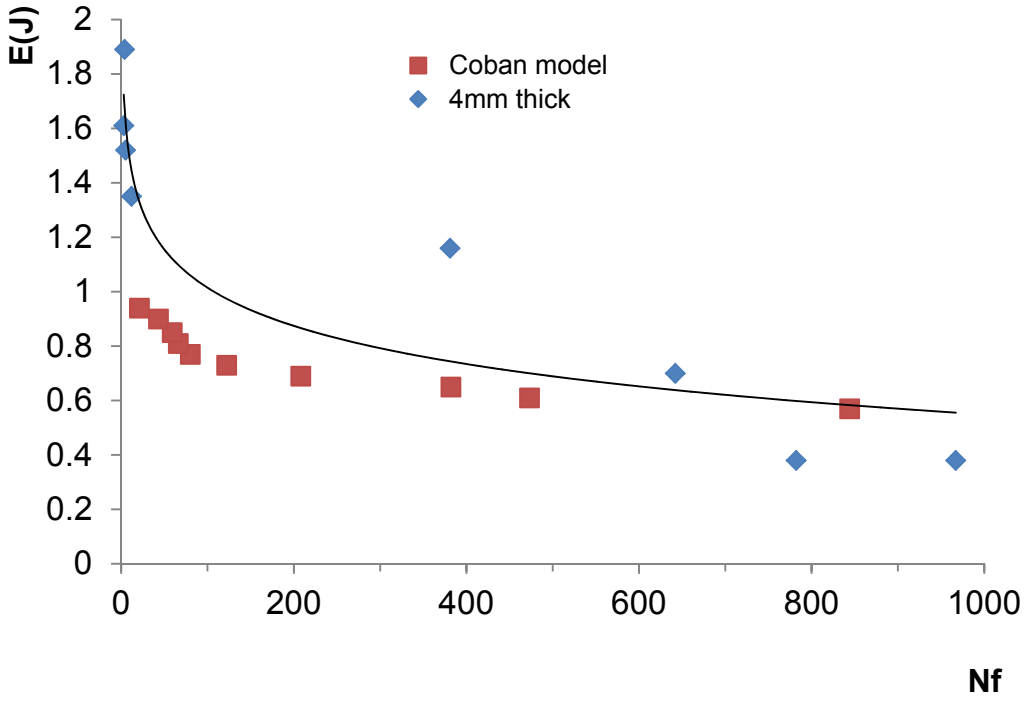


Figure 4.3 Analytical models for repetively impacted unidirectional composites.

In our case, if we called impact energy as ‘‘y” and impact number as ‘‘x” the equation of the impact-fatigue life curve can be expressed as: y=-0.20ln(x) + 1.946. The results have shown that CFRP’s are susceptible to rapid degradation and failure when subject to IF. It is also seen that IF can be characterised for the specific configuration and sample type using E-Nf graphs. Analysis of the evolution of damage in the samples during IF is required to understand the mechanisms of failure. This will be discussed in the following section.

### 4.2.2 Examination of Damaged Surfaces

Studies of specimens tested in IF were performed with a special specimen configuration for μXCT study, since as for accurate resolution of micro cracks the width of the specimen should be limited to 4-5 mm. Furthermore this specimen was notched at 1mm while the length and thickness was kept the same as Group A Table 3.4. The sample was subjected to 250,400 and 600 impacts of 0.02 Joules. It has to be noted that after every set of impacts (250,400 and 600) the specimen was removed and examined. The main μXCT scanning and reconstruction parameters

were the resolution, which was 3.5 μm, and the exposure time, that was kept at 1s. Figure 4.4 shows the dimensions of the specimen as well as the region of interest (ROI) selected for analysis.

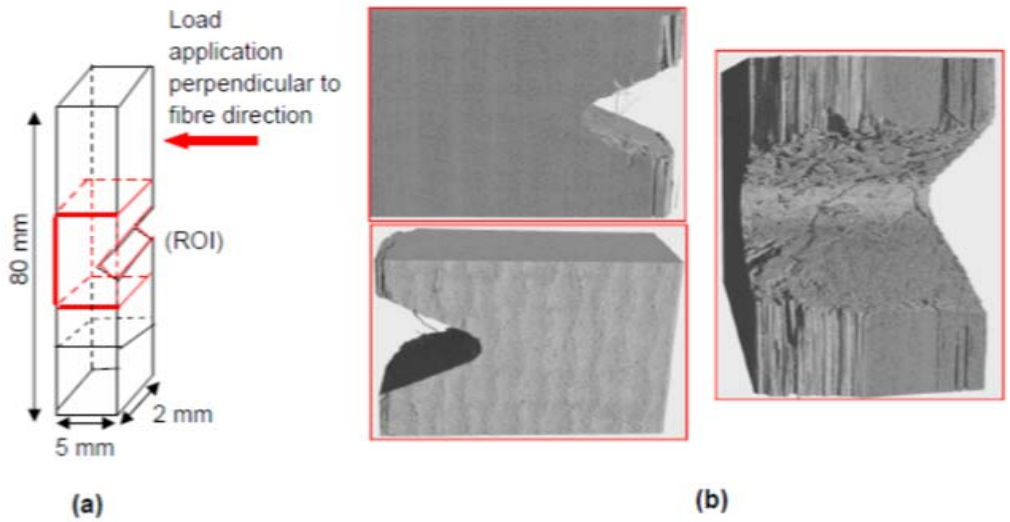


Figure 4.4(a) Specimen schematic highlighting the region of interest (ROI), (b) Side views and front view of the ROI

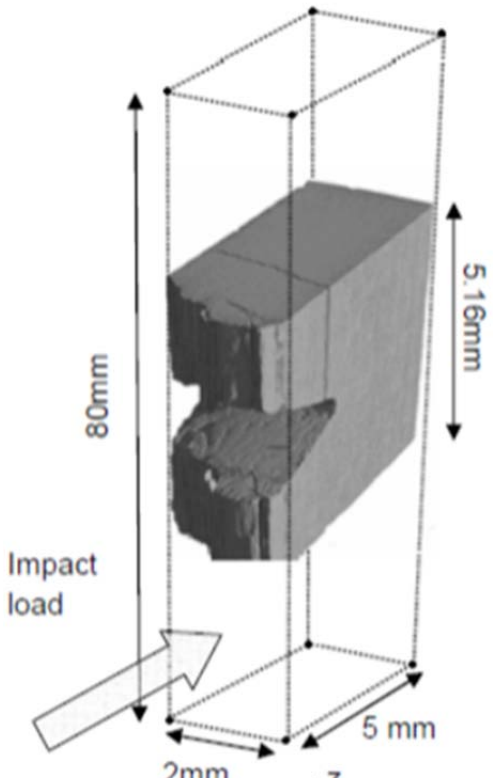


Figure 4.5 ROI schematic of the damaged volume

In Figure 4.4(b) the side and front views of the undamaged specimen from the μXCT are presented. Signs of matrix cracking and fibre pullout are visible at the edges of the sample due to the machining of the notch (front view Figure 4.4b); the cutting plane was perpendicular to the fibre direction. After 250 impacts the specimen was removed from the IF machine and was re-examined. A through thickness view of the damaged specimen at after 600 impacts can be seen in Figure 4.5

Figures 4.6-4.10 show the comparison between undamaged and damaged states of the tested specimen.

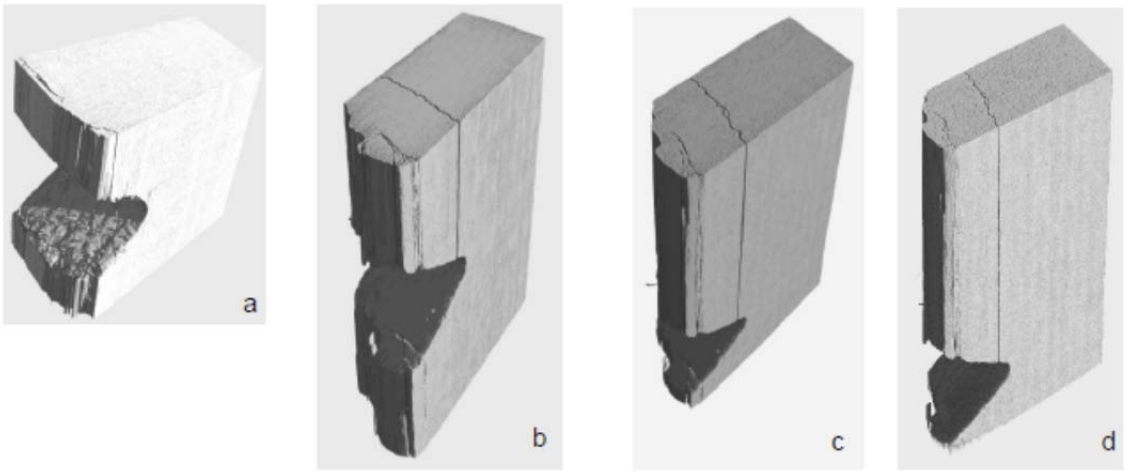


Figure 4.6 Right-side view before testing (a); after 250 impacts (b); after 400 impacts (c) and after 600 impacts (d)

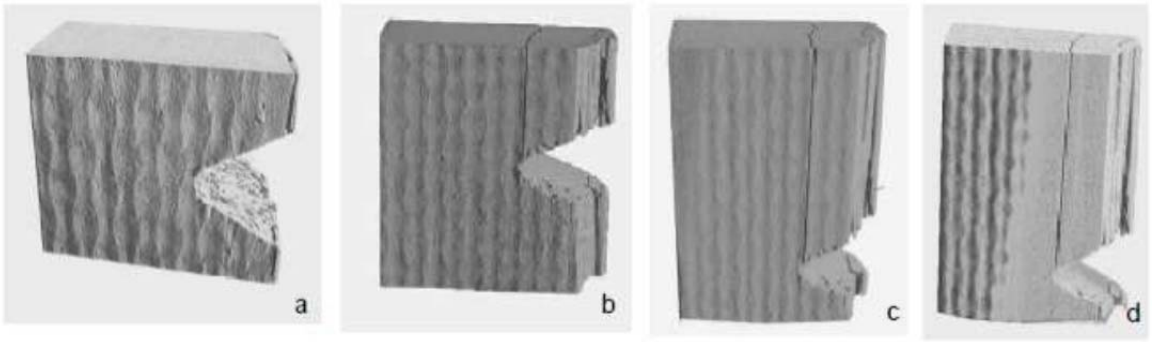


Figure 4.7 Left-side view before testing (a); after 250 impacts (b); after 400 impacts (c) and after 600 impacts (d)

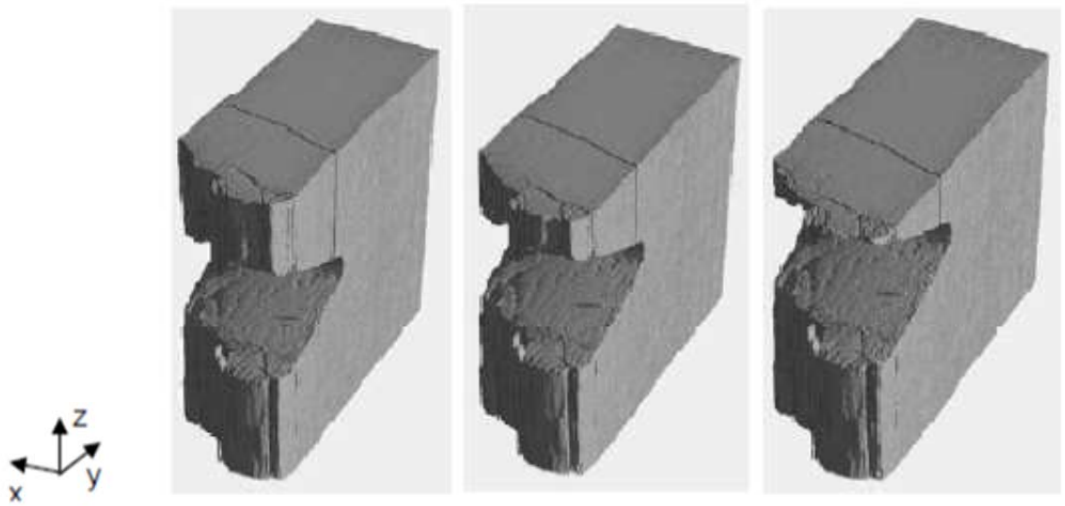


Figure 4.8 Views for successive sectioning along the z axis at 3 intervals of 0.5 mm (after 250 impacts)

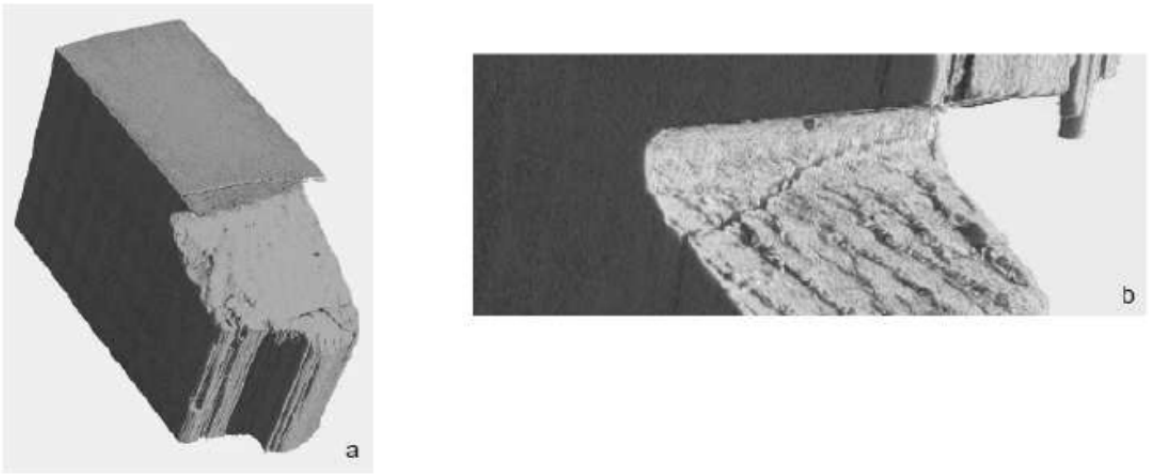


Figure 4.9 Side view indicating the relative positioning of crack (a) and notch and crack intersection with the notch (b)

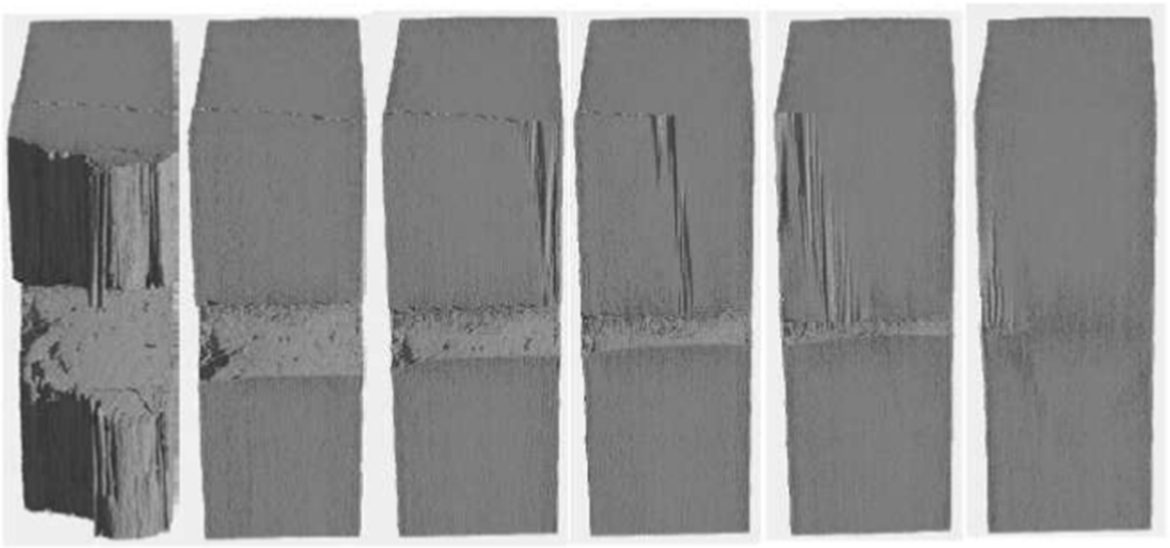

Figure 4.10 Views of successive sectioning at 5 intervals of 0.2mm along the y axis after 250 impacts (Note that the notch depth is 1mm)

A crack can be seen to be growing substantially in the fibre direction and across the sample width. The transition from one side of the specimen to the other can be seen more clearly in Figures 4.8, 4.10. In Figure 4.9 it can be observed that the crack, initially at the root of the notch, grows almost parallel to the notch tip in the x

direction and simultaneously in the z-direction. The damage in the y-direction is illustrated in Figure 4.10 that shows successive sections along this axis.

The most important failure mechanism in composites that is responsible for strength deterioration of a laminate are matrix cracks and delamination. While fibre failure is the ultimate failure mechanism, matrix cracks and delaminations can occur much earlier. Since in the case of a UD composite we deal with only one ply (This assumption lies in the fact that delamination occurs due to stiffness difference between differently oriented plies) it is reasonable to categorise the damage as intralaminar, i.e., internal within the ply. This means that the cracks present after impact are due to matrix cracking and probably, breaking of few fibres. Moreover, it can be said that fibres act as impact wave guides since matrix cracks are propagating initially along the length of the fibres. After presenting the capabilities of Micro-CT in visualising the crack propagation after a series of impacts it is important to quantify this damage. Micro-CT is capable of providing information about the total volume/area of the cracks using a region growing algorithm. This enables quantification of delamination area or the crack distribution. Figures 4.11 to 4.13 present this procedure.

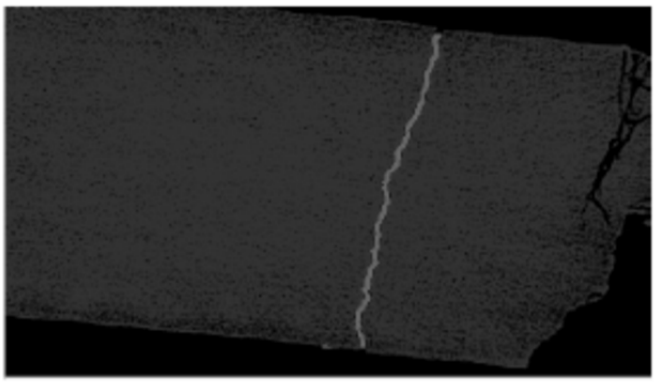

Figure 4.11 Specimen top view highlighting the capabilities of the region growing algorithm to isolate the crack area

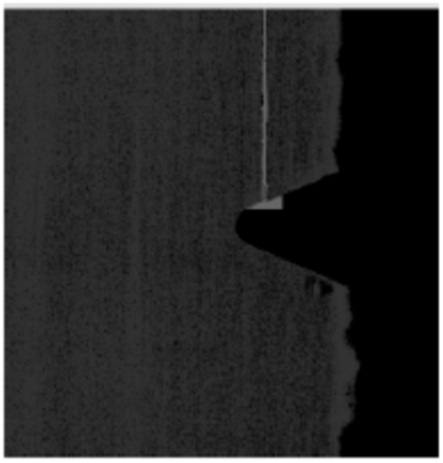

Figure 4.12 Specimen side view highlighting the capabilities of the region growing algorithm to isolate the crack area

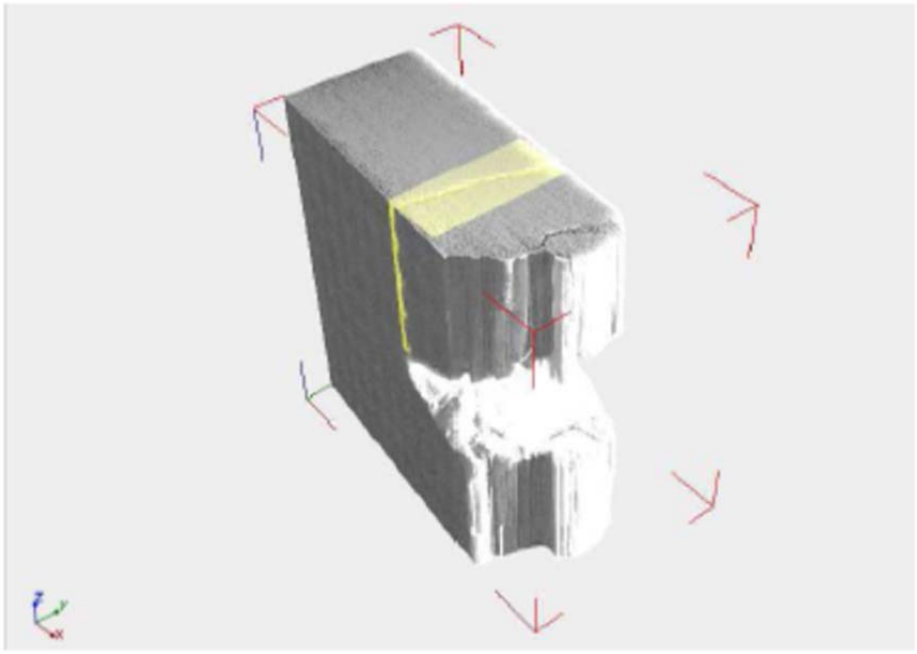

Figure 4.13  Specimen 3-D view highlighting the capabilities of the region growing algorithm to isolate the crack volume

Initially a region of interest is selected in each direction (Figs 4.11, 4.12). Then the whole 3-D profile is constructed as shown in Figure 4.11 and is 'filled' with the region growing algorithm (yellow area). After 'filling' the region of interest, information about the volume/area of the cracks can be obtained by the histogram of the region based on the grey level distribution. In our case the total crack area measured was 3 $\mu m^2$

## 4.3 Fatigue Life of Specimens Subjected to Tensile Impact Fatigue Test.

The following subsections present the results obtained from testing CFRP samples in a TIFT. Furthermore the methods that are used for to analyse the fatigue life and the fatigue damage in the 2mm and 1mm specimens are presented.

### 4.3.1 2mm Thick Specimens ($[0_4/90_4]s$)

These specimens were impacted 33000 times, to the state where intraply damage occurred and the F, t data were recorded, as shown in Figure 4.14. The force vs time response was selected at the initial life of the specimen (10 impacts), half life (16500 impacts), and 33000 impacts (total life).

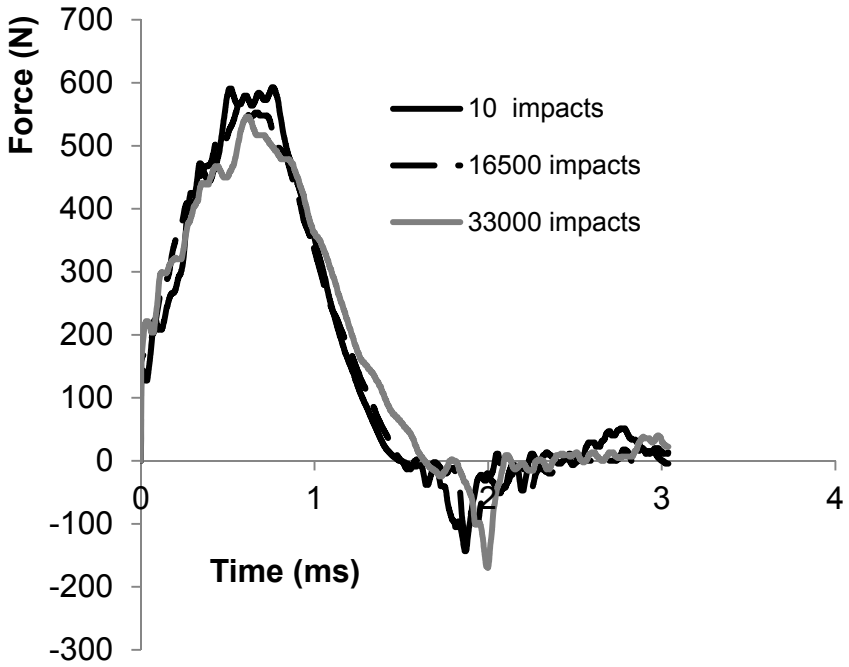


Figure 4.14 Force vs time response in various cycles of impact fatigue life

From the above graph it can be seen that the force magnitude remains reasonably unaltered between the initial stage and half life. Moreover, at total life there appears to be an increase in time and decrease in force, signs that indicate damage in the sample. This is investigated further in Figure 4.15 and in Figure 4.17. In Figure 4.15 the maximum force as a function of number of cycles can be seen for the impact fatigue test at energy level of 1 Joule. Additionally it has to be noted that data acquired up to 2000 impacts are controversial since the specimen being at the stiffest stage presented some rotation during impacting.

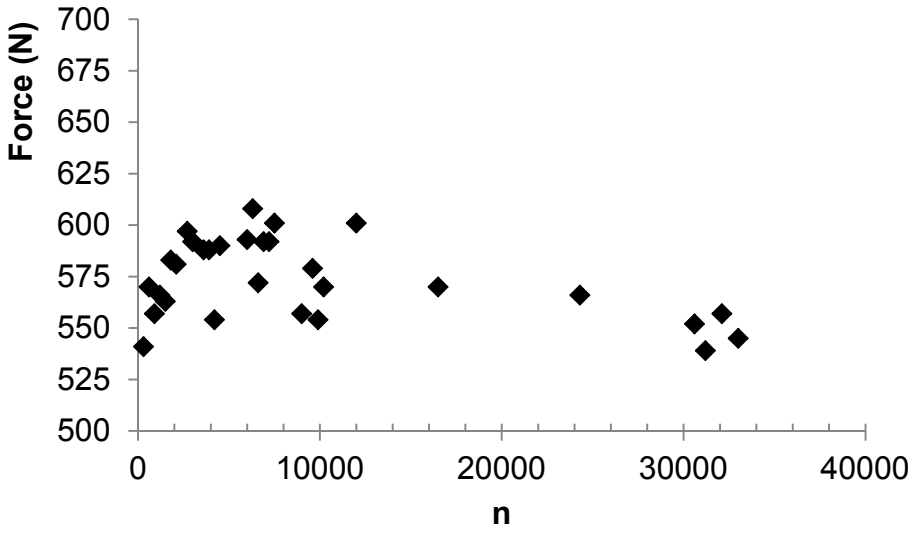


Figure 4.15 Maximum force response as a function of number of cycles (n)

At this point, is important to define the time that will be used as an additional characterising parameter. In order to model the deterioration of mechanical properties under conditions of IF the loading time was investigated. Different definitions of loading time exist [37], [25]. The parameter T' is defined as the time measured from the initial impact point until the point where the force starts decreasing after it has attained the maximum value.The parameter T'' refers to the period where maximum force is applied.In this work the $T_F$will be used because it is presenting a clear trend as seen in Figure 4.16.

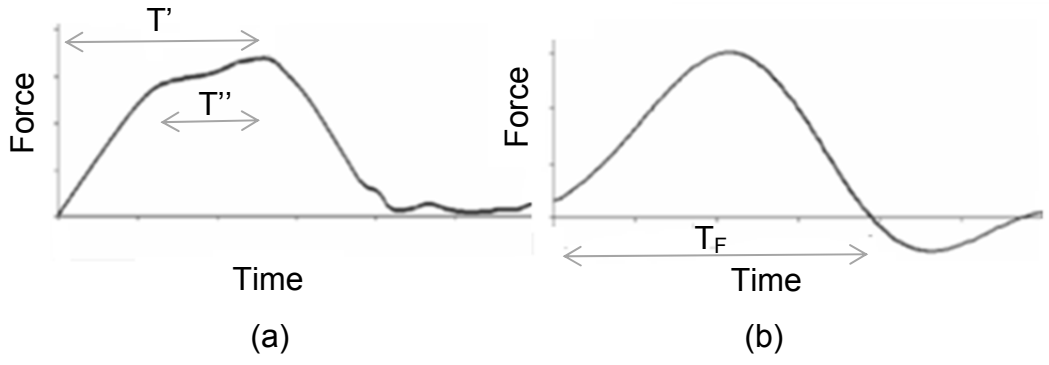


Figure 4.16 Definitions of loading time in Tanaka's model [37] (a) and in the current model (b)

The loading time ($T_F$) response shown in Figure 4.17 is more stable throughout the fatigue life span.

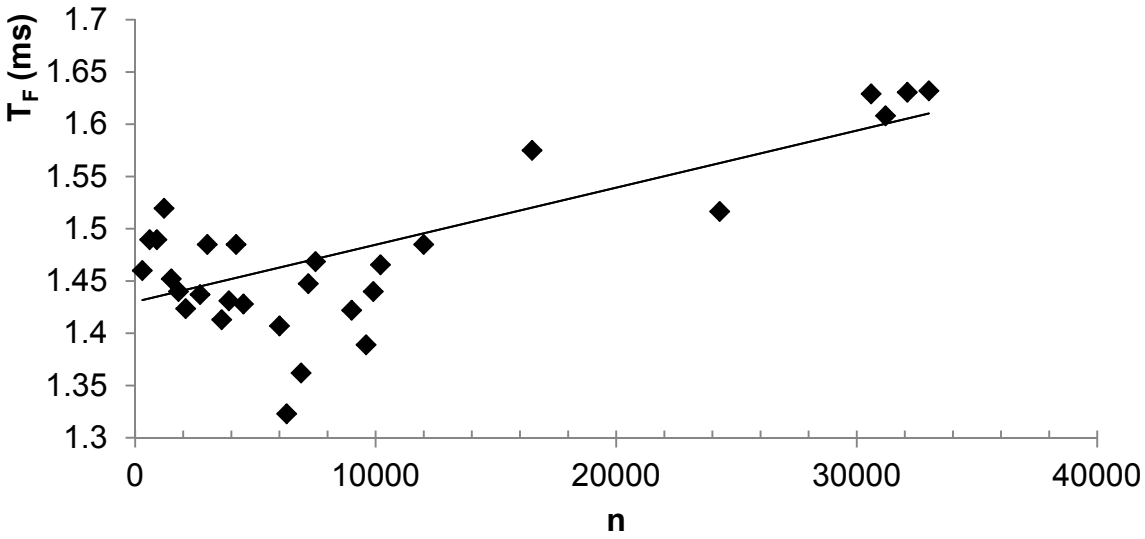


Figure 4.17 Time response as a function of cycles (n)

A typical plot showing the evolution of the $T_F$ parameter during an impact-fatigue test is given in Figure 4.18. In this plot, $T_F$ is normalised with respect to the loading time of the $10^{th}$ impact. The $10^{th}$ impact is used rather than the first in order to avoid possible errors that can be introduced by misalignments between the hammer and the impact block in the beginning of the experiment.

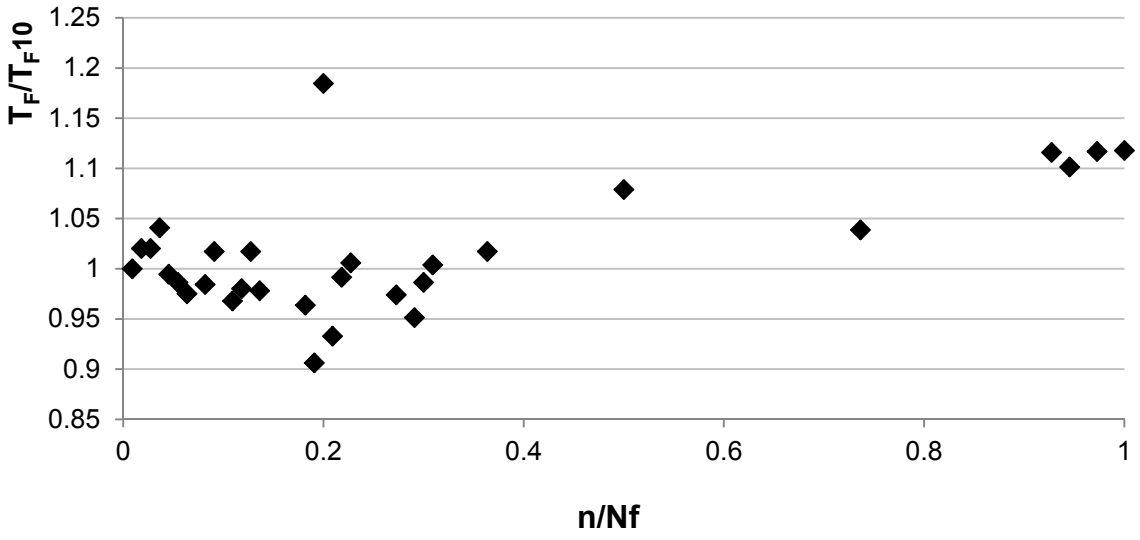


Figure 4.18 Evolution of normalised loading time during IF

It can be seen that the loading time increases towards the end of the fatigue life. Furthermore the variability in the results becomes less prominent towards the end of life which could be reasoned due to the less stiff response of the specimen and therefore fewer oscillations. The maximum force shows a sharp increase initially and then returns to the original value. When compared on a fatigue life spectrum with the time pattern as shown in Figure 4.19 it is presenting an opposite trend but with a higher scatter. With regard to their initial values, it is seen that force is reasonably constant during the test whilst the increase in the loading time is approx. 12%.

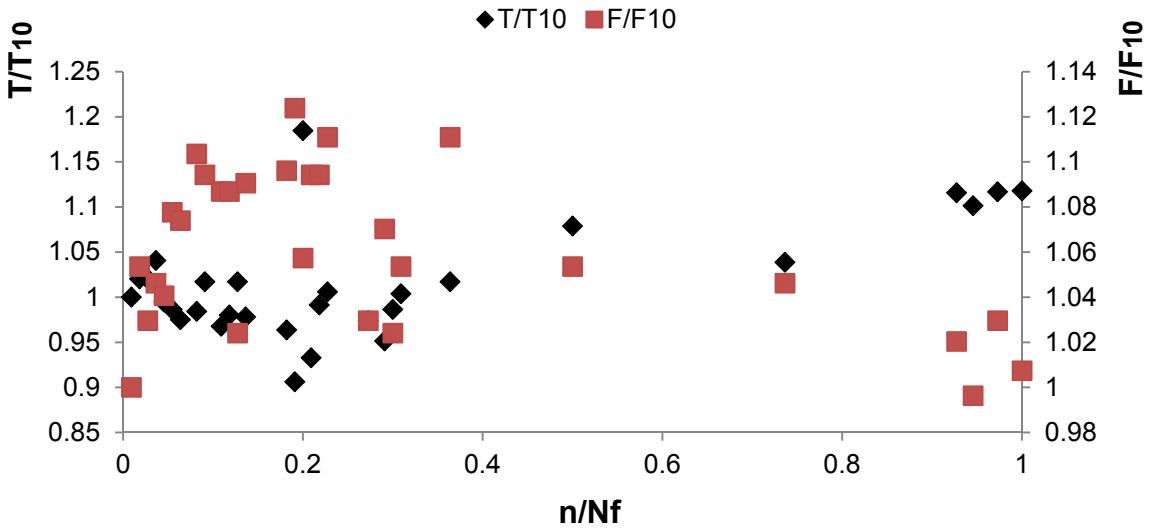


Figure 4.19 Evolution of normalised loading time and normalised maximum force during IF

The area under the force displacement graph indicates the energy absorbed elastically from our specimen for the undamaged stages. As damage progresses, this energy increases as it can be seen Figure 4.20 . Basically, the kinetic energy is converted to strain energy and then since there is no plasticity we deal with energy dissipation from formation of new cracked surfaces.

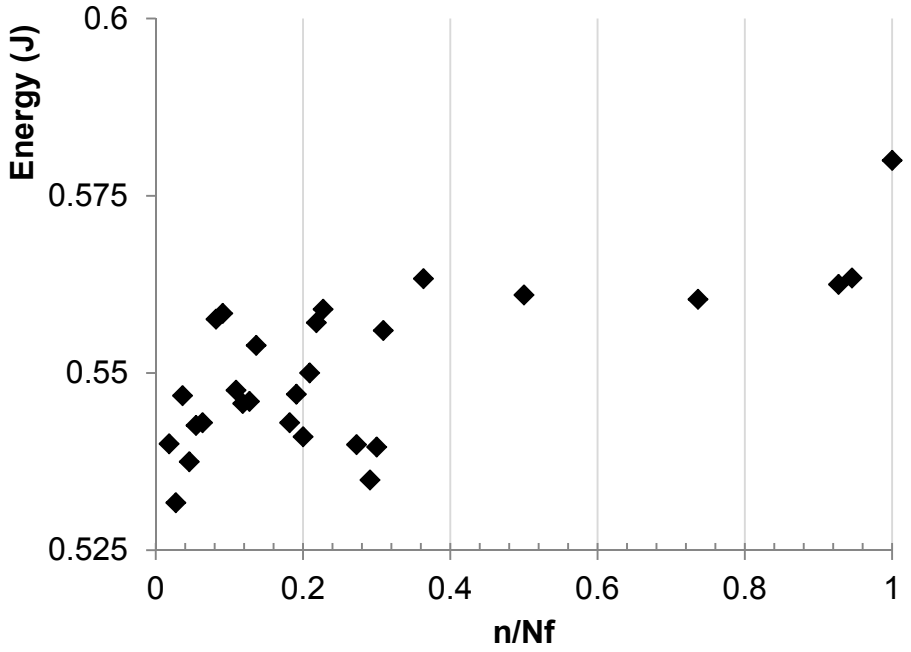


Figure 4.20 Absorbed energy at percentages of fatigue life for TIFT

The experimentation carried out concerning the TIFT involved long fibre carbon specimens. For military and commercial aircrafts, both high modulus and high strength are desirable and carbon fibres posses both of the above. Carbon fibre is preferably used in wing skins as secondary structure attached to other materials by fasteners. As, it has been said, during flight these structure will experience tensile stress wave propagations. These could be generated by either SF or IF.

The in-plane properties such the longitudinal strength and modulus are mainly a function of the fibres but also the matrix is important which is holding the fibres together and provides out-of plane strength. The out-of plane properties involve out of plane strength and modulus, as well as interlaminar strength (ILS) and compressive strength. All the above could be stated as matrix dominated properties. The fatigue process is very complex and involves several damage modes, including fibre/matrix de-bonding matrix cracking, delamination and fibre breaking. By a combination of these processes, widespread damage develops throughout the bulk

of the composite and leads to a permanent degradation in mechanical properties, notably laminate stiffness and residual strength [136].

The experimentation undertaken in this work has not been carried out before for composites. Contrasting it with literature would require literature review in fields such as: Tension-Tension fatigue (T-T) fatigue and possibly monotonic quasistatic loading. Most of the analysis will be concerned in examining our results having as platform work carried out in notched cross-ply carbon fibre composites subjected to T-T SF and quasistatic loading. Moreover the analysis/contrasting will be broken down in 2 sub-sections for the convenience of the reader.

- Residual stiffness/strength observations
- Damage mechanisms and their effect on fatigue life.

Residual stiffness and strength

Residual strength is a term used to assess the maximum stress that a structure can withstand after being fatigued at a specific load level and number of cycles. The residual strength is then contrasted with the strength that the structure possessed at the virgin state and the extend of damage is quantified. Likewise, residual stiffness is the stiffness remained in the component after testing at a certain number of cycles and load level. It has to be noted, that in our case that the maximum load that the notched crossply specimen could withstand was 14kN (Section 6.4-Experimental validation).

From the literature findings [137-140] it was suggested that under tension-tension cyclic loading, crossply carbon fibre composite laminates containing open holes experience an increase in tensile residual strength and a decrease in tensile residual stiffness.

This was reflected in our case in the F-n and T-n graphs. This can be attributed to a phenomenon called notch blunting. Since damage will be concentrated at the notch tip the local stiffness will deteriorate, but also redistribution of stresses ahead of the notch to a more uniform net section will occur. This is because effectiveness of the notch is attenuated by extensive longitudinal splitting that has as a result the increase in the residual strength as well as the fatigue life. In [139] residual stiffness and strength experimentation of 2mm thick centrally notched $[0/90]_4$s AS4/PEED

composite laminates subjected to T-T fatigue was carried out. Specimens contained a 6mm hole and fatigued at a frequency (f=10Hz). Fatigue life of specimens was exceeding 1,000,000 cycles even at 85% of the ultimate tensile strength (UTS). All the residual strengths, at levels of loading 65-90% UTS, were above the virgin state, with the increase, 10-25%, being more marked when cycled at higher stress level instead of larger amount of cycles. To the contrary residual fatigue stiffness was decreasing with increasing number of cycles presenting an initial steep falling, at 10-15% of life and a gentle decrease for the rest of life. This fall was more prominent at higher levels of loading. It was attributed according to the author to breaking of reinforcing fibers which was more serious (10-40%) and concentrated at higher applied stress level for stress levels 65%-85%. In our case a rather gradual decrease of stiffness is presented with higher trends towards the end of life, due to the non-breaking of large number of fibres.

According to [141] the fatigue strength increase presented during the fatigue life depends on the level of test loading. It was found that when fatigued at 55% of the UTS or below the residual strength increases during the early part of life and decrease later. This is due to different distribution of strain around the hole due to damage. As damage grows with number of cycles the strength of the ligaments from each side degrades. The residual axial stiffness was constantly decreasing and it was attributed to the increase of the compliance. This is exactly what happened in our case and was reflected in Figure 4.15. It has to be noted that our UTS translated to energy is 5.25J and we were testing at 1 J.

Fatigue life

Most of the findings compare and contrast the fatigues lives of notched specimens with un-notched. In [139] it was observed that notched 2mm cross-ply specimens, when fatigued under T-T conditions at an applied stress level of 85% of UTS, lasted more than 1,000,000 cycles to the contrary to un-notched where lasted only 5000 cycles .Additionally, in [140] it was revealed that for the same configuration when compared on an S-N graph in un-notched the degradation of the curve is steeper.

Higher fatigue lives tend to be observed when there is extensive longitudinal splitting as observed in [139]. This is not always the case. In [143, 144] where two carbon fibre-epoxy systems were examined under T-T fatigue conditions, the exact

opposite was observed. 2mm thick $[0/90]_4s$ specimens where fatigued containing a 5mm centrally located hole at a frequency of 5Hz. Although the untreated fibre specimens experienced higher degree of damage including longer axial splits, fatigue life was greater for treated fibres ranging from 150% to 400% when fatigue at 80-95% of UTS. It was also recorded that fatigue life at 85% of UTS for the treated was 1,000,000 cycles.

It was concluded that since the fatigue life of $[0/90]_4s$ cross-ply laminates is essentially determined by the 0 degree plies in the laminate, the 0 degree plies are sensitive to the interfacial bonding condition. Specimens with untreated fibres displayed much larger damage zone as a result of weak fibre/matrix interphase while in treated fibre adhesion was better, leading to a brittle fracture, otherwise fibres could be separated by matrix before they fail.

In terms of damage mechanisms 3 damage modes were observed; 0 degree longitudinal splitting target to the hole, 90 degree cracking that emanated from hole edge or longitudinal splits and delaminations. The final failure of the crossply was mainly found to be controlled by the ply failure (splitting, pullout, debonding) of the 0 degree ply. In the above work correlation of the damage mechanisms with the fatigue cycles was not occurred. Additionally, the specimen configuration was sub-laminate and not blocked as in our case. Contrasting our finding with T-T SF of notched blocked cross-ply specimens is not feasible since there is no relevant work in the literature. However, tensile testing of blocked ply sequences of crossly composite laminates has been performed by [142] where open hole tension characteristics of high strength glass and carbon laminates were examined. This paper is entirely static and is a good source for contrasting blocked and sublaminate CFRP sequences in terms of damage mechanisms.

Radiographs of damage progression in CFRP $[90/0]_2s$ and $[90_2/0_2]s$ open hole at percentages of the UTS revealed the following: Axial splits in the 0 degree plies from each side of the hole accompanied by matrix cracks in the 90 plies. With increasing load, the damage zone increased in size but matrix cracking occurred outside the 0 degree splits towards the laminate edge. Delaminations occurred from 75% of Soht with matrix cracking occurring outside the axial splits. The differences observed between the blocked ply and sub-laminates sequences was that the damage zone in sub-laminate is less extensive. The length of the axial splits is higher in blocked specimen because pitting a 90 degree ply between the 0 degree plies tends to arrest

the splits more. It was furthermore displayed that intralaminar damage at the notch tip provides stress relief and stress concentration is reduced since notch geometry changes and this has as a result increase in notched strength.
The above finding agree with our research as well as with the T-T fatigue findings where it was found that the extensive 0 degree splitting was the driving mechanism for the subcritical damage. This is explained explicitly in the following section.

#### 4.3.1.1 Macroscopic Evaluation of Damage in 2mm Specimens

Damage initiation and progression scenarios were assessed in both micro-CT and phenomenological manner using optical microscopy. The virgin and final stage of damage can be seen in Figure 4.21. It has to be noted that the specimen was impacted 33000 times at impact energy of 1J. The damage progression was not acquired using Xray but with direct observation. The following observation were made from this investigation.
More specifically at:

- 4000 impacts, initiation of axial splits occurred;
- 15000 impacts  inner delaminations at the hole edge appeared;
- 18000 impacts  free edge delaminations initiated at the hole level;
- 30000 the free edge delaminations were propagated along the length of the specimen;
- 32700-33000 intraply cracks governed the hole section leading to complete removal of the 90 ply;

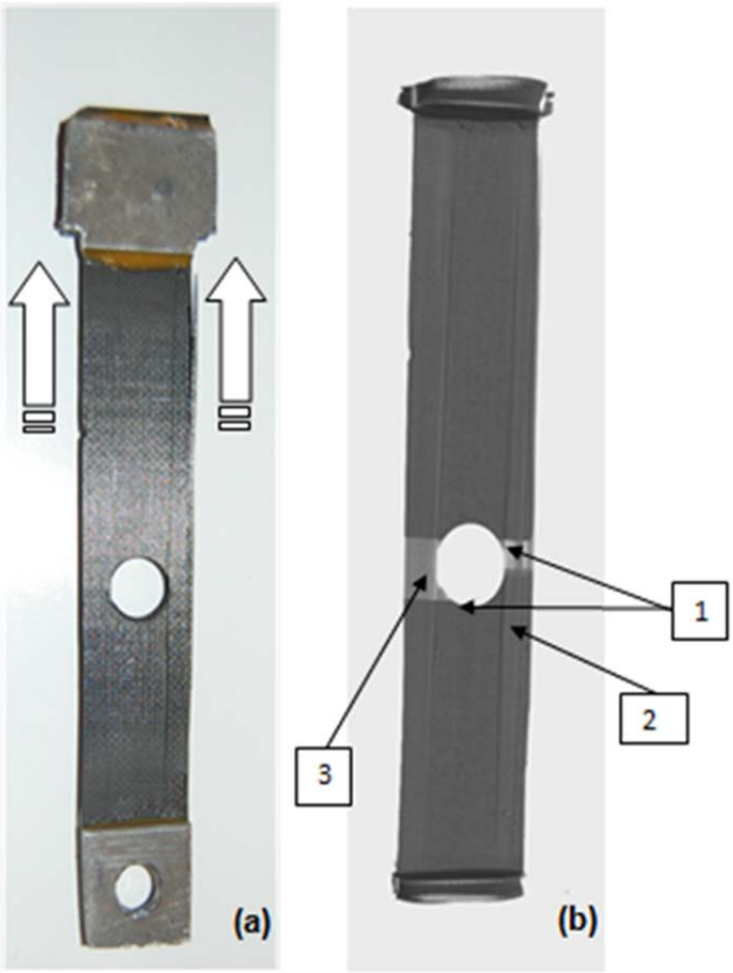


Figure 4.21(a) Specimen with arrows indicating the direction of loading, (b) Semitransparent Xray front view of the whole specimen at the final stage of damage.

The above observations could be grouped in 3 stages as shown in Figure 4.21

1. Isolated damage at the hole edge due to matrix cracking in the 90 degree plies. The above was accompanied by inner delamination at the interfaces at 45,-45 degrees from the centre of the hole that propagated towards the middle of the hole in a clockwise manner. Such delamination occurred as a result of free edges and matrix cracks produced by high interlaminar normal and shear stress that occur at that region.

2. Almost simultaneously generation of 0 degree splits occurred that increased in length in either way but always adjacent to the hole with increasing number of impacts.

3. Damage propagated across the width of the specimen in the form of delamination. As loading continued delamination at the hole and specimen free edge propagated towards each other. When they became close enough delamination through the whole specimen width occurred. Final catastrophic failure occurred when intraply matrix cracks propagated fully through the thickness and width of the hole area which has as a result the complete removal of 90 ply at the hole as shown in Figure 4.21

### 4.3.2 1mm Thick Specimens ($[0_2/90_2]s$) -Reproducibility of Results

In order to reproduce the results obtained for the 2mm thick specimen and also have a parametric study on the effect of thickness on the fatigue life, the second round of experiments involved specimens of the same balanced layup but with half the number of plies. In these samples the magnitude of the force at the final stages of damage was greater than in the 2mm samples, as seen in Figure 4.22.

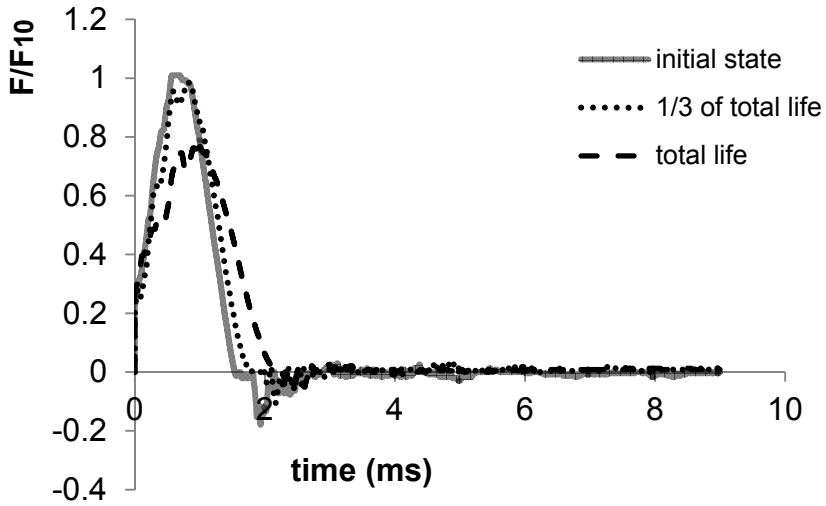


Figure 4.22 Force vs time response in various cycles of impact fatigue life

This load drop causes the residual stiffness to drop by 50%. This is shown in Figure 4.23. The stiffness data were acquired by monitoring the instantaneous force and displacement and sequently dividing the reaction force with the displacement. Three specimens were tested, specimens 1-3. Furthermore, the stiffness value has been normalised with the stiffness of the $10^{th}$ impact $K_{10}$. Although this initially was perceived as an important element that could be used as damage parameter it was contradicting with relevant literature review and the previous results. More specifically according to [8] under tension the Young's modulus does not reduce significantly in crossply laminates but only the Poisons ratio does. In other words it was proven that the in-plane properties present a maximum of 10% decrease. The reason for this load drop could be attributed to the excessive bending effect that the 1mm specimen possessed due to the impact block being too heavy for that thickness. This bending factor could be a separate study. However, it was superimposed to the IF loading in the same manner for all the specimens. The effect on the fatigue life can be seen in

Figure 4.24.

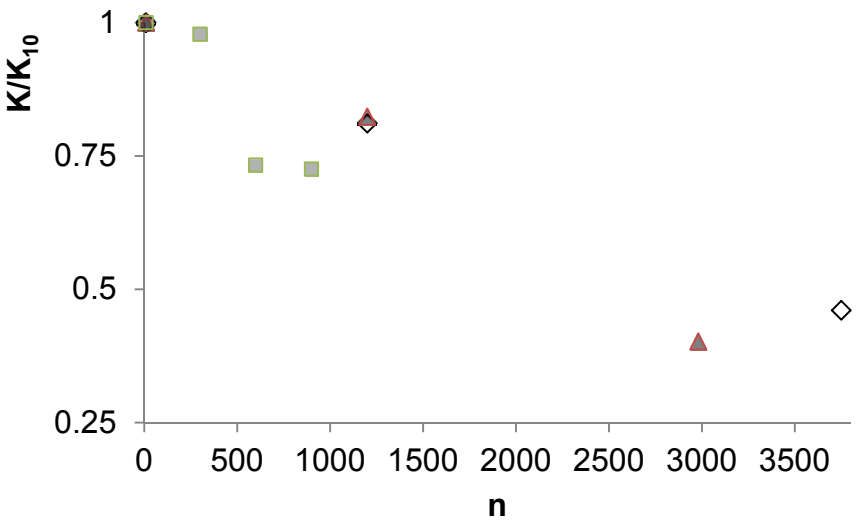


Figure 4.23 Deterioration of K with respect to number of cycles

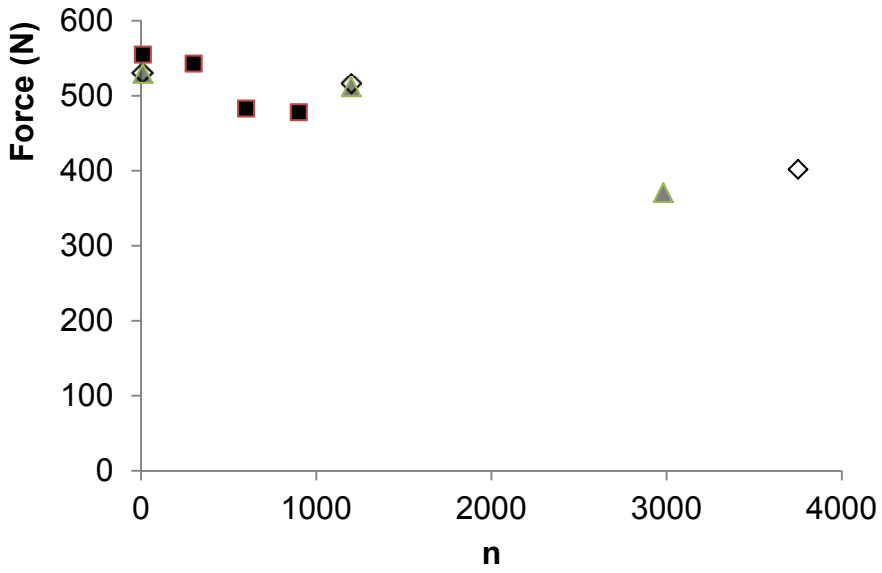


Figure 4.24 Deterioration of force response as a function of number of cycles

The preliminary objective at this point was to correlate the changes in stiffness and force with the observed damage in the sample. These two figures indicate that the studied response is changing as a function of damage accumulated in the sample as a result of the repeated impacts. This will be described in the following section.

#### 4.3.2.1 Macroscopic/Microscopic Evaluation of Damage in 1mm Specimens

Damage initiation/ progression scenarios were assessed for the 1mm specimens in the same way as with the 2mm specimens. The damage initiation and progression pattern was the same as with the 2mm but occurred at much fewer numbers of cycles. An additional microscopic evaluation took place examining the damage around the hole instead of the whole specimen. Figure 4.25 shows the inspection area as well as the sectioning procedure of the post processing of the results.

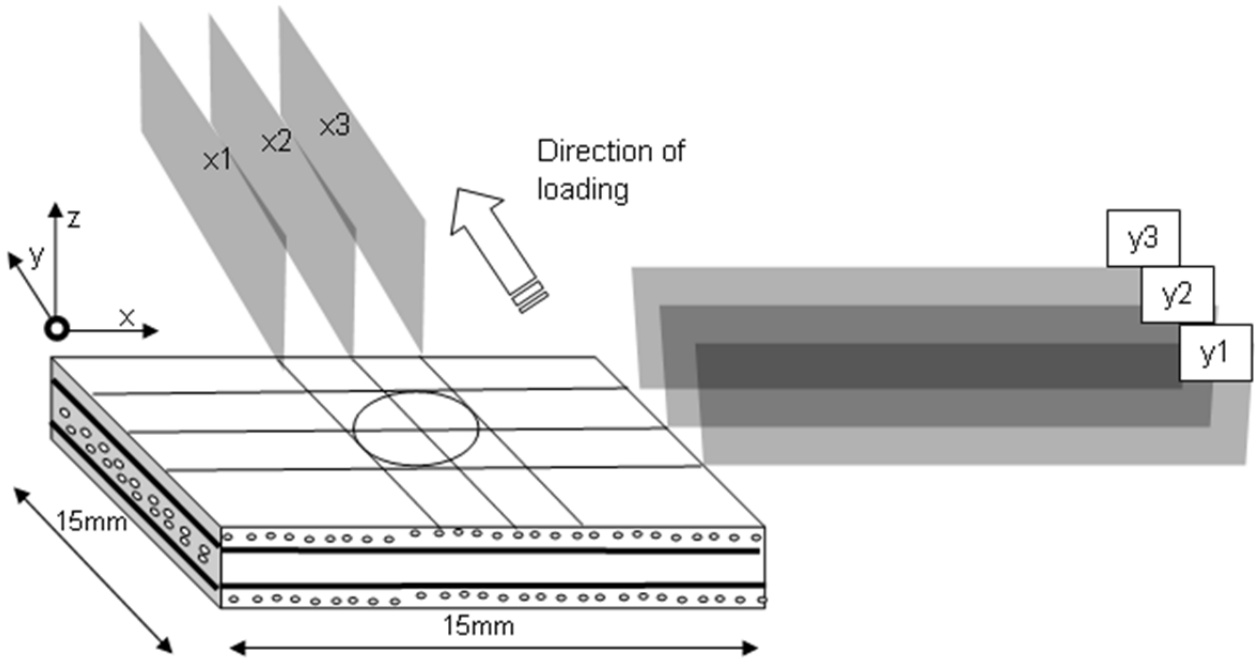


Figure 4.25 Schematic indicating the post processing procedure and direction of loading. Slices selected at the edges and centre of the hole along the x and y axes

Figure 4.26 presents the slice y1 along the y axis (x-z plane) while Figure 4.27 presents the x3 slice along x axis (y-z plane). In Figure 4.26 axial cracks can be seen to form initiated by microdefects at the virgin state Figure 4.26(a) are evolving by increasing in width and length as they reach the 90° plies Figure 4.26(b)-(d). At the final stage of damage these axial cracks are joined by delamination and complete decohesion of the 0 degree plies takes place as shown in Figure 4.26(e). In Figure 4.27 the slices along the x axis are demonstrated. Delamination signs are vivid at the area adjacent to the hole and seem to grow away from the hole along the length of the specimen. Transverse cracks in the 90° plies grow towards the 0/90 and 90/0 interfaces joining the delaminations at areas next to the drilled area.

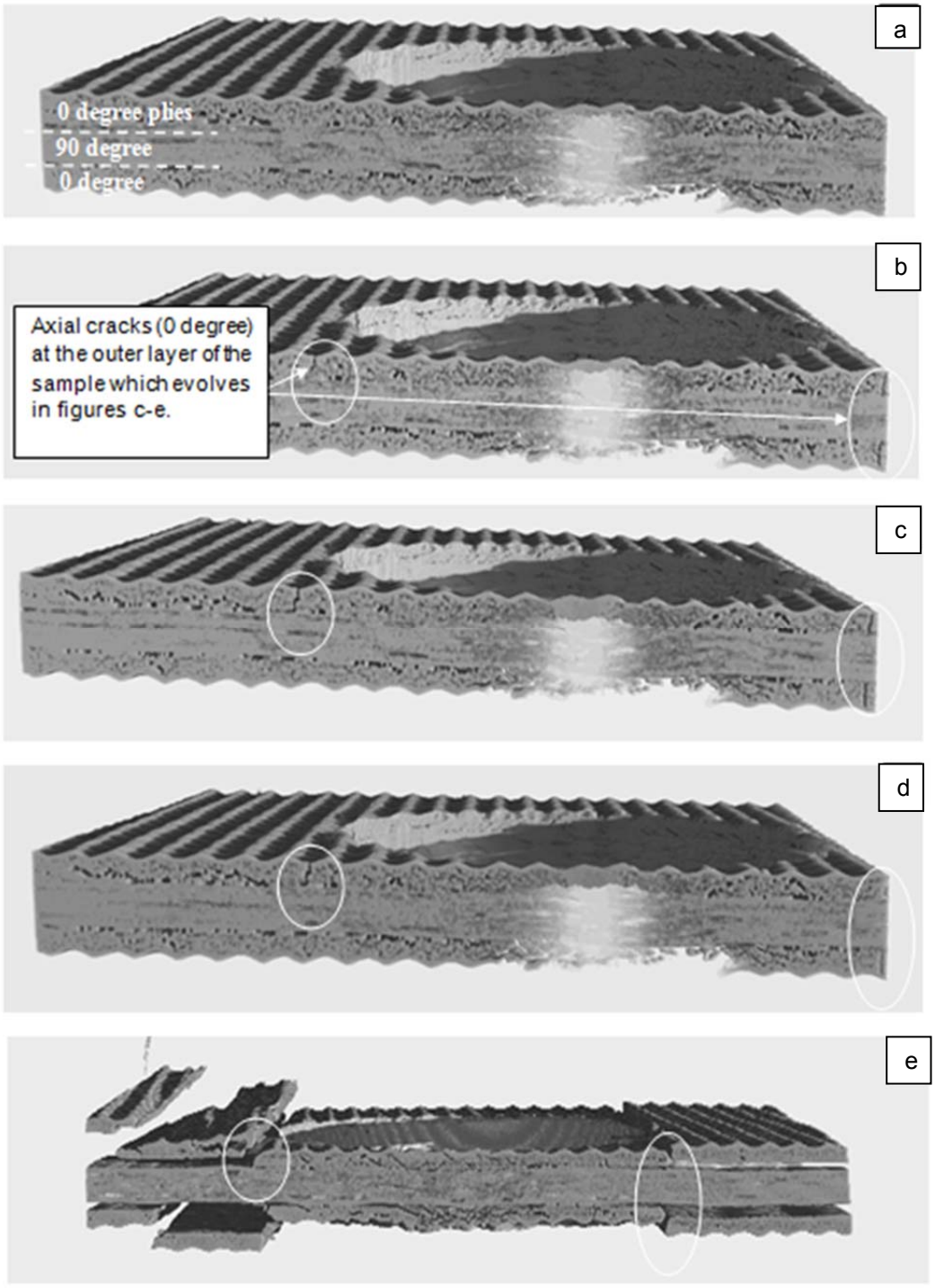


Figure 4.26 µXCT results showing individual y1 slices at a) post-manufacturing state, b) 300 impacts, c) 900 impacts, d) 1200 impacts and e) 3750 impacts (ultimate life)

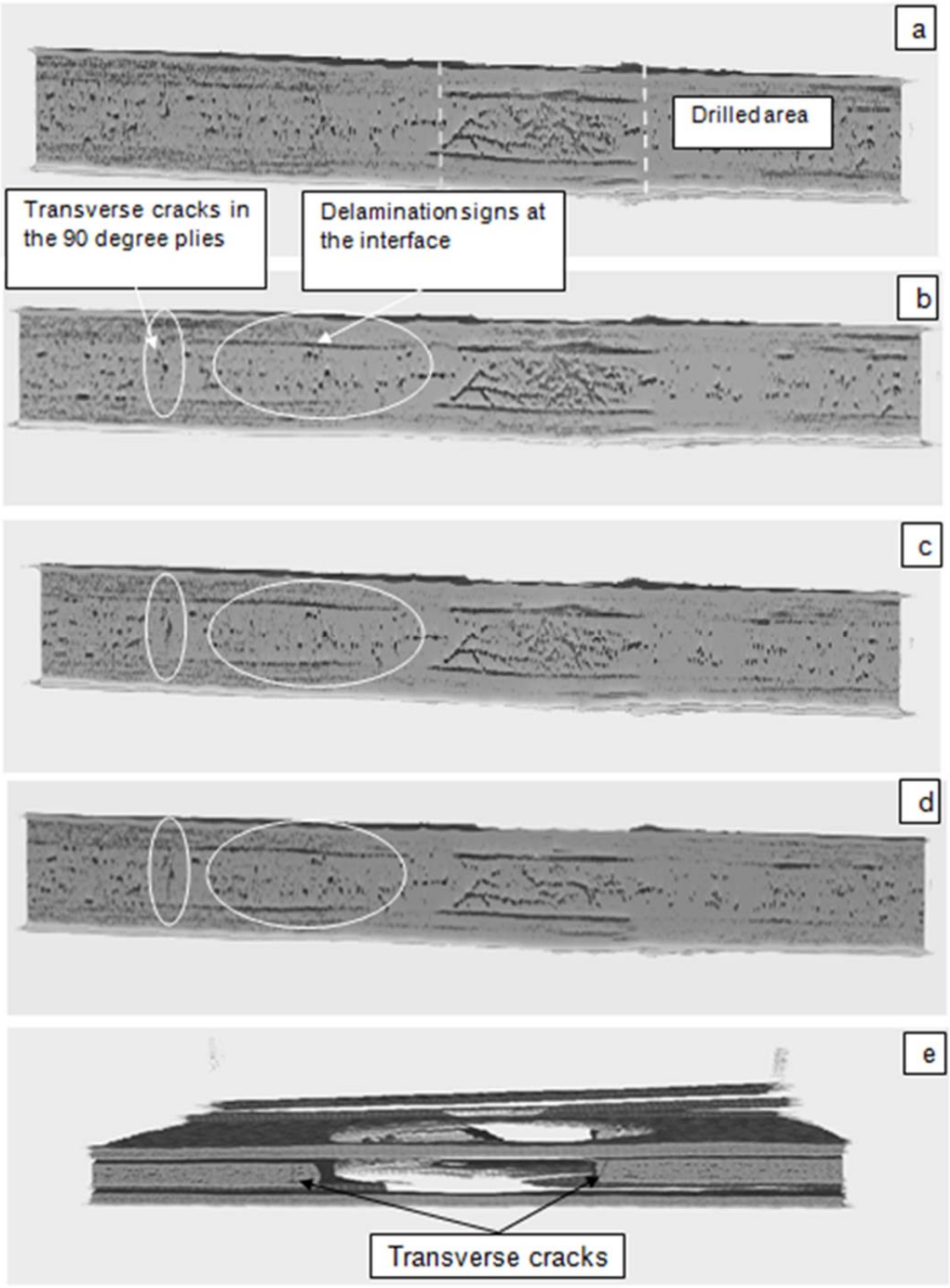


Figure 4.27 μXCTresults showing individual x3 slices at a) post-manufacturing state, b) 300 impacts, c) 900 impacts, d) 1200 impacts and e) 3750 impacts(ultimate life)

## 4.4 Summary

From the IIF test, the results will be discussed and contrasted for the two diferrent thicknesses. The impact energy associated with a given Nf is significantly lower for the 1mm thick samples than for the 4mm thick samples. A level of scatter is apparent, however, this is inevitable as fatigue is a probabilistic phenomenon. The E-Nf graphs showed that as the impact energy decreases, the number of cycles to failure will increase in a quasi-linear fashion. From the test data it is seen that in cases of IF a fatigue limit is not clearly observable, making this a potential problem in designing against IF. In an attempt to characterize the crack growth a special specimen was made with 4 mm width which allowed detailed X-ray micro CT to be carried out. Cracks seemed to grow substantially in the fibre direction and across the sample width causing matrix cracking some fibre breakage. It is proposed that fibres act as impact wave guides since matrix cracks propagate initially along the length of the fibres.

For the TIFT the discussion will be concentrated on the effect of the thickness on the fatigue life and damage mechanisms. Two thicknesses were investigated. A 2mm and a 1mm balanced and symmetric composites of the following configuration were tested $[0_n/90_m]_s$ where n=2,m=4 for the 1mm and n=4, m=8 for the 2mm specimens. It was seen that the 1mm thickness was not appropriate for truly uniaxial impact, since a bending factor, caused by the mass of the impact block altered the true uniaxial loading regime. Conclusions could be drawn therefore only for the 2mm specimen. From the 2mm experiments, it could be seen that the force response remains constant between initial stage of life, half life and total life while the time required for the force to return to zero is increasing. It can also be seen that the loading time increases after 70% of life. Furthermore the variability in the results becomes less prominent towards the end of life which could be reasoned due to the less stiff response of the specimen and therefore fewer oscillations. With regard to their initial values, it is seen that force is constant during the test whilst the increase in the loading time is approx. 12%. Accurate and detailed representation of the damage mechanisms could be captured in the case of 2mm specimen due to the high number of cycles

More specifically:

- 4000 impacts (13%Nf), initiation of axial splits occurred;
- 15000 impacts (45%Nf), inner delaminations at the hole edge appeared;
- 18000 impacts (54.5%Nf), free edge delaminations initiated;
- 30000 (91%Nf), the free edge delaminations were propagated along the length of the specimen;
- 32700-33000 (100%Nf), intraply cracks governed the gauge section.

# Chapter 5 Finite Element Modelling of Single Impacts

## 5.1. Introduction

Finite element analysis (FEA) has been extensively used in recent years, as a tool to support the study of CFRPs subjected to impact loading, mainly the drop weight scenario. Using FEA, investigation of the effect of dynamic loading on regions of stress concentration is feasible. These regions act as damage initiation points and characterisation of the transient stress distributions in the specimen.
The aim of this chapter is to develop an FEA model that can be used as a predictive tool to describe the dynamic phenomenon in detail. To fulfill this aim the steps undertaken were based on the following objectives:

- A numerical model was built, based on a hammer-aluminium specimen assembly, to compare the results acquired experimentally.
- Calibration of the model above was achieved with a mesh convergence study.
- A parametric study of the effects of altering the thickness and specimen configuration was carried out.
- A CFRP specimen was successfully modelled.
- A second numerical model was built, substituting the aluminium specimen with CFRP, in order to compare the results acquired experimentally and computationally.

## 5.2 Model Details

Under dynamic conditions, the interactions of the bodies that are in contact during an impact are extremely important. In order to develop a suitable dynamic model, calibration of the boundary conditions is conducted using an undamaged aluminium specimen. In the following subsections, the geometry, boundary conditions and the meshing will be described for the hammer, specimen and the rest of the assembly.

### 5.2.1 Geometry and Boundary conditions

The geometry of the respective FEA model is shown in Figure 5.1. The boundary conditions will be explained in relation to the figure. The model is composed of five elements. A hammer (1), an impact block (2), a support (3), a clamp (4) and the specimen (5). The hammer is modelled as a solid deformable body with a real 3D geometry, using a variable thickness for each section and materials, representing the features of the real component. The hammer rod is a hollow cylindrical part with external and internal diameters of 14 mm and 12 mm, respectively. The impact block, clamps and support were included into the model, with the size, thickness and weight of the original taken from measurements of the actual experimental parts.
For the representation of tensile-impact vice a small fixed part was included (clamp) and represented by encastred boundary conditions.
In order to decrease the time of simulations, the hammer was modelled an instant before the vertical position was attained with an initial velocity of Vo=1.48 m/s.The hammer initially was modelled as a discrete rigid body; however it was observed that some deformation was apparent in the cylindrical hammer rod section.The rest of the assembly parts were modelled as discrete deformable bodies too with the exception of the support which was modelled as rigid.

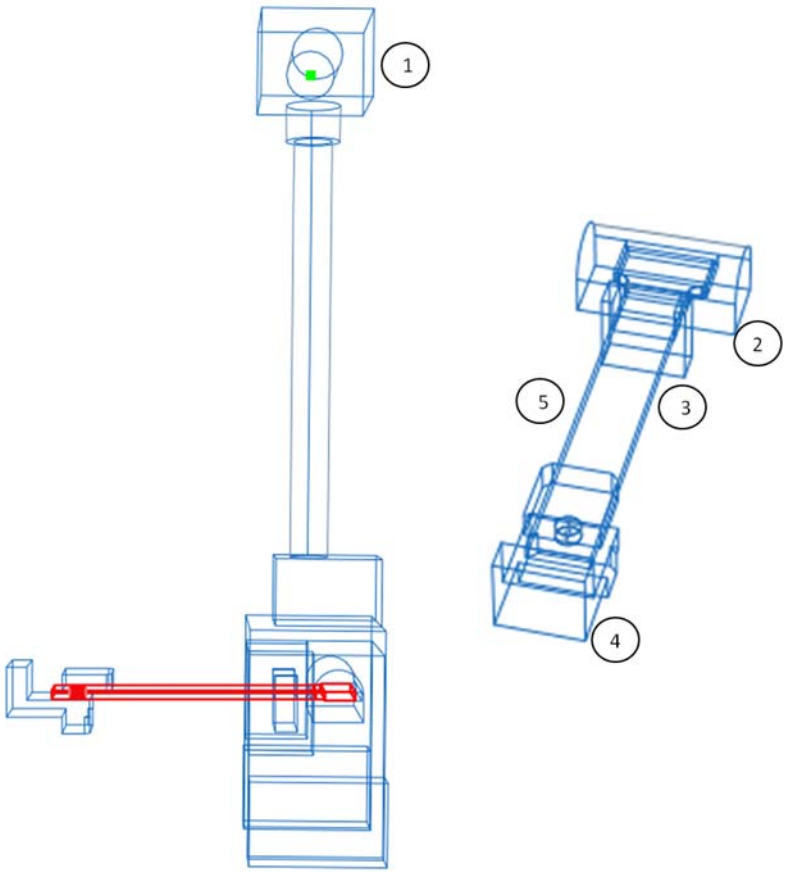


Figure 5.1 Geometry of FEM 3-D model

For the contact between the hammer and the impact blocks, a general contact algorithm with a frictionless tangential behaviour was included. In order to represent the actual pendulum scenario, a kinematic coupling constraint was introduced to allow the hammer to rotate around the x axis. The basis of this method is that all the nodes of the inner cylinder of the upper block of the hammer were kinematically coupled to the reference point at the middle of that cylinder, and then the reference point was only permitted to rotate around the x-axis.

At this point, clarification on whether it was necessary to model the whole hammer specimen interaction will be given. The reasons are: The physics of contact are different if a concentrated load or uniform pressure option was used. The localisation of damage would alter the true nature of impact. In addition, the exact magnitude of pressure at the time of impact would not be possible to know in advance. The disadvantage is that the specific analysis is computationally expensive in terms of both analysis time and CPU power.

### 5.2.2 Material Data

All the parts used in this study, except from the specimen, were assigned the properties of carbon steel. The model's elastic material properties are given in Table 5.1. These data were obtained from direct contact with the manufacturer.

Table 5.1 Elastic Material properties of carbon steel and aluminium alloy

| Part | Material | Elastic modulus (GPa) | Poisson's ratio | Density ($kg/m^3$) |
|---|---|---|---|---|
| Hammer-vice assembly | Carbon steel | 210 | 0.3 | 7850 |
| Specimen | Aluminium alloy | 67.1 | 0.3 | 2650.4 |

For determining the properties of the aluminium specimen used, and input it into the model, two aluminium specimens were manufactured in conformity with ASTM B557M-07e1 standards and tested under quasistatic conditions in an Instron tensile testing machine. The stress-strain graph is given in Figure 5.2 while the true plastic stress, stain values given in Table 5.2.

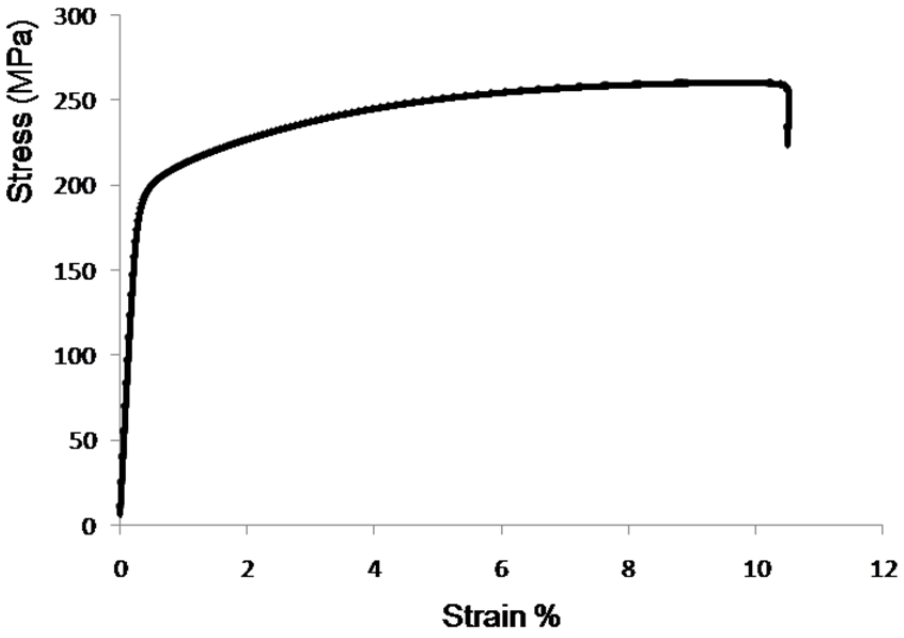


Figure 5.2 Stress vs strain diagram of aluminium specimen

Table 5.2 True plastic stress-strain values of aluminium alloy specimen used in calibration model

| Plastic stress (MPa) | Plastic strain (mm/mm) |
|---|---|
| 167.98 | 0 |
| 197.59 | 0.0014 |
| 211.59 | 0.0054 |
| 223.43 | 0.0114 |
| 233.30 | 0.0176 |
| 241.94 | 0.0239 |
| 249.62 | 0.0304 |
| 256.22 | 0.0369 |
| 262.02 | 0.0437 |
| 267.07 | 0.0504 |
| 271.51 | 0.0573 |
| 275.39 | 0.0641 |
| 278.78 | 0.0709 |
| 281.82 | 0.0778 |
| 283.39 | 0.0818 |

### 5.2.3 Element and Mesh Selection

Due to the relative complex geometry of the specimen, partition of certain regions was carried out as shown in Figure 5.3. More specifically, at the fillet area a partition was introduced in order to alleviate stress concentrations and enhance the mesh quality in the gauge section. Around the hole, a common practise is to partition in a cross configuration for the mesh to be uniform at the edges of the hole.

The hammer as well as the rest of the assembly was discretised with 4-noded linear tetrahedron C3D4 elements using a structured meshing technique. An optimised/refined mesh was introduced at the contact surface of the hammer's strikers. Linear hexahedral elements were used for the specimen and were chosen from the extensive element database of Abaqus explicit. The specimen was modelled with linear reduced integration elements of type C3D8R at the stress

concentration areas and linear fully integrated elements of type C3D8I were used for the gauge section. Reduced integration reduces running time but a drawback, is that with reduced-integration elements hourglassing can be a problem. This problem was tackled using a fine mesh around the hole area, and the enhanced hourglass control option.

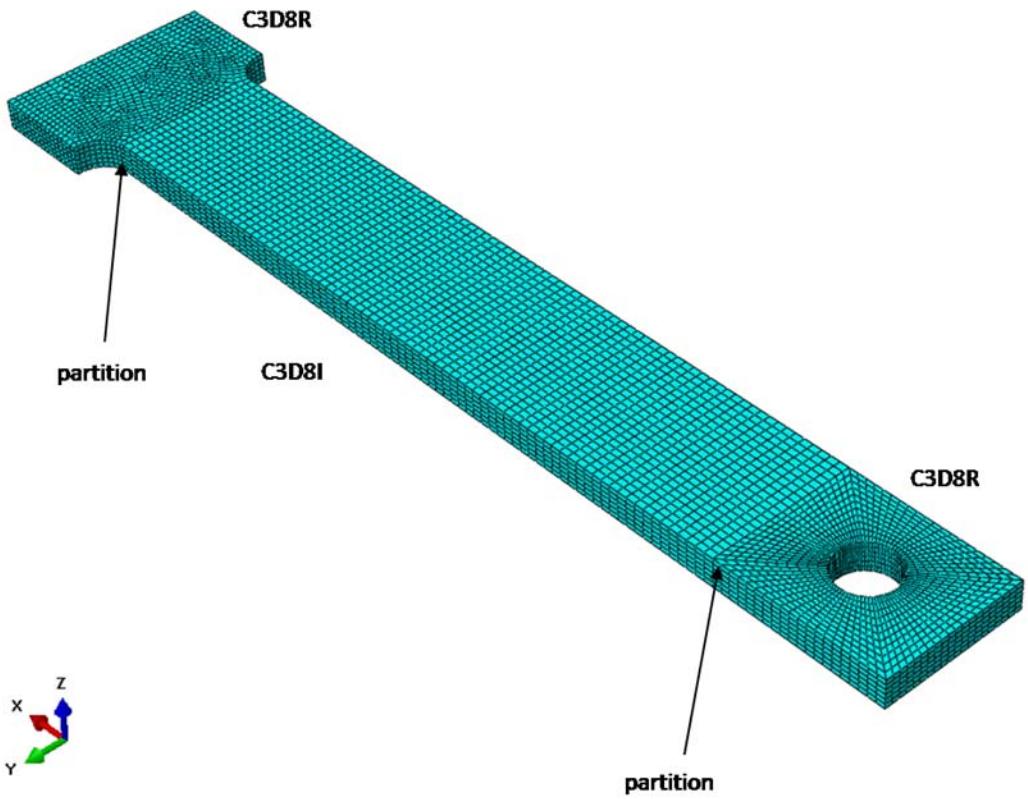


Figure 5.3 Meshed 3-D specimen indicating partitioned regions and element types used.

The C3D8I elements are enhanced by incompatible modes to improve their bending behaviour. The main reason these elements were used for the gauge section is to eliminate the parasitic shear stresses that cause the response of the C3D8R elements to be too stiff in bending. Although these elements are more expensive than C3D8R, they are more economical computationally than the second-order elements. Additionally, the incompatible mode elements use full integration and, thus, have no hourglass modes and the need for a very fine mesh is reduced. Finally, a sufficient number of linear (first order) elements provides superior results to quadratic (second order) elements, since linear elements are favourable in explicit contact problems in terms of material response and computational time.

### 5.2.4 Field/History Output Request

The experimental data acquired were the force and strain signal. Experimentally, the force signal was measured at the back of the clamp where the loadcell was located. The strain signal was acquired with a strain gauge placed at the middle of the specimen.

In order to correlate with the experimental results in the numerical model, two elements sets were created. For these sets of elements, history output requests were created. The history output is the acquisition of data during the analysis in order to analyse during post processing. The history outputs for the force and strain history were requested in the direction of the loading. Both of the history outputs were recorded every 0.02ms which was adequate for creation of the force-strain history.

### 5.2.5 Solver

Dynamic problems in the low dynamic range can be solved with Implicit or Explicit methods, both of which are available in the Abaqus solver. In an implicit dynamic analysis the stiffness matrix is inverted, and a set of simultaneous non linear equilibrium equations must be solved at each time increment. This solution is carried repetitively using the Newton–Raphson method. In an explicit dynamic analysis a large number of small time increments is performed efficiently. The use of small increments is advantageous because it allows the solution to proceed iteration free and without the need of forming tangent stiffness matrices. Contact conditions and other extremely discontinuous events are easily handled by ABAQUS/Explicit. An Implicit FEM analysis is the same as Explicit with the addition that after each increment the analysis does Newton-Raphson iterations to enforce equilibrium of the internal structure forces with the externally applied loads. Overall, for large problems presenting multiple types of non-linearity, as in our case, where multiple contacts

and stress wave propagations are present, the explicit method is favourable due to the assuring convergence that is proven to be very computational cost effective when compared with the implicit regime.

## 5.3 Dynamic modelling of Single Impact on Aluminium

### 5.3.1 Set up

In this section, the calibration of boundary conditions will be presented and contrasted with a single impact experiment on aluminium. In order to gain an understanding of the dynamics of single impact, a simple tensile-impact test was conducted using an aluminium plate. A semiconductor strain gauge glued to the middle of the plate was used to measure the dynamic strain during an impact produced using the impact testing machine described in section 3.4.2. The reaction force signal was measured during the impact of the hammer with energy of 1J and a velocity of 1.46m/s and is presented in Figure 5.4. It can be seen, that the signal's approach time is similar to the restitution period i.e., elastic impact.

The second type of data that was captured was the axial strain as shown in Figure 5.4. This was acquired from the strain gauge that was placed at the top of the aluminium specimen. It may be expected in a pure tensile impact that the strain signal should be similar to the force signal but out of phase. The last feature is due to the fact that the force sensor is at a greater distance than the strain gauge. However, in Figure 5.4 there is no obvious time lag between the two signals or great difference in damping behaviour up to 0.6ms. The theoretical expected maximum strain value for an aluminium alloy bar with a rectangular gauge section of 15 mm x 3 mm, elastic modulus of 67.1 GPa, impacted in tension with a load of 558N should be approximately $0.18\times10^{-3}$, which gives an error of 16.6% between theoretical and experimental results. It should be noted, that similar experiments with standard electrical resistance strain gauges were not able to generate usable results because of the high noise and lower frequency response.

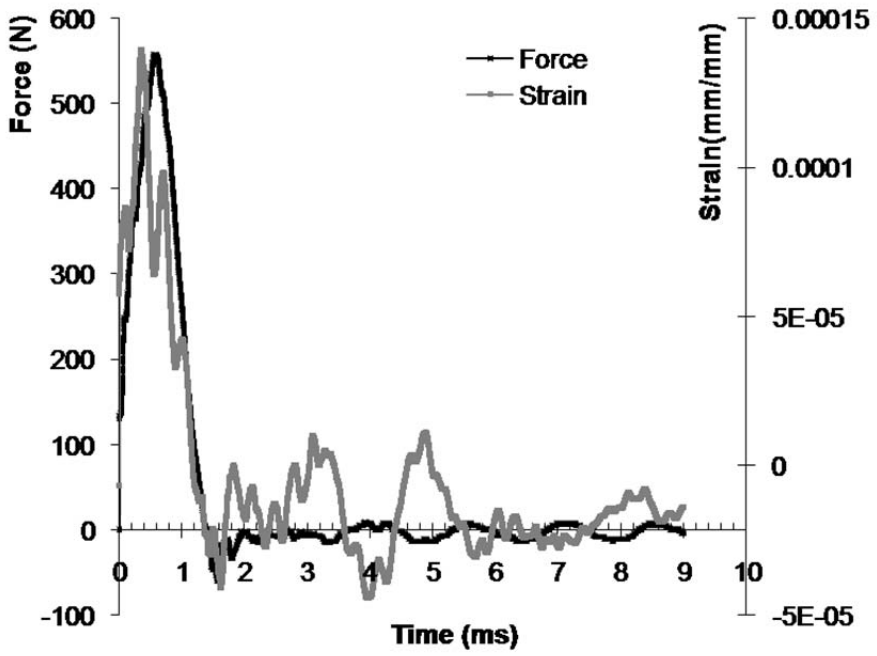


Figure 5.4 Experimental force and strain response for aluminium specimen

### 5.3.2 Numerical Validation

To compare the force and strain response history of experiment and simulations, the reaction force of the element set at the back of the clamp was recorded in the history output of Abaqus/Explicit. Figure 5.5 presents a comparison with the experimental data as well as the mesh results from the convergence convergence study.

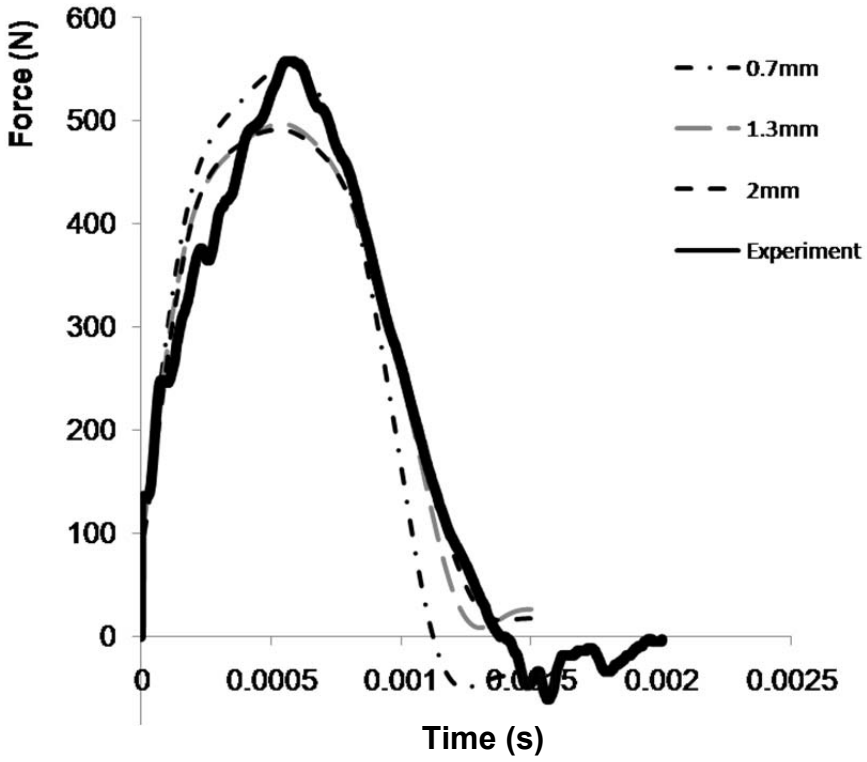


Figure 5.5 Experimental and numerical results for aluminium specimen at different element sizes

It has to be noted that in the numerical results a noise reduction filter was introduced. The Butterworth filter was used on the raw force–time data. Its main purpose was to attenuate the high frequency noise. The second order LowPass (LP) Butterworth filter was applied with a 2.3 kHz cut-off frequency. The cut-off frequency is the frequency above which the filter attenuates at least half of the input signal. From the figure above it can be observed that with mesh refinement the magnitude of the force matches ideally, however the period of the signal is getting smaller. This could be due to the fact that compliance of the system has not been incorporated in the model which may affect the energy dissipation. However, the general rule is that the finer the mesh the better the capturing of the stress wave signals. Large transitions in the mesh should be avoided since stress concentrations are induced.

Comparing the strain data, contributed ın deciding the optimum element size since for the 0.7 mm the strain data presented good correlation. The strain-time graph is presented in the figure below.

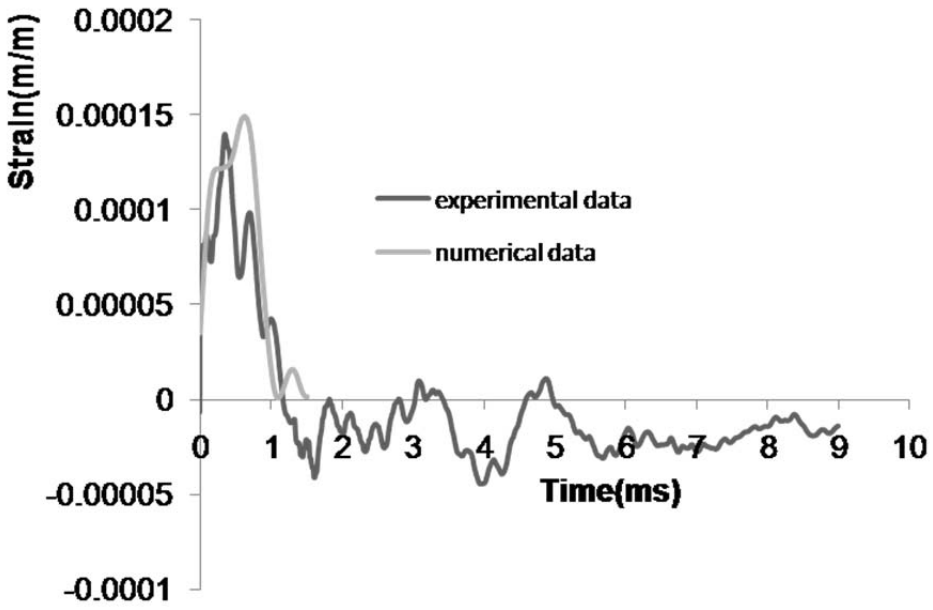


Figure 5.6 Experimental and numerical results for aluminium specimen at 0.7mm element size

The simulation time for the single impact was set to 1.5 ms to reproduce only the specimen-hammer interaction. During that period, the model reproduced the experiment in terms of the trend, strain amplitude and contact time with insignificant errors. Due to the dynamic nature of loading of the aluminium specimen, oscillations in the response of both the model and the experiment were apparent. In the dynamic stress wave has been captured throughout the impact duration in the model. Distributions of the maximum principal stress within the aluminium specimen at different moments were acquired as shown in the figure. In general, it can be observed from these stress distributions over several time increments that due to the sudden imposing of the load, elastic stress-waves were generated and propagated in different directions in the specimen, and those stress waves produced accompanied strain waves.

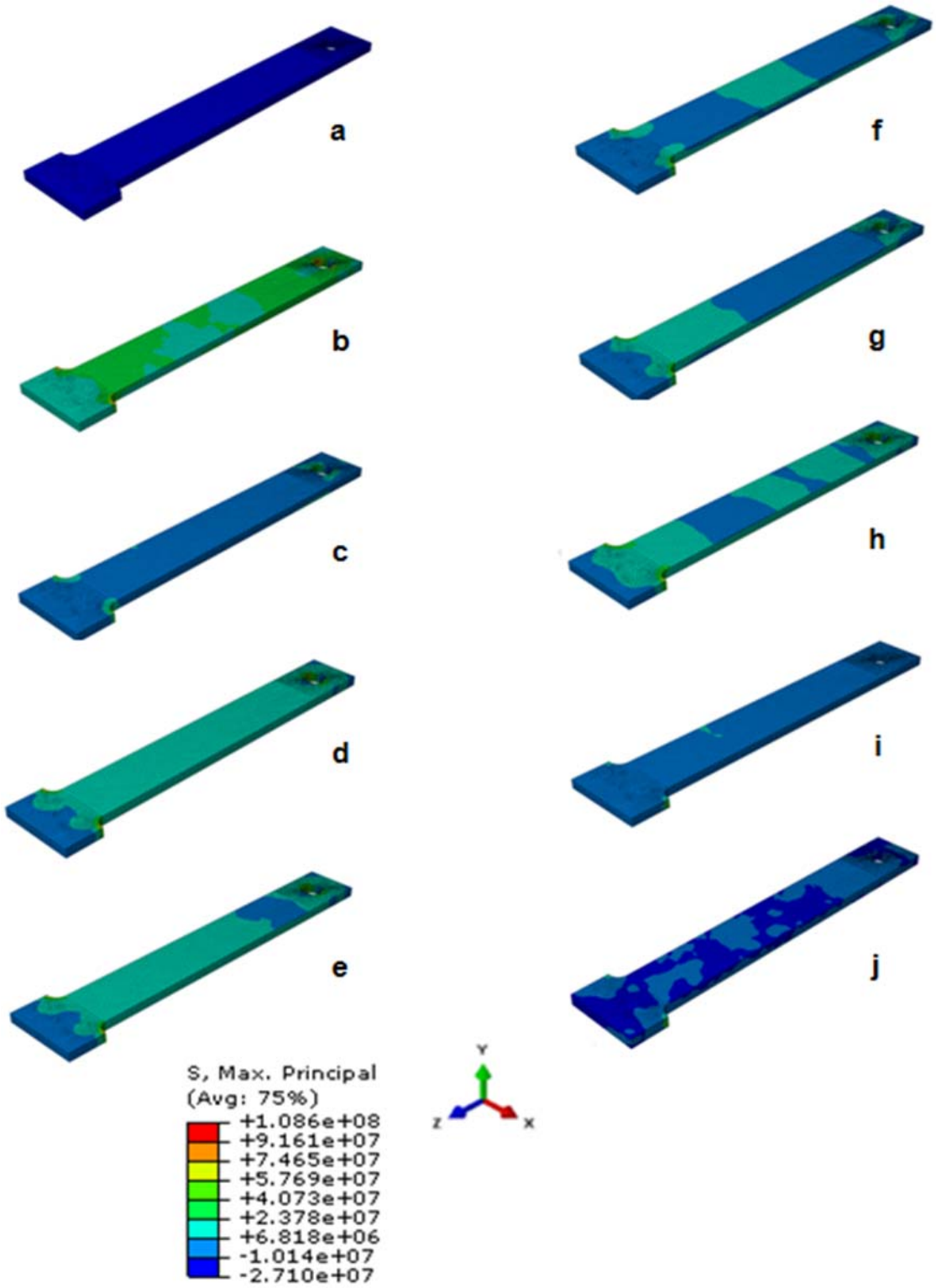


Figure 5.7 Maximum principal stress distribution (Pa) at different time increments a)0.075ms, b)0.225ms, c)0.45ms, d)0.6ms, e)0.825ms, f)0.9ms, g)0.975ms ,h)1.05ms, i)1.425ms, j) 1.5ms.

### 5.3.3 Parametric Studies

Parametric studies were also carried out to investigate the effects of altering the geometry by a) decreasing the thickness, b) introducing a hole in the middle of the specimen. The stiffness of the specimens is altered in both cases, reflected in the following graph by changes in the initial slope and period duration, and the effect is prominent after the retraction of the hammer which occurs after 0.6 ms in all 3 cases.

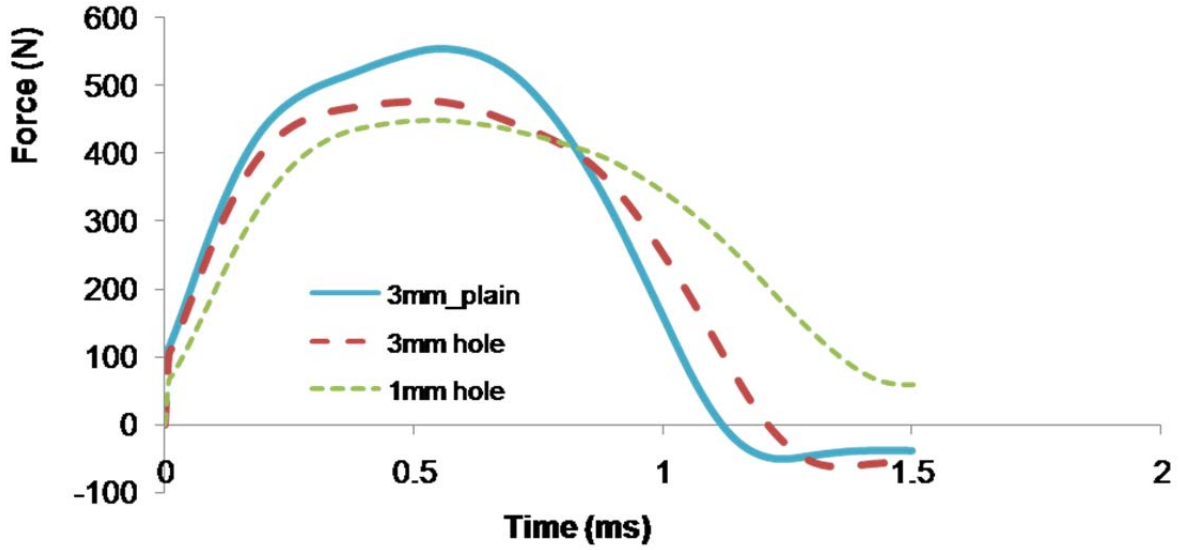


Figure 5.8 Effects on the force response when altering thickness and introducing a hole.

The modelling has been proven to be adequate for the preliminary aluminium specimen since the numerical force history matches the experimental data. However additional work is required for modelling the composite specimen in the dynamic analysis and this will be presented in the following section.

## 5.4 Dynamic modelling of single impact on CFRP containing a centrally located hole

The modelling work undertaken in the previous section, served the purpose of calibrating the boundary conditions using an aluminium specimen and matching the force vs time data. The next step was to substitute the aluminium specimen with the

CFRP composite. In order to do so, decisions on the partitioning, material model as well as element type had to be investigated. The chart in

Figure 5.9 shows the options available when modelling a composite and highlights the most efficient route for our case. The dashed line denotes the initial route followed prior to the introduction of damage in the specimen. After the introduction of damage the second route was followed. The choices made and the reasoning behind them will be discussed in the following subsections.

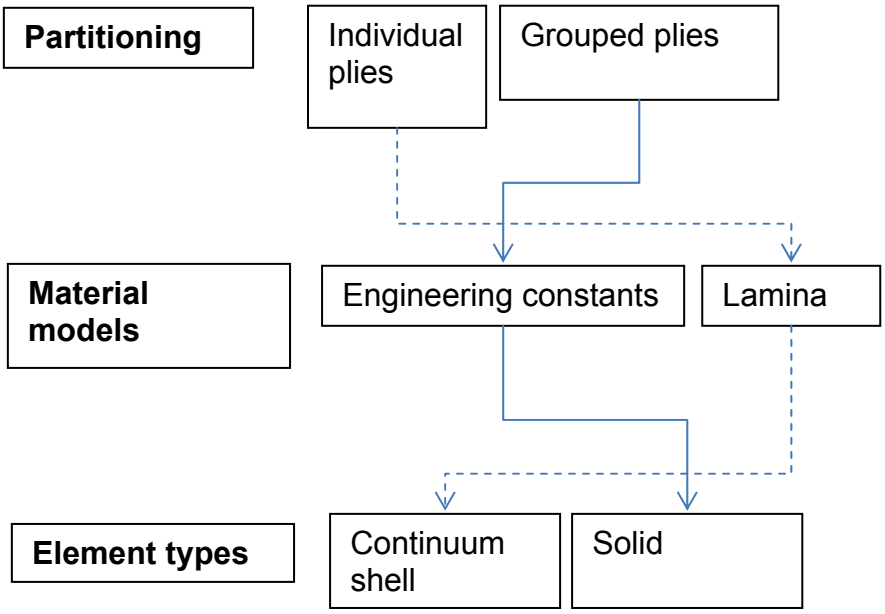


Figure 5.9 Pre damage (dashed line) and after damage (normal line) modelling methodology of CFRP lay-up

### 5.4.1 Partitioning

Figure 5.10(a) shows a common technique when modelling composites. Here, a thickness of 1mm is partitioned 8 times at 0.125mm intervals which represents the actual ply thickness. In this way modelling of the composite uses only 1 coordinate system, changing the angle of the plies in respect to this for multidirectional lay-ups. The drawback with this technique is that it's computationally expensive and could be time consuming when modelling thick composites. An alternative method, which is

favourable in our case because we do not deal with too many different orientations, is based on the grouping of plies, which can be seen in Figure 5.10(b). It should be noted that both methods were investigated in initial quasistatic tests and produced the same results.

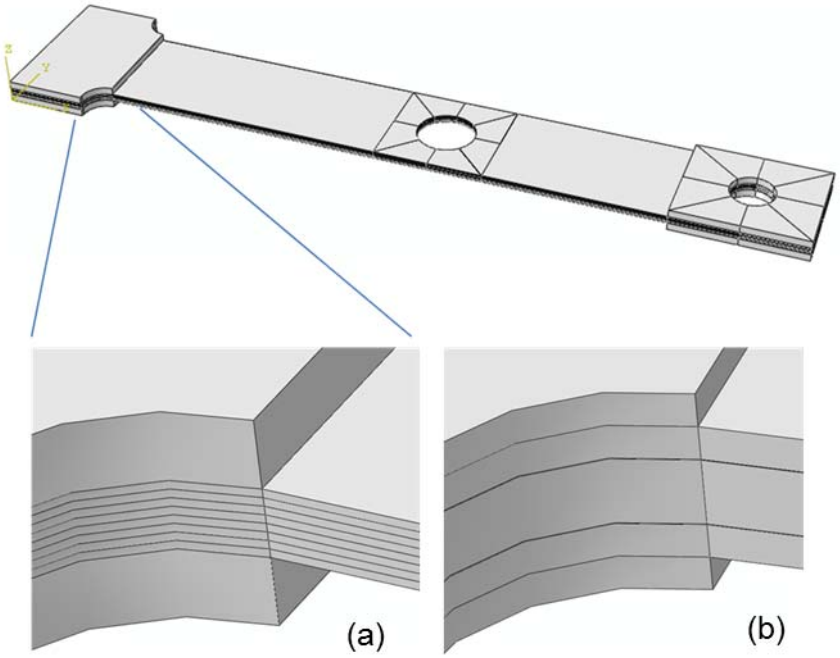


Figure 5.10 Ply by ply modelling vs grouping of plies

### 5.4.2 Material Models

In order to model the CFRP composite, a linear elastic behaviour was assumed because the specific composite is quasi-brittle and presents negligible plasticity. The material models, available in Abaqus explicit, which could be used are the lamina and engineering constants. Both of these models are used to specify orthotropic elastic properties with the only difference that the first one assumes plain stress conditions.

In the case of lamina, plane stresses condition exist where $\sigma_{33}=0$, such as in a shell element, and only 5 constants are required. More specifically the values of $E_1, E_2, v_{12}, G_{12}, G_{13}$ and $G_{23}$. The shear moduli $G_{13}$ and $G_{23}$ are included because they may be required for modelling transverse shear deformation in a shell element. The Poisson's ratio is given as $v_{21}=\left(\frac{E_2}{E_1}\right)v_{12}$. In this case the stress-strain relations for the in-plane components of the stress and strain are of the form

$$\begin{Bmatrix}\varepsilon_1\\ \varepsilon_2\\ \gamma_{12}\end{Bmatrix}=\begin{pmatrix}1/E_1 & -v_{12}/E_1 & 0\\ -v_{12}/E_1 & 1/E_2 & 0\\ 0 & 0 & 1/G_{12}\end{pmatrix}\begin{pmatrix}\sigma_{11}\\ \sigma_{22}\\ \tau_{12}\end{pmatrix}$$

In the case of engineering constants, nine material constants are required $E_1, E_2, E_3, v_{12}, v_{13}, v_{23}, G_{12}, G_{13}$ and associated with the material's principal directions. The stress-strain relations are of the form

$$\begin{Bmatrix}\varepsilon_{11}\\ \varepsilon_{22}\\ \varepsilon_{33}\\ \gamma_{12}\\ \gamma_{13}\\ \gamma_{23}\end{Bmatrix}=\begin{pmatrix}1/E_1 & -v_{21}/E_2 & -v_{31}/E_3 & 0 & 0 & 0\\ -v_{12}/E_1 & 1/E_2 & -v_{32}/E_3 & 0 & 0 & 0\\ -v_{13}/E_1 & -v_{23}/E_2 & 1/E_3 & 0 & 0 & 0\\ 0 & 0 & 0 & 1/G_{12} & 0 & 0\\ 0 & 0 & 0 & 0 & 1/G_{13} & 0\\ 0 & 0 & 0 & 0 & 0 & 1/G_{23}\end{pmatrix}\begin{Bmatrix}\sigma_{11}\\ \sigma_{22}\\ \sigma_{33}\\ \sigma_{12}\\ \sigma_{13}\\ \sigma_{23}\end{Bmatrix}$$

Both material models were tried but each one works with a different technique. For example, the lamina material model works with the individual ply partitioning technique while the engineering constants with the grouped plies

### 5.4.3 Element Types

Element types that could be used to represent the CFRP are continuum shell and continuum solid elements on shell homogeneous and solid homogeneous sections

respectively. Again, the continuum shell elements are used with the lamina material model and ply by ply modelling technique while solid elements are used with engineering constants and grouped plies.

From a modelling point of view, discretisation wise, continuum shell elements look like three-dimensional continuum solids, but their kinematic and constitutive behaviour is similar to conventional shell elements. Continuum shell elements are proven to be accurate in contact modelling since they employ two-sided contact taking into consideration the respective changes in thickness**.** These elements, are assigned to solid parts, and Abaqus determines the thickness from the geometry of the part. In other words, one element per ply is allowed.

### 5.4.3 Results/Experimental validation

Both approaches resulted in similar results. The properties used for modelling the composite are presented in Table 5.3. Figure 5.11 illustrates the stress state at the maximum impact force point occurring in 0.65ms shown in Figure 5.12. The Von Mises stresses at tha point are approximately 380 MPa. The results show a good correlation between experimental and numerical methods and establish the starting point for the insertion of the cohesive zone elements in order to model damage under multiple impacts.

Table 5.3 T700/LTM45 individual ply properties (1 = fibre direction)
Nominal thickness 0.128mm

| $E_{11}$ | $E_{22}=E_{33}$ | $G_{12}=G_{13}$ | $G_{23}$ | $v_{12}=v_{13}$ | $v_{23}$ |
|---|---|---|---|---|---|
| 127GPa | 9.1GPa | 5.6GPa | 4GPa | 0.32 | 0.4 |

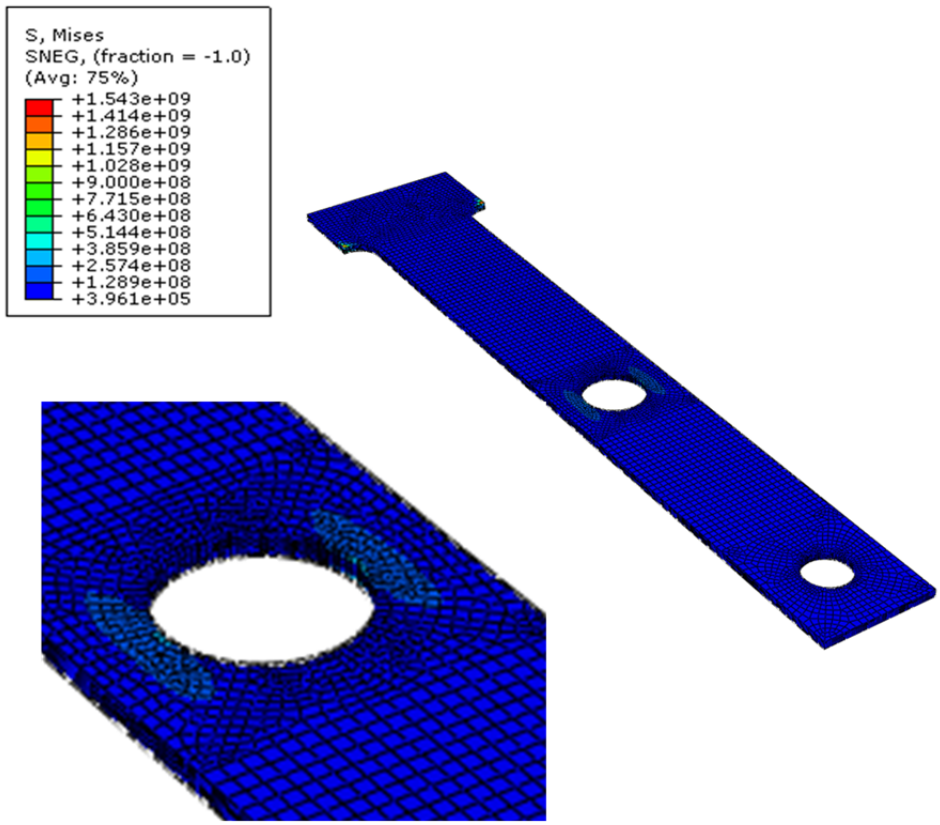


Figure 5.11 Von-Mises stresses at the area of stress concentrations at 0.65ms, ROI stress level equal to 518 MPa.

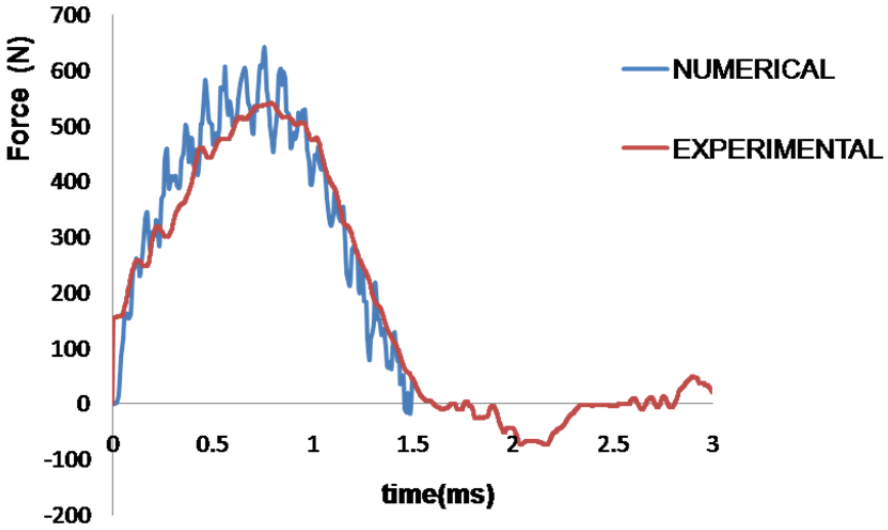


Figure 5.12 Comparison of Impact force history between experimental data and numerical analysis for 1mm CFRP specimen

In order to do so the principal stresses contour in the direction of the loading can be utilised to determine the potential damage areas. In Figure 5.13 the region around the hole which has four zero degree upper and lower plies is subjected to a maximum axial stress of 508 MPa while the middle ninety degree plies are subjected to lower stress values.

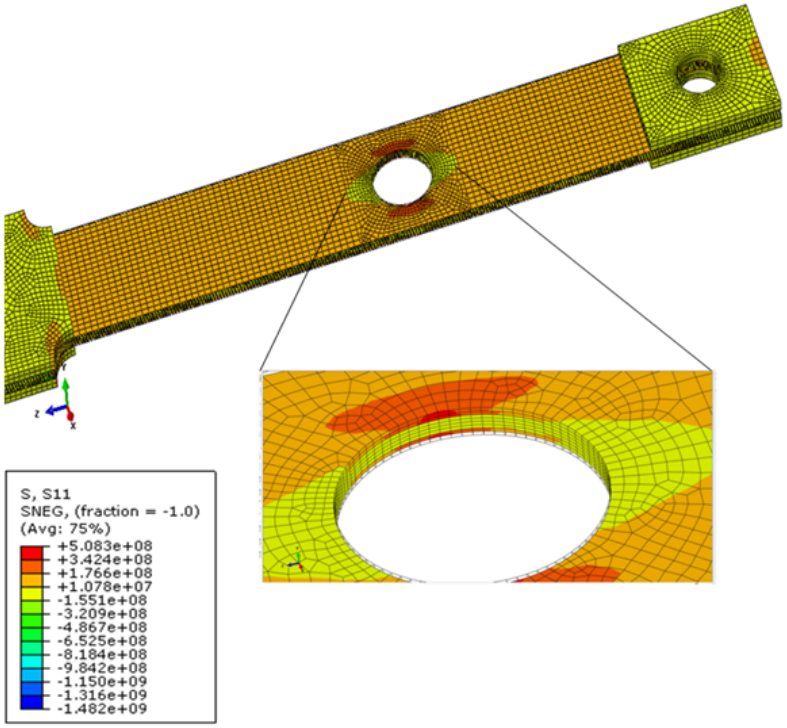


Figure 5.13 Areas of potential damage initiation in the top and bottom 0 degrees plies as well as delamination initiation at the 0/90 and 90/0 interfaces.

After identifying the stress pattern of stress concentration points which are related to damage initiation, extensive experimental work was carried out in order to observe the damage propagation behaviour of the composite under multiple impacts. This is presented in the following Chapter.

## 5.5 Summary

In this chapter the foundation for the numerical model was laid. A 3D transient model was successfully constructed in Abaqus Explicit based on the actual experimental configuration. Strain and force data were successfully simulated for a single impact

initially using an aluminium specimen. After calibration of the boundary conditions, using the aluminium specimen, successful modelling of a carbon fibre specimen was carried out using two techniques. The results matched the experimental data. The output of this chapter gives confidence in modelling damage under dynamic loading that will be discussed in the following Chapter.

# Chapter 6 Finite Element Modelling of Damage

## 6.1 Introduction

In the previous chapter it was demonstrated that FEA is a feasible tool to investigate the effects of dynamic loading on regions of stress concentration in composites. These regions act as damage initiation points, which under multiple impacts can grow in different directions. In the experimental work undertaken, the damage growth areas patterns were identified and investigated. Damage was categorised in 3 groups; Matrix cracks, axial splits and delamination. These damage modes will be investigated numerically by means of cohesive zone elements (CZE) in this chapter. These elements will be placed in experimentally predefined areas and a cohesive bilinear law will dictate their damage behaviour, i.e. damage initiation and damage propagation.

The aim of this chapter is to investigate the applicability of CZE in predicting damage under dynamic conditions in tension. To fulfil this aim the steps undertaken were based on the following objectives:

- Calibration of CZE parameters in a quasistatic model investigating only delamination.
- Incorporation of matrix cracks and axial splits in the above model and experimental validation using the global stiffness as a correlation parameter.
- Insertion of CZE in the dynamic model and investigation of static cohesive zone parameters based on the force response.

## 6.2 Quasi-static Experiment

Before including damage in the dynamic problem, calibration of the CZE parameters was undertaken by conducting a standard open hole quasistatic test on a $[0_4/90_4]_s$ composite. Following that, validation of the results was carried out with a numerical model. The parameters that needed to be investigated before continuing to a dynamic problem, where inertia effects would be superimposed, were:

- Cohesive element size required for convergence
- Penalty stiffness
- Damage initiation parameters
- Damage propagation parameters

Initially a tensile test was undertaken in conformity with ASTM D5766/D5766M-11 standards. The standard states that for a balanced and symmetric specimen the geometry recommendations should be according to Table 6.1, Figure 6.1.

Table 6.1 Specimen dimensions and configuration for quasi-static test

| Fiber orientation | Balanced,symmetric (crossply) |
|---|---|
| Width (w) | 36mm |
| Length (L) | 250mm |
| Thickness (h) | 2.5mm |
| Tabs | Emery cloth |

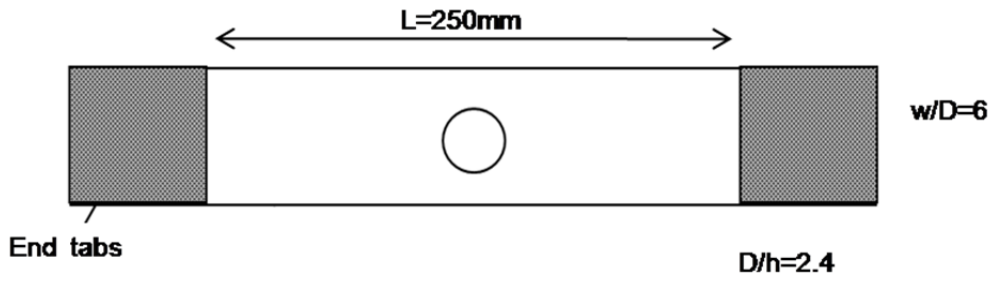


Figure 6.1 Specimen configuration for quasistatic test

Ultimate strength is calculated based on the cross-sectional area, neglecting the presence of the hole and the test is considered successful only if the failure passes though the hole in the specimen

A servo-hydraulic fatigue testing machine with digital control and computer data logging was used in the quasi-static tensile testing and essential data were acquired such as maximum force/failure force and crosshead displacement at the point of failure. The sampling rate was set at 5 data recordings per second which allowed accurate capture of the force/displacement data. The load cell capacity was 200kN.The failure load was calculated as the average of the maximum force reached by two specimens tested at a displacement rate of 0.08 mm/s which is the minimum rate specified by the standards. The tests were conducted under ambient conditions.

## 6.3 Quasi-static Numerical Model Considerations

The quasistatic experiment was predominantly undertaken in order to estimate the failure load of the specimen, and will be used as an input to the model in the form of uniform pressure. The resulting numerical stiffness will be then correlated with the experiment. The $1/8^{th}$ symmetry was used in the analysis, which is a common practice for balanced and symmetric composites, and allows a significant reduction of computational time which was proven to be a major issue. Figure 6.2 illustrates the boundary conditions for the numerical model.

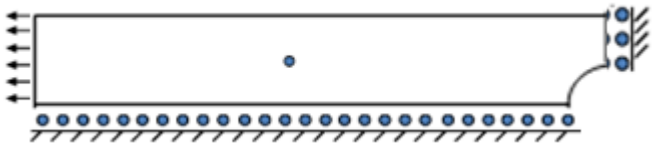

Figure 6.2 Boundary conditions for 1/8$^{th}$ symmetry model

In order to capture the damage development the use of CZE was introduced as shown in Figure 6.3 and Figure 6.4. For the convenience of the reader the full model and quarter symmetry model are shown. This is done because in the dynamic analysis only half symmetry can be used due to the fact that the hammer cannot be simplified further than half symmetry. For the insertion of the elements, partitions were made of 10 micron thickness. The usual practise to determine the area required for insertion, is to determine the resin rich thickness of the interface. Most authors use between 1 and 100 microns.

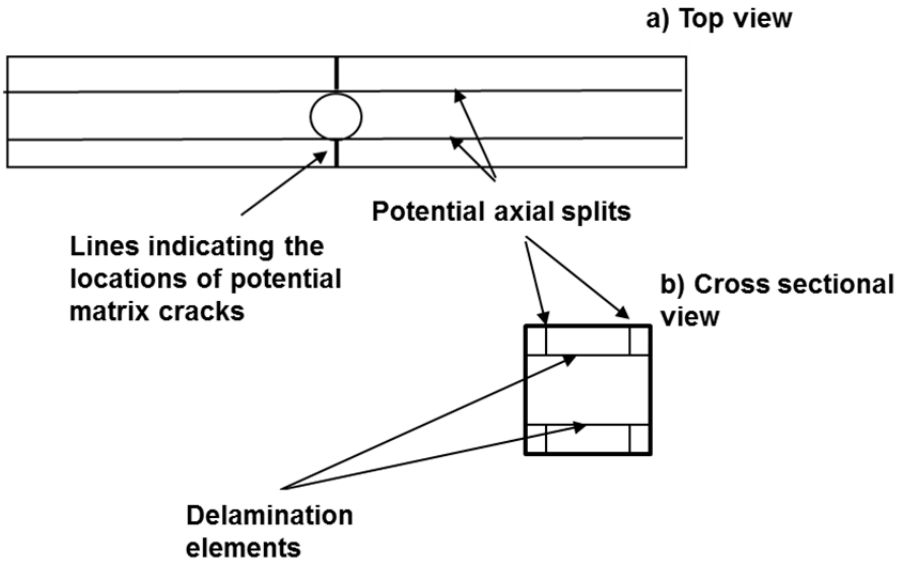


Figure 6.3 Position of cohesive elements at partitioned regions

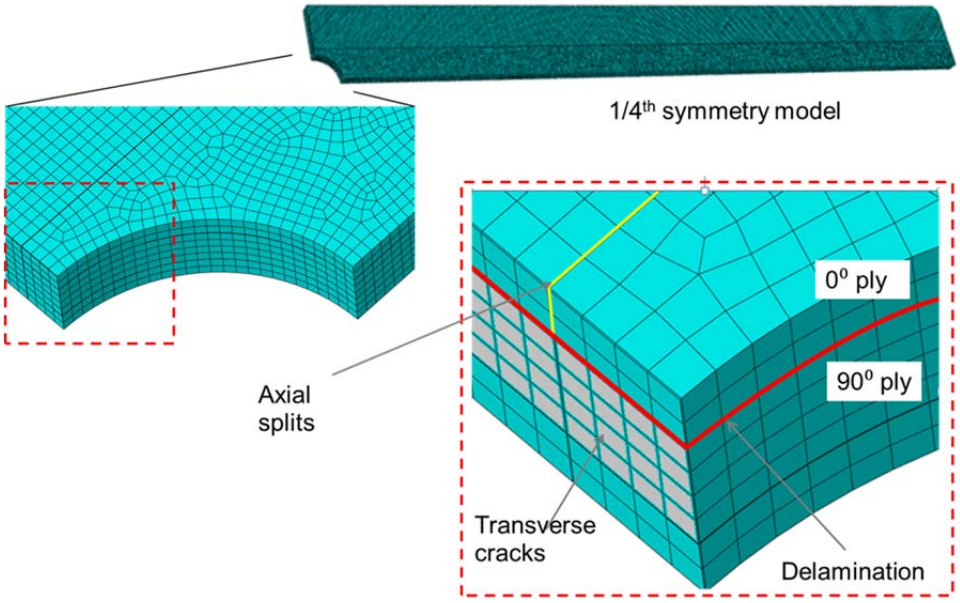


Figure 6.4 Quarter symmetry model highlighting dominant damage modes. Axial splits (yellow line), transverse cracks (grey line) and delamination (red line).

CZE are becoming popular for modelling subcritical damage and delamination in composites. The elements used in this study are discrete elements of ideally zero thickness that ensure perfect bonding between initially coincident nodes. Their constitutive behaviour follows a bi-linear traction separation law shown in Figure 6.5.

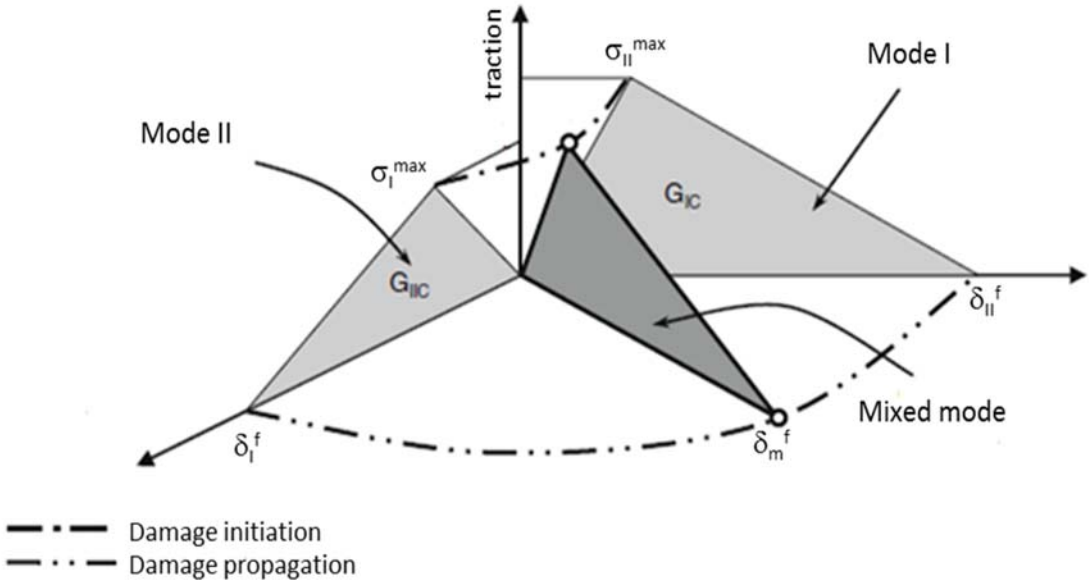


Figure 6.5 Mixed mode traction displacement relationship for cohesive elements

A detailed description of the two-dimensional form of the bi-linear traction-separation curve is shown in Figure 6.6. The parameters that govern this traction-separation law are described below.

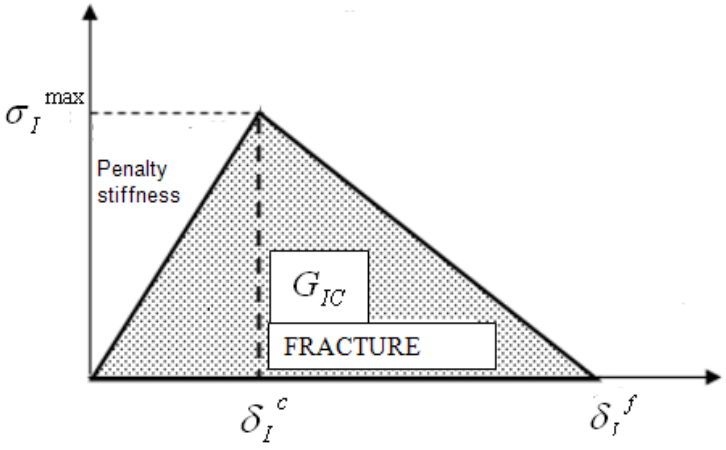


Figure 6.6 Simplified Schematic of traction separation law for mode I

- The interfacial strength $\sigma^{max}$ is the maximum separation strength that denotes the damage initiation point

- The damage onset displacement $\delta^c$ is the displacement related to σmax
- Maximum opening displacement $\delta^f$ is the point of absolute decohesion of surfaces
- Strain energy release rate $G_{IC}$ is equal to the energy required to create a unit area of a newly fully formed crack and equals the area under the graph.
- Penalty stiffness K is the initial stiffness of the cohesive law and represents the stiffness of the interface where the crack will form.Ideally this value should be infinitely high in order to ensure perfect bonding between the surfaces but care should be taken since a very high value can introduce compliance problems in the system.

An analytical approach successfully used by [128] indicates that the ratio of the transverse modulus of the surrounding material (matrix) and its thickness is adequate to calculate the cohesive-zone stiffness. This is given by the following relation.

$$K=E_{33}/t$$

Based on this relation, a value of interface stiffness of $9.1x10^{15}$ N/m$^3$ was used in this study, assuming an interface thickness of 10 μm. The application of CZE requires a detailed discretization. The number of elements $N_e$ in the cohesive-zone is determined according to $N_e=l_{cz}/l_e$ given in [129], where $l_{cz}$ is the length of cohesive-zone and $l_e$ is the mesh size in the direction of crack propagation. Cohesive elements of size 0.25 mm x 0.25 mm with thickness of 10 μm were defined for computationally effective simulations.

In order to account for mode mix, the mixed mode damage onset displacement and interfacial strength are introduced. The damage onset criterion is given by the following quadratic relation:

$$\sqrt{\left[\frac{\max(\sigma_I,0)}{\sigma_I^{max}}\right]^2+\left[\frac{\sigma_{II}}{\sigma_{II}^{max}}\right]^2}=1$$

The damage evolution criterion is given by the following power law energy failure criterion:

$$\left[\frac{G_I}{G_{IC}}\right]^a + \left[\frac{G_{II}}{G_{IIC}}\right]^a = 1$$

Where a takes values between 1 and 2 and is a parameter derived from mixed mode tests. $G_{IC}$, $G_{IIC}$ are the critical energy release rates for Modes I, II respectively. Table 6.2 summarises the properties of the plies as well as the CZE properties used for damage modelling under quasistatic conditions.

Table 6.2 T700/LTM45 individual ply properties (1 = fibre direction)
Nominal thickness 0.128mm [130-131]

**Elastic properties**

| $E_{11}$ | $E_{22}= E_{33}$ | $G_{12}= G_{13}$ | $G_{23}$ | $v_{12}=v_{13}$ | $v_{23}$ |
|---|---|---|---|---|---|
| 127GPa | 9.1GPa | 5.6GPa | 4GPa | 0.32 | 0.4 |

**CZE properties**

| $G_{Ic}$ | $G_{IIc}$ | a | $\sigma_I^{max}$ | $\sigma_{II}^{max}$ |
|---|---|---|---|---|
| 0.14N/mm | 1N/mm | 1 | 60MPa | 90MPa |

The optimum element size, required for convergence, was investigated initially by considering only one element with two plies and a cohesive zone in the middle. Following that, a real life model was built as shown in Figure 6.7 but with only delamination damage mode. Figure 6.7 shows a convergent study with fully damaged elements (SDEG=1). The term SDEG refers to the stiffness degradation variable tha the explicit regime of Abaqus 6.11 uses.

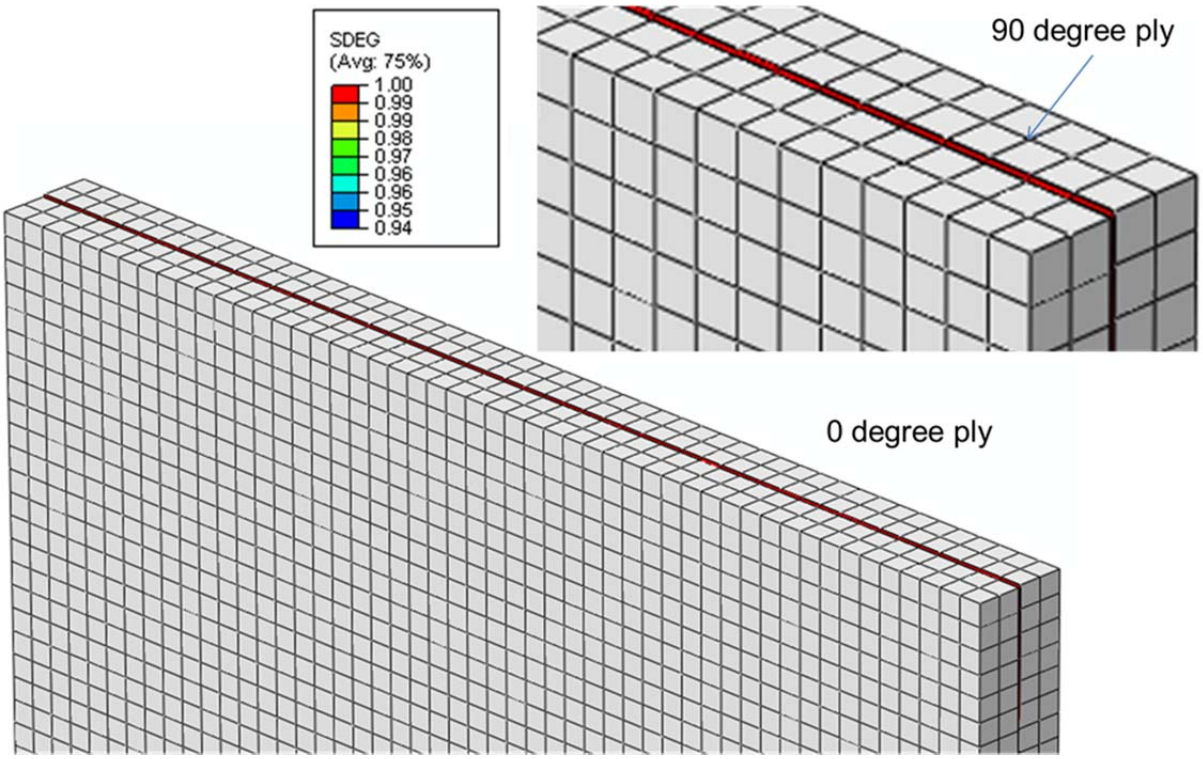


Figure 6.7 Interlaminar delamination of quasistatic model

It was proven, that convergence occurs when using an element size of 0.25mm which is twice the laminate thickness, and agrees with relevant literature. This resulted in a uniform damage pattern along the length of the specimen as shown in

Figure 6.8. The problem size was equivalent to 270090 elements. It has to be noted that 213928 linear hexahedral solid elements C3D8R were used to model the composite while 56162 linear hexahedral cohesive elements of type COH3D8 were used to model the delamination zone.

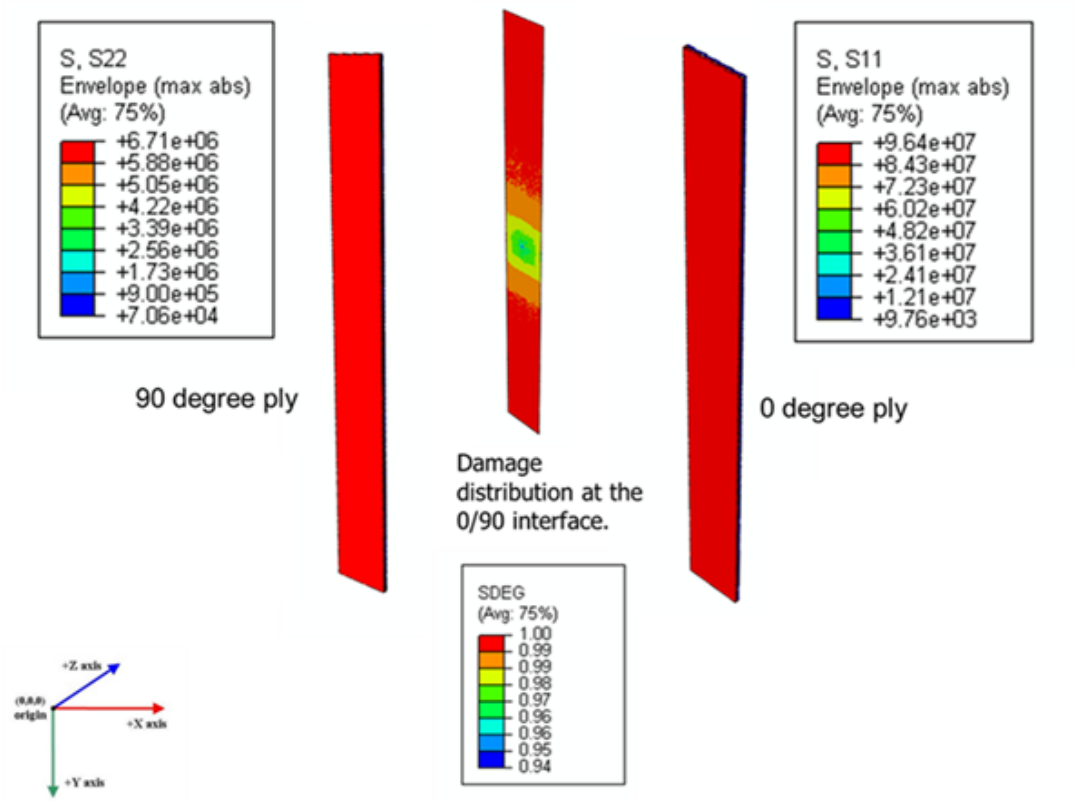


Figure 6.8 Damage distribution and principal stress values during delamination.1 refers to y direction

Due to the size of the problem, as well as the damage (non-linearity) the Abaqus explicit solver was chosen. The drawback of the explicit solver is the analysis time. For that reason an additional option of the mass scaling was investigated. With mass scaling the mass density of the material is artificially increased from $\rho$ to $\rho'$.

As a result the wave speed is decreased. The wave speed of the material is given by

$$Vc=\sqrt{\frac{E}{\rho}}.$$

Decreasing the wave speed, results in a higher step time in the analysis, and as a result a lower computational time. The relationship between the step time and wave speed is given by the following equation:

$$\Delta t = \frac{\text{Element\_size}}{Vc}$$

A mass scaling option of 80 resulted in a 50% decrease of the computational time which was 6 days and 16 days for 0.25 and 0.1mm minimum element size respectively. It should be noted that the value of 80 was not chosen arbitrarily. When mass scaling option is used, the criterion that validates that not an excessive value is used, is the kinetic energy of the model. If the kinetic energy is a fraction of the total energy, approximately 10% or less, then the analysis is acceptable. In our case it was 7.89%. Higher values can introduce inertia effects and a static analysis is by definition nonexistent. Up to this date mass scaling option is not feasible for dynamic effects. In Figure 6.9 the normal and shear stress distributions in the plies can be seen.

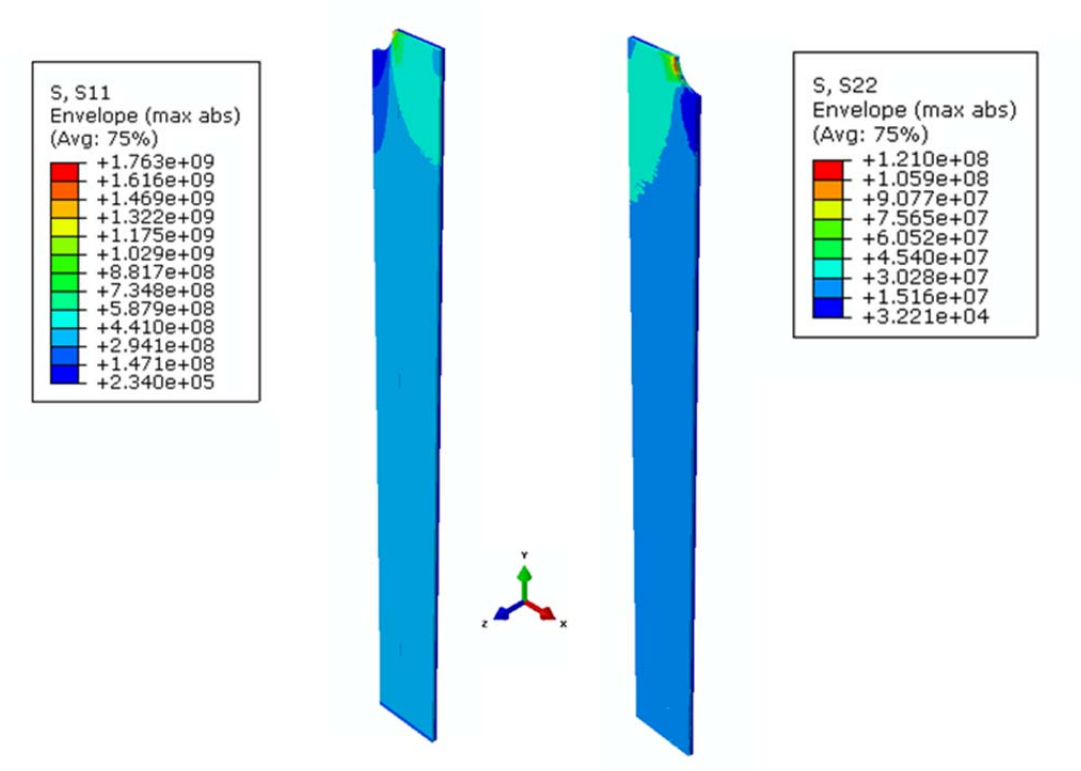


Figure 6.9 Normal (for the 0 degree ply) and shear (for the 90 degree ply) stress distributions in the 1/8$^{th}$ symmetry model.

## 6.4 Experimental Validation

A global behaviour correlation between the experimental and numerical model can be seen in the force vs displacement graph in Figure 6.10. The force vs displacement graph is used to compare the numerical and experimental results instead of the stress-strain graph. The reason is that the stress distribution is not uniform in the specimens containing a hole but is approximately 3 times higher in the areas of stress concentration. The stiffness predicted from the numerical model (FEA) is very close to experimentation (EXPERIMENT).The initial part of the graph follows well the experimentation. Non-linearities in the plot arising from damage, such as matrix cracks, axial splits and delamination.

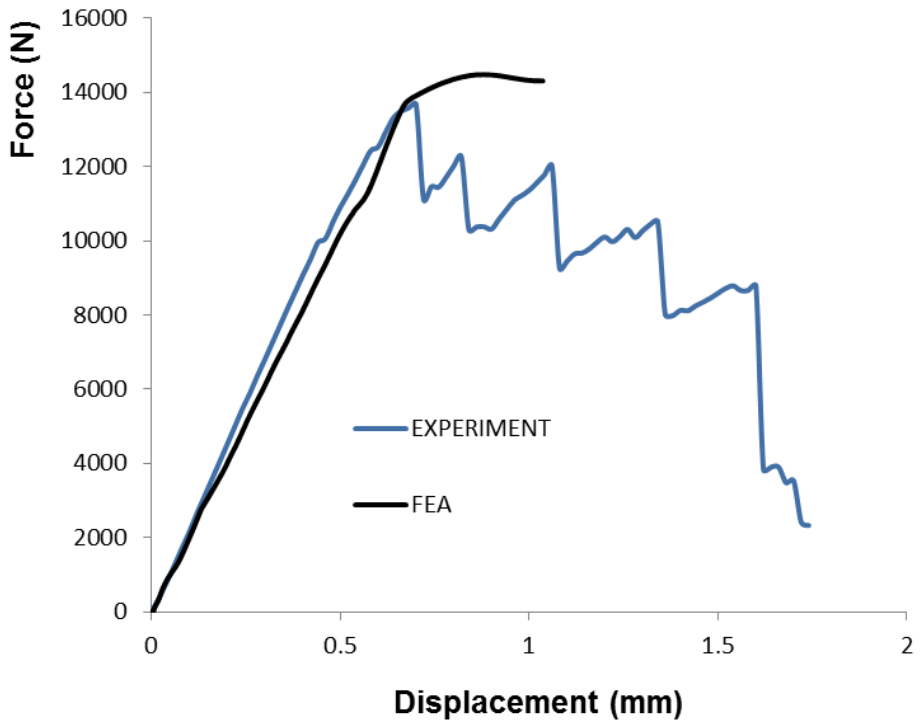


Figure 6.10 Stress-strain graph for experimentation and numerical results.

The damage initiation and progressions was investigated in an area close to the hole, as seen in Figure 6.11.The main reasons were a) the stress distribution in the section away from the notch is uniform as it can be seen in the previous figures, (b)

is the region of interest. In Figure 6.12 the damage progression is visualised by removing the plies.

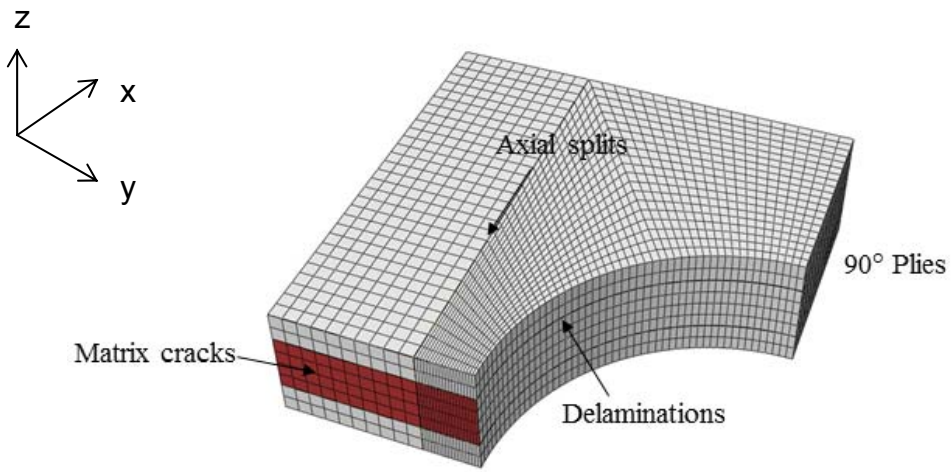


Figure 6.11 One-quarter model of central section of specimen. Individual partitions for insertion of CZE are shown for each different damage mode.

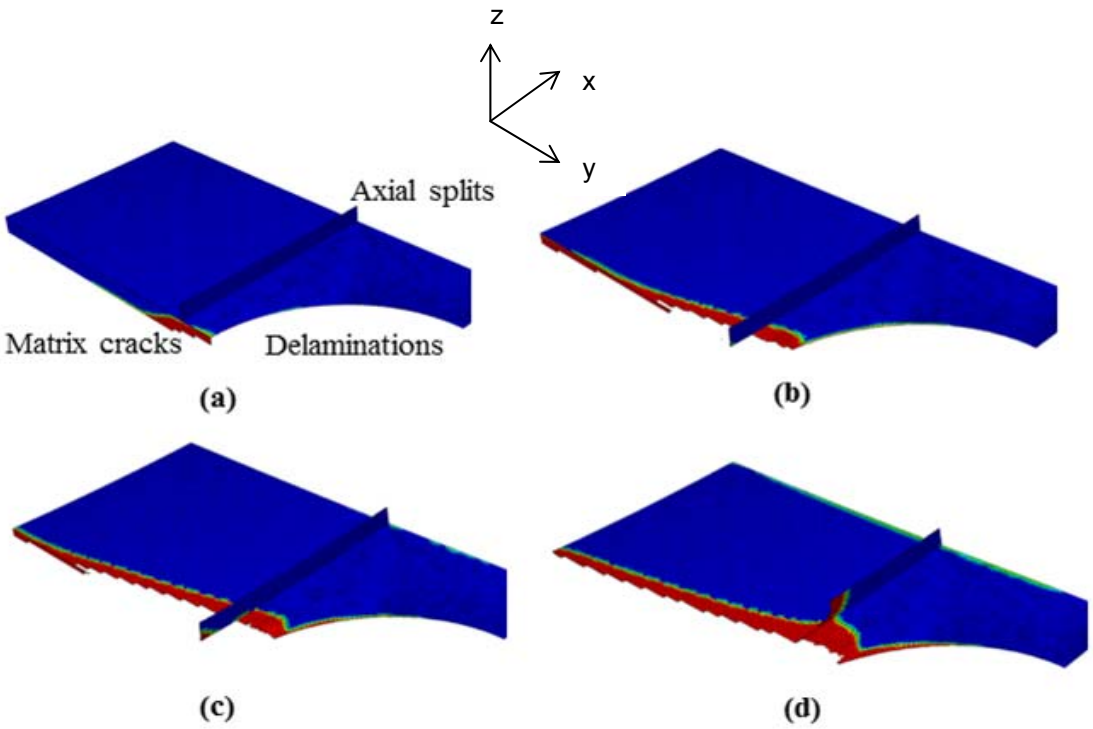


Figure 6.12 Isolated CZE sections highlighting damage progression in notched area

The damage scenarios are as follows:

1. Isolated damage at the hole edge due to matrix cracking in the 90 degree plies. The above was reinforced by inner delamination at the interfaces that propagated towards the middle of the hole in a clockwise manner.
2. Almost simultaneously generation of 0 degree splits occurred that increased in length but always adjacent to the hole.
3. Damage propagated across the width of the specimen in the form of delamination.

In the model above, key decisions were made that were included in the dynamic problem.

a) The usual practise in modelling composites is to use the lamina material model which assigns properties to each ply and allows a detailed examination of through thickness property distributions. However, since the configuration is crossply ($0_4/90_8/0_4$) and interlaminar stresses occur only at the interfaces a ply by ply modelling strategy would only increase computational time and geometric complexity.

b) After the insertion of the CZE, at predetermined areas that were identified experimentally, it was revealed that the element size required for convergence was 0.25mm which is double the thickness of each individual ply. What that means is that if the lamina material model was used, which assigns 1 element through the thickness of the ply, it would be compulsory to have an element size half of what is required for convergence and therefore the computational cost would increase.

## 6.5 Dynamic Damage Model

An important element of the successful simulation of damage lies in the cohesive zone properties. Although quasistatic numerical and experimental results agree there is question about whether the same properties should be used under dynamic conditions. Two papers relevant to this subject were found. One experimental and one numerical. According to [132], at very high rates of strain the structure responds in a local mode and the magnitude of the energy dissipated in mechanisms such as delamination may become important. However extensive testing undertaken by the author on carbon fibre/epoxy composites showed that the Mode I interlaminar toughness does not vary with strain rate. More specifically for epoxy resins it was proved that they do not exhibit a significant rate-dependent behaviour whereas tougher systems such as the latest generation of thermoplastic-based composites do.

Numerical work on the subject has also been performed [133]. A rate independent cohesive law using static fracture toughness was assumed for dynamic crack growth, which had been shown to be sufficient in previous dynamic fracture studies [134-135]. Based on the above two findings, and the fact that in the experimental test undertaken the velocities are much less than 10m/s (1.48m/s) it could be assumed that the problem lies in the low dynamic range. So, modelling of the specimen under dynamic conditions containing all the damage modes was carried out.

Initial modelling resulted in 88hrs of running time for half of the analysis with 4X6 core processors. The whole specimen is meshed with a mesh of 0.25 mm which of course increased the computational time which significantly depends on the minimum element size. For that reason, half symmetry conditions were implemented for the hammer and specimen. In that way, the calculation time for each step will be reduced significantly. Symmetry conditions (x-symmetry) were applied also at the rest of the assembly so number of elements involved was halved. Further reduction of mesh at areas of hammer that were not involved in the contact were further involed.

As it has been said before, the total running time is mainly based on the minimum element size which could not be altered. An overall decrease of 23% in time was achieved. It has to be noted that a mass scaling option could not be used since in transient problems altering the density can result in problems with the wave propagation results in a wrong estimation of the reaction forces.

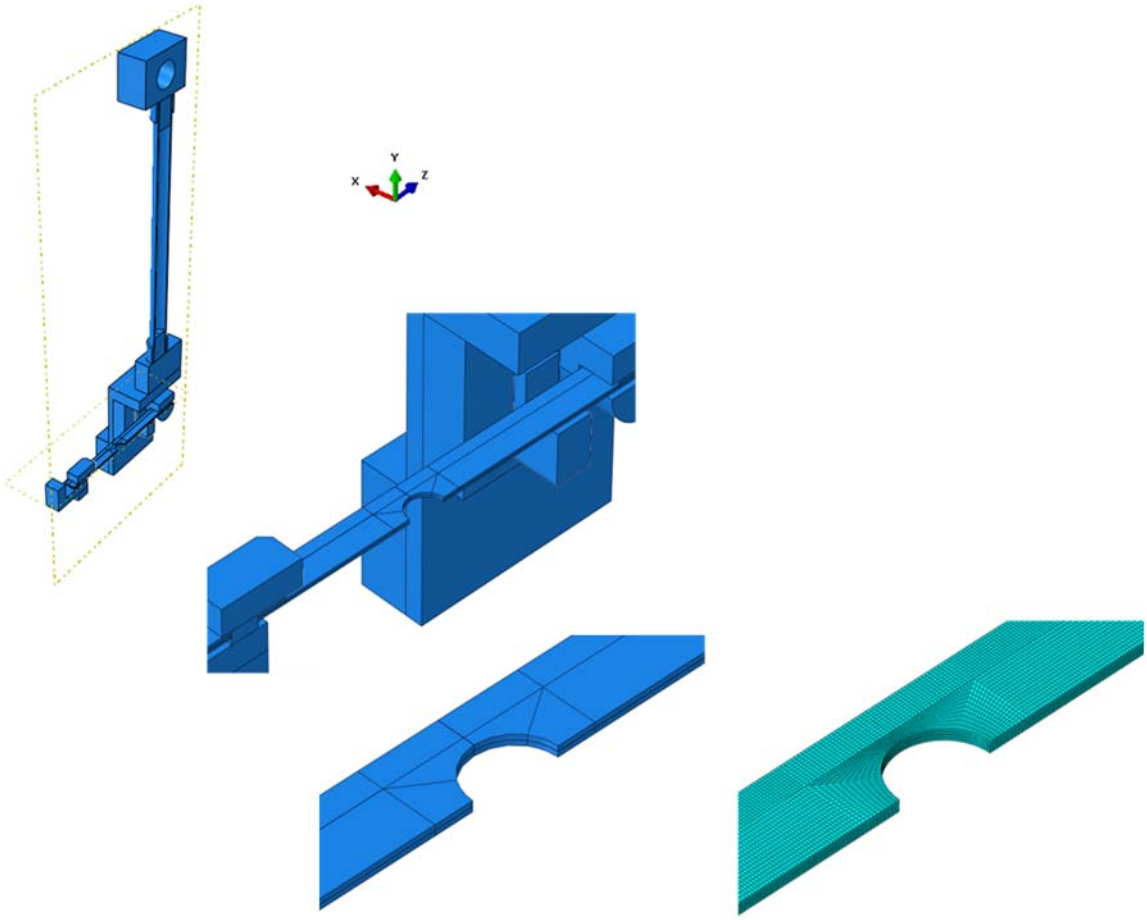


Figure 6.13 X-symmetry conditions for hammer-specimen assembly

Initial results of a single impact of a specimen that contained all the damaged modes revealed identical results (force-time response) to the virgin specimen. For that reason, manipulation of the cohesive zone parameters (CZP) was undertaken to investigate the effect on the overall stiffness response of the system. More specifically, 5 parameters were modified: the penalty stiffness, $G_I/G_{II}$ ratios and the $\sigma_I,\sigma_{II}$ ratios.

Table 6.3 Parametric study of input data for CZP

| | $\sigma_I$ (MPa) | $\sigma_{II}$ (MPa) | $G_I$ (J/m$^2$) | $G_{II}$ (J/m$^2$) | K(N/m) |
|---|---|---|---|---|---|
| **Model 1** | 60 | 90 | 140 | 1000 | $9.1x10^{15}$ |
| **Model 2** | 30 | 45 | 140 | 1000 | $9.1x10^{15}$ |
| **Model 3** | 120 | 180 | 140 | 1000 | $9.1x10^{15}$ |
| **Model 4** | 60 | 90 | 70 | 500 | $9.1x10^{15}$ |
| **Model 5** | 60 | 90 | 70 | 250 | $9.1x10^{15}$ |
| **Model 6** | 60 | 90 | 140 | 1000 | $9.1x10^{16}$ |

The output of the parametric studies revealed minimal impact on the force time response i.e., the stiffness of the system. Manipulating the damage initiation parameters resulted in an increase/decrease of time required for damage to form. Reducing damage initiation values, keeping the same stiffness and damage evolution parameters had as a result a belated complete decohesion of the surfaces but the damage pattern sequence was not influenced significantly. Reducing damage propagation value, keeping the rest of the parameters the same had as a result an earlier complete decohesion of the cohesive zone. It has to be noted that when the stiffness was increased by an order of magnitude, (Model 6), the damage pattern was erratic and was not representing reality.

Overall, the damage pattern/sequence was initiating from the ends of the specimen and was moving towards the middle of the specimen as shown in Figure 6.14. In this figure the composite plies have been removed and only the CZE are shown. Matrix cracks and axial splits are barely damaged to the contrary to the delamination zone which presents to be the dominant damage mode (Mode II). The in plane shear stresses that in real life are responsible for this delamination are shown in Figure 6.15.

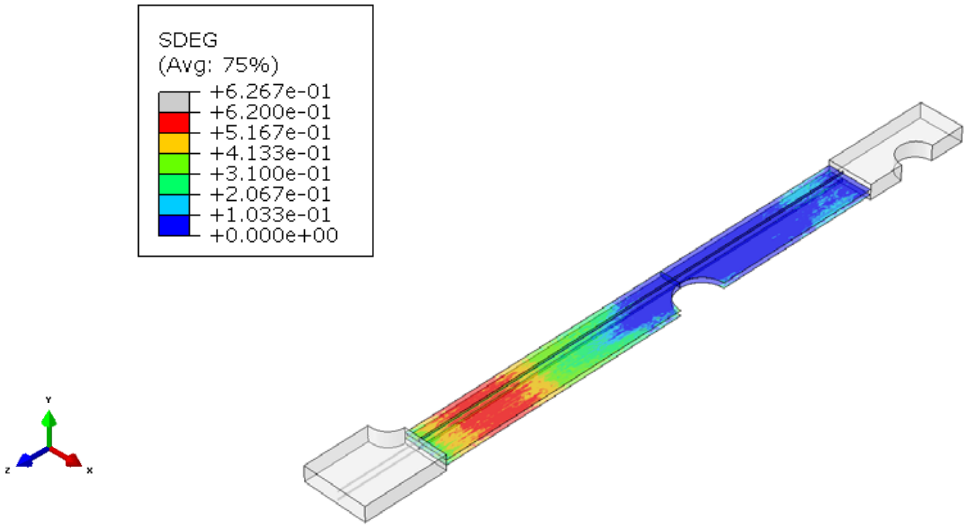


Figure 6.14 Damage pattern at the final stage of the analysis t=1.5ms

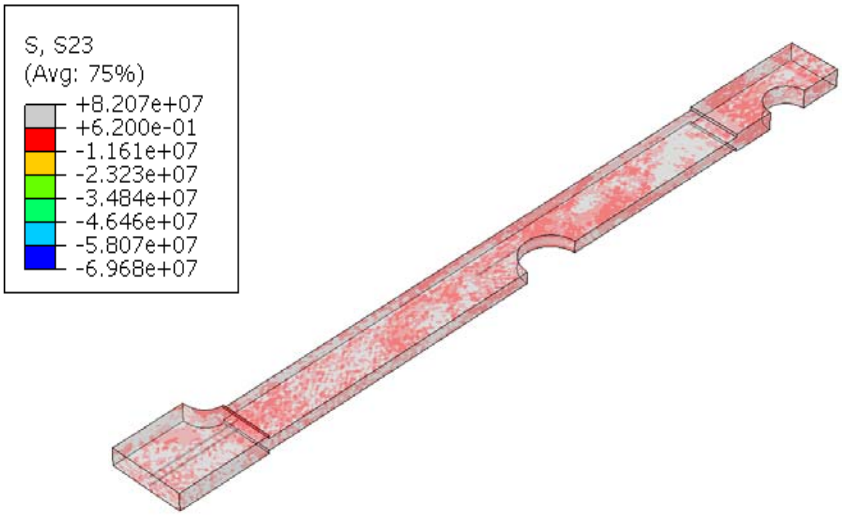


Figure 6.15 Shear stress pattern at final stage of damage

The evolution of damage at percentages of duration of the impact is shown in the following figure.

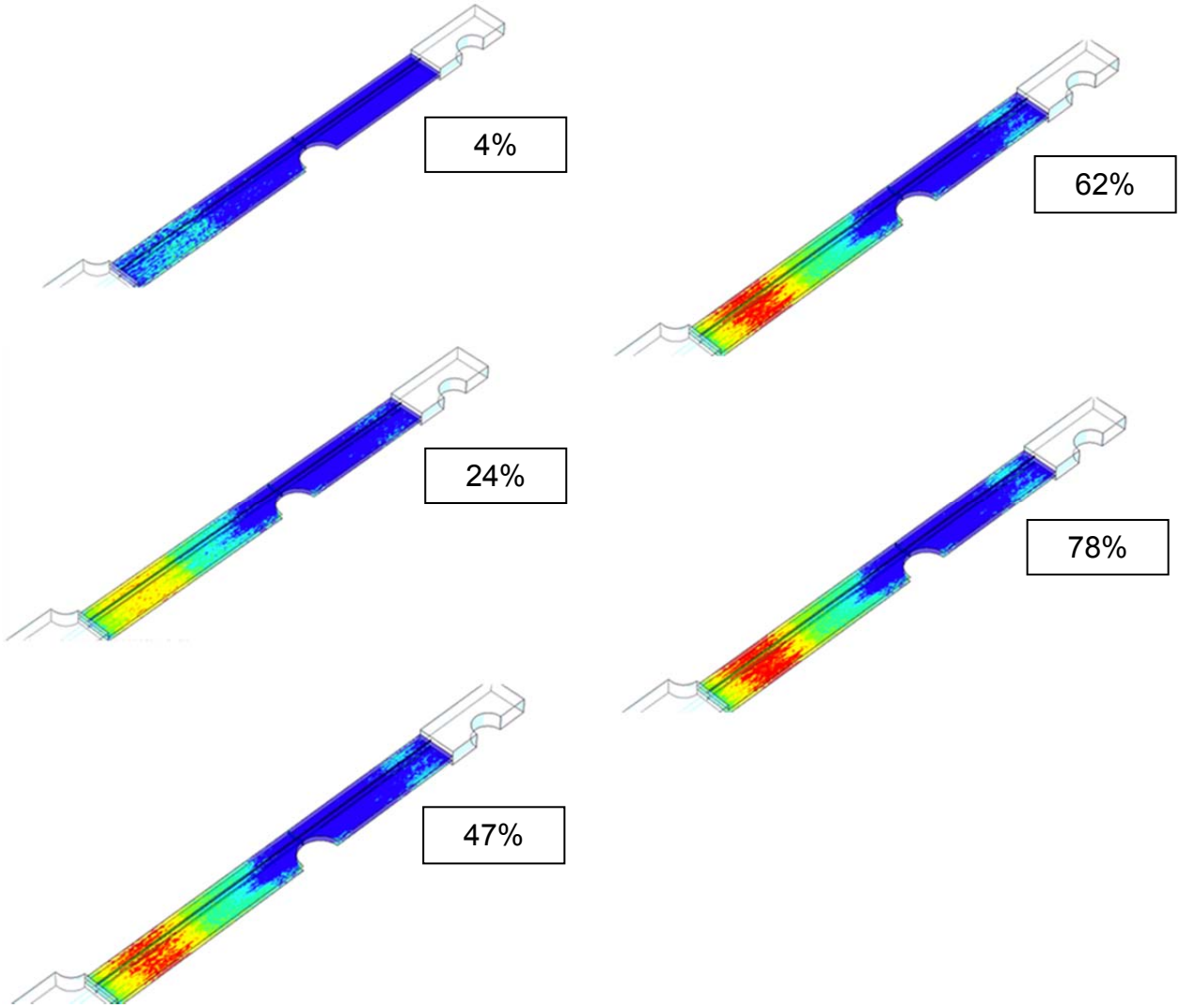


Figure 6.16 Damage evolution at percentages of the impact duration for t=1.5ms

In model 1 (Figure 6.14), an island formation of damage was observed. The fact damage is not continuous initially was perceived to be an element size problem. For that reason multiple models were built, substantially decreasing the mesh from 0.25mm to 0.1mm. The non-continuous damage formation was still apparent. An analytical calculation based on minimum step time required for convergence was undertaken to investigate if the mesh was the issue. It was revealed that this was not the case. The 2 possible problems were a) the explicit algorithm, b) multiple stress wave reflections. Regarding the explicit algorithm studies have showed that although is highly favourable in non linear problems due to convergence accuracy, the very detailed interpolation could result is a scatter in the stress patterns. More specifically,

the explicit dynamic analysis of Abaqus utilises an explicit time integration scheme which requires minor time increments to be implemented for the accurate convergent solution. These intervals solely depend on the highest natural frequency of the structure. In dynamic problems, and in general in non-linear problems, the highest frequency of the model will continually change which influences the stability limit i.e., the value of the minimum time increment. During automatic time incrementations, as with our case, accurate capturing of the dynamic stress wave depends on this time increment. This proved to be the problem that resulted in a non-uniform damage pattern. This argument can further be reinforced by the analysis of Section 5.3.2 in Figure 5.7 where due to the sudden imposing of the load, elastic stress-waves were generated and propagated in different directions in the aluminium specimen in a scattered manner.

Regarding the multiple stress wave reflections it could be said that due to dynamic loading the stress waves interacting with the natural frequencies of the material are producing concentrated strain areas, while in the static case at the same force level the strain contour is uniform.

The fact that the damage is not influencing the stiffness response means that all the load is being taken by the ply. The subcritical damage investigation undertaken is being carried out in the matrix. All the damage modes that are being represented by cohesive zone elements are being given matrix properties. The specimen is loaded in the fibre direction while the damage investigation using CZM is considering damage within the matrix (delamination, matrix cracks, axial splits). The entire load is therefore been taken predominantly by the fibres in the 0 degree direction.
Commenting on
Figure 6.16, on the evolution of damage, it could be said that is quite symmetric with respect to top and bottom plies. The largest evolution happens up to half life of the impact while after the peak force has been reached the damage scenarios remain relatively constant. It is worth commenting on the fact that the matrix cracks as well as the axial splits present minimum damage scenarios. Quantificantion of damage could be done in the case that island formation was not prominent.

## 6.6 Summary

In this chapter the steps required for the fulfilment of the damage modelling were presented. A 3D transient model was successfully constructed in Abaqus Explicit and the geometry and configuration of the cohesive zone was applied successfully. The cohesive zone properties used were first contrasted with the quasistatic case were the global stiffness was used as the validation parameter. Following the quasistatic case, further literature review revealed that for low dynamic range and for epoxy matrix the static cohesive zone parameters can be used. After implementation and with the aid of parametric studies focussing on the shifting of the five predominant cohesive zone parameters it was revealed that damage has negligible effect on the force time response and that altering the properties did not make any difference. The reason, stiffness response is unaltered is due to the fact that the load is being taken by the ply. The subcritical damage investigation undertaken is being carried out in the matrix. All the damage modes that are being represented by cohesive zone elements are being given matrix properties. The specimen is loaded in the fibre direction while the damage investigation using CZM is considering damage within the matrix (delamination, matrix cracks, axial splits).

# Chapter 7 Discussion

## 7.1 General

Small mistakes in design of components and structures subjected to fatigue conditions can spread at dangerous rates. In CFRP structures such as the fuselage and wings of planes could even be fatal. Applicability of long fibre CFRP, especially for aircrafts is really large because they posses tailor made properties such as: High specific tensile strength and stiffness, low speed impact strength, respectable fracture toughness and resistance to crack propagation as well as ability to get repaired. Typical damage scenarios during flight include hail impact, wind gusts as well as impact with foreign objects. These discrete damage events represent a serious threat to polymeric composites and their thin skinned components. Additionally, aircraft structures are subjected to various loading regimes during flight such as: tension, compression, bending and torsion. For example, the applied tensile stress, until yield limit, should be considered for the fuselage. Here, specific tensile strength is important. For the wings, both tensile and compressive stresses are important parameters to consider. For that reason, stiffness of the CFRP material used for the wing is crucial.

High cycle conditions are determined by speed of cruise, altitude flight loads, failure conditions. Normally are designed for a lifetime of approximately 25,000 hours which for a typical service life represents 70,000 flight hours. Damage quantificiation of the components is feasible when they are subjected to SF conditions. In industry the

way the service life is predicted, for SF conditions, is by simplifying the stress pattern by a method such as the rainflow counting tool and subsequently quantification of the cumulative damage is carried out by relations such as the P-M rule. As a result, S-N graphs are generated and based on them estimation of the fatigue life is feasible for different stress levels.

In the case of IF, a maximum stress magnitude can hardly be used as a sole parameter as the same level of this parameter can correspond to different levels of the applied energy, depending on the loading conditions, especially impact velocity [28]. Additionally, the majority of the authors in section 2.6.3 reported that crack growth rates in polymers are higher under IF than SF and that cracks propagate in a more unstable fashion. The study of impact fatigue IF started at approximately the same time as SF, however, is far less investigated especially for high cycles. The literature available is predominantly concentrated on the residual strength degradation and energy absorbing capabilities of composites subjected to a limited number of impacts under drop weight scenarios. Conclusions from single impact tests or impacts in the order of tens can not be used to predict the behaviour CFRPs under IF.

In this thesis high cycle impact fatigue experiments were carried out utilising two experimental configurations. The first experimental set-up involved an Izod tester. Although the Izod testing device is used mainly for evaluation of fracture toughness under a single impact, in our case was used for evaluation of fatigue life. Additionally, the plane of impact was perpendicular to the ply plane of the laminates. This was the first element of novelty. Moreover, the specimens contained a v-shaped notch in the mid section which was the second element of the novelty. Most of the authors that examined Izod fatigue life conducted their experiments under flexural conditions i.e., the plane of impact was parallel to the plane of the reinforcement and also their experimentation involved stress concentration free specimens.

The second experimental set-up involved a Charpy tester modified to conduct impacts but parallel to the direction of reinforcement. The specimens were subjected to dynamic loads in the longitudinal direction in the same way they would be subjected in a zero-tension SF test. The element of novelty is the research on the fatigue life of CFRP specimens under tensile dynamic condition in the low dynamic range. Additionally, contrast with an equivalent S-N graph in the future could

potentially reveal and quantify the difference between IF and SF with respect to the service life of components. It has to be noted that also numerical verification of a single tensile impact in CFRP was carried out for this test, were the force-displacent graph was used for the correlation

The following sections highlight the main findings of experimentation as well as numerical analysis which was carried out for the second experimental set-up

## 7.2 Experimentation and damage assessment

As mentioned before, in this project, two impact fatigue tests were performed. We will refer to the Izod as Izod impact fatigue test (IIFT) and to the modified Charpy as tensile impact fatigue test (TIFT).

For the IIFT, two groups of specimens were tested. The dimensions were kept the same except from the thickness which was altered in order to observe the effect on the fatigue life and contrast the reproducibility of results. The specimens were subjected to multiple impacts and the F-t response was captured using a dynamic load cell. The impact testing was terminated when specimens presented a clean cut through the mid-section were the notch was located.

As it was mentioned previously, a stress parameter could not be used to construct an S-N graph. Instead, absorbed energy was used which also agrees with relevant litearature [59].The E-Nf graphs were used to analyse the fatigue life and showed that as the impact energy decreases, the number of cycles to failure will increase in a quasi-linear fashion. A level of scatter is apparent, however, this is inevitable as fatigue is a probabilistic phenomenon. The equation of the impact-fatigue life curve can be expressed as: $y=-0.20\ln(x) + 1.946$. The results have shown that CFRP's are susceptible to rapid degradation and failure when subject to IF. Finally, is important to note that a fatigue threshold was not clearly identifiable, to the contrary to [59], making this a potential problem in designing against IF.

With respect to the TIFT, additional work was performed. The scope of the second experimentation was not only the fatigue life assessment but also detailed damaged

assessment which was carried out in frequent intervals of fatigue life with the aid of micro X-CT. In that way any residual stiffness degradation signs presented during testing could easily be attributed to the evolution of the identified damage mechanisms.

For the TIFT, two groups of specimens were tested. The dimensions were kept the same except for the thickness which was halved. The specimens were subjected to multiple impacts and the F-d, F-t response was captured using a tension-compression load cell. Additionally the strain time response was captured utilising a strain gauge at the mid-section. The impact testing was terminated when specimens presented an intra-laminar crack through the thickness of the 90 degree plies.

Analyzing the F-t response it was observed that the magnitude of the reaction force remained unaltered between initial life, half life and final life. However, at more detailed interval of life it was shown that the force presented an initial increase and then returned to the magnitude corresponding to the virgin state. The increase in the force at the very early stages of life can be attributed to a phenomenon called notch blunting. During this phenomenon the effectiveness of the notch was attenuated by the extensive longitudinal splitting that occurred. Additionally, the subquent decrease can be attributed to different distribution of strains around the hole with increasing number of cycles and damage. As damage grows, mainly the axial splits and delaminations, with number of cycles the strength of the ligaments from each side degrades.

To the contrary, the contact time, which is time required for the reaction force to return to zero, was constantly increasing. This was attributed to evolution of micro defects which propagated to form initially axial splits across the length of the specimen and tangential to the hole. With increasing number of impacts, but always having the axial splits as a driving mechanism, delamination between the free ends and the edges of the hole occurred that led to complete removal of the 90 plies which contained matrix cracks at the early stages of life.

Analyzing the F-d response i.e the absorbed energy, interestingly enough it could be said that it increases at the very last stages (above 70% of life) rather than gradually. In other words the intralaminar cracking contributes the most in the energy dissipation, while subcritical damage has a minimal effect on the global stifness.

Finally, the damage behaviour of the crossply configuration under dynamic loading could be said to be the same as with any monotonically quasistatic case with the important element being the appearance of each damage mode relative to number of cycles.

## 7.4 Numerical stress analysis and validation

As it has been mentioned in previous chapter the IF phenomenon if far less studied in comparison with SF. On top, most of the modelling work available is related to a single impact or limited number of impacts under flexural (Izod test) or through thickness (Drop weight test) conditions. The validation of the numerical work with respect to the experimentation normally takes place by comparing and contrasting reaction force-displacement, reaction force-time responses. Additionally, qualitiative and quantitative damage analysis is feasible since the level of visualisation modules in the post processors of most modelling softwares is above satisfactory.
In this work the Abaqus 6.11 modelling tool was utilised for pre and post-processing. The Abaqus explicit solver was utilised for accurate interpolation of the field quantities.
Uniaxial tensile impact model have been built in the past for examination of viscoelastic response in single lap joints by [28]. The authors utilised a 2-D model and a fracture mechanics approach because they were examining a macro crack in an adhesive between 2 CFRP plates.
In our work damage is propagating in all three directions. Damage modes such as matrix cracks, axial splits and delamination as well as their combination require a 3D model.

One may ask, why simulating the whole hammer-specimen interaction and not just replace the hammer with a concentrated load or a pressure magnitude. This could be answered in two ways. Firstly, when contact is present, the mechanisms of deformation are unique. In other words a concentrated load would result in a far more localised case while the exact determination of the impact area for the

pressure option would again be tricky. Secondly, the step input required for the force signal would be extremely difficult to duplicate and model.

In terms of mesh and boundary conditions the problem was tackled as efficiently as possible. Due to the nature of the problem and the large number of elements involved computational time was highly placed in the objectives list. Having computational efficiency in mind, initially, an aluminium specimen was used as a specimen, due to the isotropic behaviour that possesses, so at least high material non-linearity would not be present in the model. Parametric studies for the mesh convergence were undertaken and it was decided that the optimum size was 0.7mm. This decision was drawn after investigation of two factors. The force–time response and the strain-time response. The force time response was acquired for a set of elements at the area where the load cell was while the strain-time response at a central section of the specimen.

Following the calibration process using the aluminium specimen, successful modelling of the composite under investigation was the new task. Experimentally two thicknesses were tried, 2mm and 1mm. A balanced and symmetric composite [0n/90m]s configuration was used. This was decided with respect to modelling convenience. Firstly, symmetry conditions could be applied and secondly, grouping of plies was feasible. Finally, a relatively non-complex damage scenario could be investigated further on just by introducing CZE at the interfaces.

Two different modelling techniques were undertaken. A ply by ply method and a grouping method. Of course, the second method proved to be more computationally efficient. The experimental and numerical data were in agreement and this set the foundation for incorporation of damage in the numerical model which was the next main task.

Referring to modelling the damage, due the multiple novelty elements, it was decided to investigate the damage in a quasistatic scenario first. This was decided mainly on the fact that our problem lies is the low dynamic range. On top, the dynamic cohesive zone parameters were not available at the time. Since all three damage modes were about to be investigated using only CZE (Axial splits, delamination and matrix cracks), defining an accurate sweep direction path for the cohesive zone elements was crucial. The way that the opening displacements are

represented in the model for Modes I, II is by setting a sweep direction in the direction that the crack is propagating in real life. This resulted in tremendous difficulties when attempting to tie the mesh of the plies with the mesh of the cohesive zone elements. Additional problems occured when trying to establish a criterion for solution convergence. Element size is always an issue but in damage modelling could be proved to be a major factor. Through literature review and analytical calculations, based on the minimum step time, it was agreed that an element size of 0.25mm or less would result in a successful simulation of the damage propagation.

Having solved the mesh issue and the element size required for convergence it was time to implement the exact boundary conditions for the dynamic problem. All damage modes were implemented in the same way as with the quasistatic case. However, the effects that are present in the dynamic cases produced concentrated damage areas. Additionally, we were not sure whether to use the static cohesive zone parameters in the model. After a literature survey, it was decided that the problem was in the low dynamic range (speeds<10m/s) and that for epoxy material the static cohesive zone parameters could be used because they are not rate dependent in the low dynamic range. Eitherway, it was a starting point and it was proven that the cohesive zone properties did not result in a large difference. The damage pattern was proved to be extremely non-continuous with patches of damage that although were representing locations that experimentaly were prone to damage it was impossible to quantify them. The reason behind this is the explicit solver of Abaqus. During impacts in the low dynamic range the response is dominated by the impactor and composite-specimen assembly mass rather the impact velocity. In this type of dynamic response, to the contrary to high velocity tests, most of the energy is absorbed in an elastic manner and in internal damage initiation/propagation. The explicit dynamic analysis of Abaqus utilises an explicit time integration scheme which requires minor time increments to be implemented for the accurate convergent solution. These intervals solely depend on the highest natural frequency of the structure. In dynamic problems, and in general in non-linear problems, the highest frequency of the model will continually change which influences the stability limit i.e., the value of the minimum time increment. During automatic time incrementations, as with our case, accurate capturing of the dynamic stress wave depends on this time increment. This proved to be the problem that resulted in a non-uniform damage

pattern. This argument can further be reinforced by the analysis of Section 5.3.2 in Figure 5.7 where due to the sudden imposing of the load, elastic stress-waves were generated and propagated in different directions in the aluminium specimen in a scattered manner.

Finally, the fact that altering the cohesive zone parameters did not influenced the stiffness response means that the entire load is being taken by the 0 degree ply.The subcritical damage investigation undertaken is being carried out in the matrix. All the damage modes that are being represented by cohesive zone elements are being given matrix properties. The specimen is loaded in the fibre direction while the damage investigation using CZM is considering damage within the matrix (delamination, matrix cracks, axial splits). The entire load is therefore been taken predominantly by the fibres in the 0 degree direction.

# Chapter 8 Conclusions and Future work

## Conclusions

- In the Izod test the E-Nf graphs were used to analyse the fatigue life and it was revealed that as the impact energy decreases, the number of cycles to failure will increase in a quasi-linear fashion. Additionally, a fatigue limit was not clearly identifiable, making this a potential problem in designing against IF.

- A special Izod specimen (4 mm width) in necessary for the detailed X-ray micro CT to be carried out. The crack was growing substantially in the fibre direction and across the sample width causing matrix cracking and probably breaking of some fibres which act as impact wave guides since matrix cracks are propagating initially along the length of the fibres.

- For the uniaxial impact test, the experimentation undertaken showed that for 1mm thick $[0_2/90_2]$s LTM45/T700 laminates the fatigue life was approximately 10% of what it was for $[0_4/90_4]$s laminates as well as less consistent.

- Regarding the numerical validation a 3D model and a full assembly reconstruction is necessary. Firstly, when contact is present, the mechanisms of deformation are unique. A concentrated load would result in a far more localised case while the exact determination of the impact area for the pressure option would again be tricky. Secondly, the step input required for the force signal would be extremely difficult to duplicate.

- Through literature review and analytical calculations, based on the minimum step time, it was agreed that an element size of 0.25mm or less would result in a successful simulation of the damage propagation in both quasistatic and dynamic cases.

- Static cohesive zone parameters can be used in dynamic model as long as it lies in the low dynamic range (speeds<10m/s) and for epoxy matrix material.

- The subcritical damage investigation undertaken is being carried out in the matrix. All the damage modes that are being represented by cohesive zone elements are being given matrix properties. The specimen is loaded in the fibre direction while the damage investigation using CZM is considering damage within the matrix (delamination, matrix cracks, axial splits). The entire load is therefore been taken predominantly by the fibres in the 0 degree direction.

**Future work**

- **Incorporation of ply-failure criterion**

As it was observed the subcritical damage is not influencing significantly the stiffness of the structure when it is loaded uni-axially. This means that 'diluted damage' or fibre breakage and wear are needed for altering the in-plane stiffness. Diluted damage could be modelled by incorporating a failure criterion for the plies. A viable

suggestion is the Hashin 3-D criterion for long fibre composites. Abaqus database contains a 2-D failure criterion and thus a Vumat subroutine is needed.

- **Incorporation of cyclic inertia effects and cycle jump strategy**

In order to model the progressive stiffness reduction a cycle jump strategy is needed. Fatigue damage accumulation, for number of cycles greater than 10000 cannot be analysed with a cycle by cycle analysis because this would be computationally inefficient. As it has been said experimentally it was observed that a valid interval for cycle jump would be 2000 cycles.

- **Residual stiffness and progressive damage model for full characterisation of the IF phenomenon**

In this thesis, experimentally we utilised a fatigue life model, using the energy parameter in the E-Nf graph. However for full characterisation of the IF phenomenon other techniques complementary to the fatigue life models exist.
Broadly speaking a residual stiffness/strength model could be used where the reduction in strength/stiffness could be correlated with the number of cycles. In addition a progressive damage model such as the Paris law could be created for each of the damage modes, although this would prove to be extremely challenging.

## -References-

[1] J.Ekh, "Multi-fastener single lap joints in composite structures," *PhD Thesis,Royal Institute of technology, Stockholm*, 2006.

[2] J. C. Williams and E. A. Starke, "Progress in structural materials for aerospace systems," *Acta Materialia,* vol. 51, pp. 5775-5799, 11/25, 2003.

[3] Carl T. Herakovich, *Mechanics of Fibrous Composites.* John Wiley & Sons, 1998.

[4] F. L. Matthews, *Finite Element Modelling of Composite Materials and Structures.* CRC, 2000.

[5] V.V.Silberschmidt, "MSc structural integrity report," Loughborough University, 2008.

[6] J.M. Berthelot, "Transverse cracking and delamination in cross-ply glass-fibre and carbon-fibre reinforced plastic laminates: Static and fatigue loading," *Journal of Applied Mechanics Review,* vol. 56, pp. 111-147, 2003.

[7] Y. Qingda and B. Cox, "Cohesive models for damage evolution in laminated composites," *International Journal of Fracture,* vol. 133, pp.107-137, 2005.

[8] Ramesh R. Talreja, "Damage Mechanics and Fatigue Life Assessment of Composite Materials," *International Journal of Damage Mechanics,* vol. 8, pp. 339-354, 1 October 1999.

[9] K.W. Garrett and J.E. Bailey, "Multiple transverse fracture in 90° cross-ply laminates of a glass fibre-reinforced polyester," *Journal of Materials Science,* vol. 12, pp.157-168, 1977.

[10] L. Boniface, P.A. Smith, M.G. Bader, and A.H. Rezaifard, "Transverse Ply Cracking in Cross-Ply CFRP Laminates--Initiation or Propagation Controlled?"*Journal of Composite Materials,* vol. 31, pp. 1080-1112, 1997.

[11] A.L. Highsmith and K.L. Reifsnider, "Stiffness reduction mechanisms in composite laminates," *ASTM Digital Library,* vol. 775, pp. 103-117, 1982.

[12] S.G. Lim and C.S. Hong, "Prediction of transverse cracking and stiffness reduction in cross-ply laminated composites," *Journal of Composite Materials,* vol. 23, pp. 695-713, 1989.

[13] D. Flaggs, "Prediction of tensile matrix failure in composite laminates," *Journal of Composite Materials,* vol. 19, pp. 29-50, 1985.

[14] Z. Hashin, "Analysis of cracked laminates: a variational approach," *Journal of Mechanics of Materials,* vol. 4, pp. 121-136, 1985.

[15] R. Talreja, "Modeling of damage development in composites using internal variables concepts," *Damage Mechanics in Composites ASME,* vol. 12, 1987.

[16] E.A. Armanios, "Interlaminar fracture of composites," *Key Engineering Materials,* vol. 37, 1991.

[17] A.S.D. Wang, N.N. Kishore, and C.A. Li, "Crack development in graphite-epoxy cross-ply laminates under uniaxial tension," *Composites Science and Technology,* vol. 24, pp. 1-31,1986.

[18] S.R. Hallett, B.G. Green, W.G. Jiang, and M.R. Wisnom, "An experimental and numerical investigation into the damage mechanisms in notched composites," *Composites Part A: Applied Science and Manufacturing,* vol. 40, pp. 613-624, 2009.

[19] M.R. Wisnom and F.K. Chang, "Modelling of splitting and delamination in notched cross-ply laminates," *Composites Science and Technology,* vol. 60, pp. 2849-2856, 2000.

[20] S.R. Hallett, W.G. Jianga, B. Khana, and M.R. Wisnom, "Modelling the interaction between matrix cracks and delamination damage in scaled quasi-isotropic specimens," *Composites Science and Technology,* vol. 68, pp. 80-89, 2008.

[21] S.W. Tsai and E.M. Wu, "General Theory of Strength for Anisotropic Materials," *Journal of Composite Materials,* vol. 5, pp.58-80, 1971.

[22] Z. Hashin, "Failure Criteria for Unidirectional Fiber Composites," *Journal of Applied Mechanics,* vol. 47, pp. 329-334,1980

[23] J. Schijve et al., *Fatigue of Structures and Materials.* Academic publishers, 2004.

[24] R. D. Adams, *Adhesive Bonding: Science, Technology and Applications.* Egully.com, 2005.

[25] J.P Casas-Rodriquez, "Damage in adhesively bonded joints: sinusoidal and impact fatigue," *Loughborough University,* December 2008.

[26] W. Van Paepegem and J. Degrieck, "A new coupled approach of residual stiffness and strength for fatigue of fibre-reinforced composites," *Int. J. Fatigue,* vol. 24, pp. 747-762, 2002.

[27] J. R. Schaff and B. D. Davidson, "Life Prediction Methodology for Composite Structures. Part I—Constant Amplitude and Two-Stress Level Fatigue," *Journal of Composite Materials,* vol. 31, pp. 128-157, January 01, 1997.

[28] V.V.Silbercshmidt , J.P Casas-Rodriquez, and I.A.Ashcroft, "Impact fatigue in adhesive joints," *Journal of Mechanical Engineering Science*,vol. 222,pp. 1981-1994, 10,2008.

[29] T.E. Stanton and L. Bairstow, "The resistance of materials to impact", *Proc. Inst. Mech. Engrs*, pp.889-919, 1908.

[30] A.A. Johnson and D.N. Keller,"The impact fatigue properties of pearlitic plain carbon steels", *Fatigue Engng.Mater.Struc,*vol. 4, pp. 279-285, 1981

[31] A. Johnson, "Impact Fatigue-An Emerging Field of Study," *Engineering Integrity,* vol. 15, pp. 14-20, 2004.

[32] J. Yu, P. K. Liaw and M. Huang, "The impact-fatigue fracture of metallic materials," *JOM Journal of the Minerals, Metals and Materials Society,* vol. 51, pp. 15-18, 1999.

[33] T. Tanaka, H. Nakayama and K. Kimura, "On the impact crack growth behaviour of metallic materials," *Fatigue & Fracture of Engineering Materials & Structures,* vol. 8, pp. 13-22, 1985.

[34] K. J. A. R. Mukarami. *Soc. Mater. Sci. Japan 31,* pp. 690,1982.

[35] T. Tanaka, K. Kinoshita and H. Nakayama, "Crack opening behavior near crack tip in impact fatigue," *Int. J. Fract.,* vol. 29, pp. 39-44, 1985.

[36] M. Niinomi, K. Uwai, T. Kobayashi and A. Okahara, "Impact fatigue properties of epoxy resin filled with SiO2 particles," *Eng. Fract. Mech.,* vol. 38, pp. 439-449, 1991.

[37] T. Tanaka, K. Kinoshita and H. Nakayama, "Effect of loading time on high-cycle range impact fatigue strength and impact fatigue crack growth rate," *JSME International Journal.Ser.1, Solid Mechanics, Strength of Materials,* vol. 35, pp. 108-116, 1992.

[38] G.C. Adams, "Impact fatigue of polymers using an instrumented drop Tower Device," *Instrumented Impact Testing of Plastics and Composite Materials*, S.L. Kessler, G.C. Adams, S.B. Driscoll, and D.R. Ireland, Ed. ASTM ST, 1987, pp 281-301.

[39] I. Yamamoto, T. Higashihara and T. Kobayashi, "Effect of silica-particle characteristics on impact/usual fatigue properties and evaluation of mechanical characteristics of silica-particle epoxy resins," *JSME International Journal Series A,* vol. 46, pp. 145-153, 2003.

[40] Gomaa A.I., Hamdy A.H. and A. Moet, "Subcritical crack propagation under cyclic stress impulse," *Int. J. Fract.,* vol. 53, pp. 187-199, 1992.

[41] G. Marsh, "Forceful measures," *Reinforced Plast.,* vol. 48, pp. 36-39, 2004.

[42] B. Harris, *Fatigue in Composites: Science and Technology of the Fatigue Response of Fibre-Reinforced Plastics.* Woodhead Publishing, 2003.

[43] T. Sınmazçelik, A. A. Arıcı and V. Günay, "Impact–fatigue behaviour of unidirectional carbon fibre reinforced polyetherimide (PEI) composites," *J. Mater.Sci.,* vol. 41, pp. 6237-6244, 2006.

[44] K. Bijoysri, R. Rao and N. Venkataraman, "Low velocity impact fatigue studies on glass epoxy composite laminates with varied material and test parameters-effect of incident energy and fibre volume fraction," *J Reinf Plast Compos,* vol. 14, pp. 1150-1159, 1995.

[45] R. Roy, B. Sarkar, A. Rana and N. Bose, "Impact fatigue behaviour of carbon fibre-reinforced vinylester resin composites," *Bull. Mater.Sci.,* vol. 24, pp. 79-86, 2001.

[46] Q. Yuan, K. Friedrich and J. Karger-Kocsis, "Low-energy charpy impact of interleaved CF/EP laminates," *Applied Composite Materials,* vol. 2, pp. 119-133, 1995.

[47] B. Schrauwen and T. Peijs, "Influence of matrix ductility and fibre architecture on the repeated impact response of glass-fibre-reinforced laminated composites," *Applied Composite Materials,* vol. 9, pp. 331-352, 2002.

[48] M. V. Hosur, S. M. Waliul Islam, U. K. Vaidya, A. Kumar, P. K. Dutta and S. Jeelani, "Dynamic punch shear characterization of plain weave graphite/epoxy composites at room and elevated temperatures," *Composite Structures,* vol. 70, pp. 295-307, 2005.

[49] M. V. Hosur, S. M. Islam, U. K. Vaidya, P. K. Dutta and S. Jeelani, "Experimental studies on the punch shear characterization of satin weave graphite/epoxy composites at room and elevated temperatures," *Materials Science and Engineering A,* vol. 368, pp. 269-279, 2004.

[50] M. J. Hiley, L. Dong and J. Harding, "Effect of strain rate on the fracture process in interlaminar shear specimens of carbon fibre-reinforced laminates," *Composites Part A,* vol. 28, pp. 171-180, 1997.

[51] J. M. Lifshitz and H. Leber, "Response of fiber-reinforced polymers to high strain-rate loading in interlaminar tension and combined tension/shear," *Composites Sci. Technol.,* vol. 58, pp. 987-996, 1998.

[52] M. V. Hosur, A. Abraham, S. Jeelani and U. K. Vaidya, "Studies on the Influence of Through-the-Thickness Reinforcement on Low-Velocity and High Strain Rate Response of Woven S2-Glass/Vinyl Ester Composite," *J. Composite Mater.,*vol. 35, pp. 1111, 2001.

[53] W. J. Cantwell, P. T. Curtis and J. Morton, "Impact and subsequent fatigue damage growth in carbon fibre laminates," *Int. J. Fatigue,* vol. 6, pp. 113-118, 1984.

[54] K. K. Stellbrink and R. M. Aoki, "Effect of defect on the behaviour of composites," *Progress in Science and Engineering of Composites,* pp. 853-860, 1982.

[55] G. Dorey, "Fracture of composites and damage tolerance," *AGARD Pract.Considerations of Design, Fabric.and Tests for Composite Mater.12,* 1982.

[56] T. Yuanjian and D. H. Isaac, "Combined impact and fatigue of glass fiber reinforced composites," *Composites Part B: Engineering,* vol. 39, pp. 505-512, 2008.

[57] D. A. Wyrick and D. F. Adams, "Residual strength of a carbon/epoxy composite material subjected to repeated impact," *J. Composite Mater.,* vol. 22, pp. 749, 1988.

[58] Y. Q. Ding, Y. Yan and R. McIlhagger, "Effect of impact and fatigue loads on the strength of plain weave carbon-epoxy composites," *J. Mater. Process.Technol.,* vol. 55, pp. 58-62, 1995.

[59] M. O. Bora, O. Coban, T. Sinmazcelik, I. Curgul and V. Gunay, "On the life time prediction of repeatedly impacted thermoplastic matrix composites," *Mater Des,* vol. 30, pp. 145-153, 2009.

[60] O. Çoban, M. O. Bora, T. Sinmazcelik, I. Curgul and V. Gunay, "Fracture morphology and deformation characteristics of repeatedly impacted thermoplastic matrix composites," *Mater Des,* vol. 30, pp. 628-634, 2009.

[61] L. Kärger, J. Baaran, A. Gunnion and R. Thomson, "Evaluation of impact assessment methodologies. Part I: Applied methods," *Composites Part B: Engineering,* vol. 40, pp. 65-70, 2009.

[62] S. Guinard, O. Allix, D. Guédra-Degeorges and A. Vinet, "A 3D damage analysis of low-velocity impacts on laminated composites," *Composites Sci. Technol.,* vol. 62, pp. 585-589, 2002.

[63] J. P. Hou, N. Petrinic and C. Ruiz, "A delamination criterion for laminated composites under low-velocity impact," *Composites Sci. Technol.,* vol. 61, pp. 2069-2074, 2001.

[64] H. Y. Choi and F. K. Chang, "A model for predicting damage in graphite/epoxy laminated composites resulting from low-velocity point impact," *J. Composite Mater.,* vol. 26, pp. 2134, 1992.

[65] E. F. Rybicki and M. F. Kanninen, "A finite element calculation of stress intensity factors by a modified crack closure integral," *Eng. Fract.Mech.,* vol. 9, pp. 931-938, 1977.

[66] D. J. Elder, R. S. Thomson, M. Q. Nguyen and M. L. Scott, "Review of delamination predictive methods for low speed impact of composite laminates," *Composite Structures,* vol. 66, pp. 677-683, 2004.

[67] D. Xie and S. B. Biggers Jr., "Strain energy release rate calculation for a moving delamination front of arbitrary shape based on the virtual crack closure technique. Part I: Formulation and validation," *Eng. Fract. Mech.,* vol. 73, pp. 771-785, 4, 2006.

[68] M. Quaresimin, M. Ricotta, L. Martello and S. Mian, "Energy absorption in composite laminates under impact loading," *Composites Part B: Engineering*, vol. 44, pp. 133-140, 1, 2013.

[69] B. Vieille, V. M. Casado and C. Bouvet, "About the impact behavior of woven-ply carbon fiber-reinforced thermoplastic- and thermosetting-composites: A comparative study," *Composite Structures,* vol. 101, pp. 9-21, 7, 2013.

[70] P. N. B. Reis, J. A. M. Ferreira, P. Santos, M. O. W. Richardson and J. B. Santos, "Impact response of Kevlar composites with filled epoxy matrix," *Composite Structures*, vol. 94, pp. 3520-3528, 12, 2012.

[71] Kashtalyan M, Soutis C, “Stiffness degradation in cross-ply laminates damaged by transverse cracking and splitting”, *Composites Part A*, vol. 31(4), pp.335-51, 2000.

[72] Maimí P, Camanho PP, Mayugo JA, Dávila CG. “A continuum damage model for composite laminates: Part II - Computational implementation and validation. Mechanics of Materials”, vol.39(10), pp.909-19, 2007.

[73] Turon A, Davila CG, Camanho PP, Costa J, “An engineering solution for mesh size effects in the simulation of delamination using cohesive zone models. Engineering Fracture Mechanics”, vol.74(10), pp.1665-82, 2007.

[74] Wisnom MR, Hallett SR, “The role of delamination in strength, failure mechanism and hole size effect in open hole tensile tests on quasi-isotropic laminates”, *Composites Part A*, vol.40(4), pp.335-42, 2009

[75] T. Adam, N. Gathercole, H. Reiter and B. Harris, "Life prediction for fatigue of T800/5245 carbob-fibre composites: II. Variable-amplitude loading," *Int. J. Fatigue,* vol. 16, pp. 533-547, 1994.

[76] N. Gathercole, H. Reiter, T. Adam and B. Harris, "Life prediction for fatigue of T800/5245 carbon-fibre composites: I. Constant-amplitude loading," *Int. J. Fatigue,* vol. 16, pp. 523-532, 1994.

[77] M. H. R. Jen and C. H. Lee, "Strength and life in thermoplastic composite laminates under static and fatigue loads. Part II: Formulation," *Int. J. Fatigue,* vol. 20, pp. 617-629, 1998.

[78] Q. D. Yang, D. J. Shim and S. M. Spearing, "A cohesive zone model for low cycle fatigue life prediction of solder joints," *Microelectronic Engineering,* vol. 75, pp. 85-95, 2004.

[79] H. A. Whitworth, "A stiffness degradation model for composite laminates under fatigue loading," *Composite Structures,* vol. 40, pp. 95-101, 1997.

[80] W. X. Yao and N. Himmel, "A new cumulative fatigue damage model for fibre-reinforced plastics," *Composites Sci. Technol.,* vol. 60, pp. 59-64, 2000.

[81] S. Erpolat, I. A. Ashcroft, A. D. Crocombe and M. M. Abdel-Wahab, "Fatigue crack growth acceleration due to intermittent overstressing in adhesively bonded CFRP joints," *Composites Part A: Applied Science and Manufacturing,* vol. 35, pp. 1175-1183, 2004.

[82] P. C. Paris and F. Erdogan, "A critical analysis of crack propagation laws," *Journal of Basic Engineering,* vol. 85, pp. 528-534, 1963.

[83] T. L. Anderson, *Fracture Mechanics: Fundamentals and Applications.* CRC Pr I Llc, 1995.

[84] G. Irwin, "Linear fracture mechanics, fracture transition, and fracture control," *Eng. Fract. Mech.,* vol. 1, pp. 241-257, 1968.

[85] D. Gross and T. Seelig, *Fracture Mechanics: With an Introduction to Micromechanics.* Springer Verlag, 2006.

[86] D. Broek, *Elementary Engineering Fracture Mechanics.* Martinus nijhoff, 1982.

[87] J. R. Rice, "A path independent integral and the approximate analysis of strain concentration by notches and cracks," *Journal of Applied Mechanics,* vol. 35, pp. 379-386, 1968.

[88] I. Maekawa, "The influence of stress wave on the impact fracture strength of cracked member," *Int. J. Impact Eng.,* vol. 32, pp. 351-357, 2005.

[89] J. R. Rice, "Mechanics of crack tip deformation and extension by fatigue,".*ASTM STP 415, Am.Soc.Testing Mats.,pp. 247-311,* 1967.

[90] R. C. McClung, "Crack closure and plastic zone sizes in fatigue," *Fatigue & Fracture of Engineering Materials & Structures,* vol. 14, pp. 455-468, 1991.

[91] E. F. J. Von Euw, R. W. Hertzberg and R. Roberts, "Delay effects in fatigue crack propagation," *Stress Analysis and Growth of Cracks,* pp. 230-259, 1972.

[92] O. E. Wheeler, "Spectrum loading and crack growth," vol. 94, pp. 181-186, 1997.

[93] R. Krueger, "Virtual crack closure technique: History, approach, and applications," *Appl. Mech. Rev.,* vol. 57, pp. 109, 2004.

[94] F. G. Buchholz, H. Grebner, K. H. Dreyer and H. Krome, "2D-and 3D-applications of the improved and generalized modified crack closure integral method," *Comput. Mech.,* vol. 88, 1988.

[95] E. F. Rybicki, D. W. Schmueser and J. Fox, "An energy release rate approach for stable crack growth in the free-edge delamination problem," *J. Composite Mater.,* vol. 11, pp. 470, 1977.

[96] M. R. Wisnom and S. R. Hallett, "The role of delamination in strength, failure mechanism and hole size effect in open hole tensile tests on quasi-isotropic laminates," *Composites Part A: Applied Science and Manufacturing,* vol. 40, pp. 335-342, 2009.

[97] Zahid Rizwan Khokhar, "Finite-element analysis of delamination in CFRP laminates: effect of material randomness," *Loughborough University,* April 2010.

[98] D.S. Dugdale, "Yielding of steel sheets containing slits," *Journal of the Mechanics and Physics of Solids,* vol. 8, pp. 100-104, 1960.

[99] G.I. Barenblatt, "The mathematical theory of equilibrium cracks in brittle fracture," *Journal of Advances in Applied Mechanics,* vol. 7, pp. 55-129, 1962.

[100] A.C ORIFICI, I. HERZBERG, R.S THOMSON, "*Review of methodologies for composite material modeling incorporating failure* ," *Composite Structures,* vol. 86, pp.194-210, 2008.

[101] S. Sridharan, *Delamination Behaviour of Composites.*Cambridge uk: Woodhead Publishing, 2008.

[102] A. Needleman, "A Continuum Model for Void Nucleation by Inclusion Debonding," *Journal of Applied Mechanics,* vol. 54, pp. 525-531, 1987.

[103] A. Needleman, "An analysis of tensile decohesion along an interface," *Journal of the Mechanics and Physics of Solids,* vol. 38, pp. 289-324, 1990.

[104] V. Tvergaard and J.W. Hutchinson, "The relation between crack growth resistance and fracture process parameters in elastic–plastic solids," *Journal of the Mechanics and Physics of Solids,* vol. 40, pp. 1377-1397, 1992.

[105] V. Tvergaard, "Effect of fibre debonding in a whisker-reinforced metal," *Journal of Materials Science and Engineering,* vol. A125, pp. 203-213, 1990.

[106] G.T. Camacho and M. Ortiz, "Computational modelling of impact damage in brittle materials. ," *International Journal of Solids and Structures,* vol. 33, pp. 2899-2938, 1996.

[107] P. H. Geubelle and J. S. Baylor, "Impact-induced delamination of composites: a 2D simulation," *Composites Part B: Engineering,* vol. 29, pp. 589-602, 1998.

[108] Borg, R., Nilsson, L. and Simonsson, K., "Simulating DCB, ENF, and MMB experiments using shell elements and a cohesive zone model," *Composites Science and Technology,* vol. 64, pp. 269–278, .

[109] Camanho, P.P., Davila, C.G. and Pinha, S.T., "Fracture analysis of composite co-cured structural joints using decohesion elements," *Fatigue and Fracture of Engineering Materials and Structures,* vol. 27, pp. 745–757, 2004.

[110] A. Corigliano, " Formulation, identification and use of interface models in the numerical analysis of composite delamination," *International Journal of Solids and Structures,* vol. 30, pp. 2779–2811, 1993.

[111] De Borst, "Numerical aspects of cohesive-zone models," *Engineering Fracture Mechanics,* vol. 70, pp. 1743–1757, 2003.

[112] Schellekens, J.C.J. and de Borst, R., "Schellekens, J.C.J. and de Borst, R..On the numerical modeling of edge delamination in composites." *Key Engineering Materials,* vol. 121-122, pp. 131-160,1996 .

[113] Wells, G.N., De Borst, R. and Sluys, L.J., "A consistent geometrically non-linear approach for delamination."*International Journal for Numerical Methods in Engineering,* vol. 54, pp. 1333–1355, 2002.

[114] C. Hexcel, "Hexply 8552 Product data,", 2010.

[115] A. Krishnamoorthy, S. Rajendra Boopathy, K. Palanikumar and J. Paulo Davim, "Application of grey fuzzy logic for the optimization of drilling parameters for CFRP composites with multiple performance characteristics," *Measurement,* .

[116] Volume Graphics product, "Application software for analysis and visualization of industrial computer tomography/voxel data reference manual," Heidelberg-Germany, 2009.

[117] E Maire, L Babout, J Y Buffiere and R Fougeres, "Recent results on 3D characterisation of microstructure and damage of metal–matrix composites and a metallic foam using x-ray tomography," *Mat SciEng A– Struct,* vol. 319, pp. 216–219, 2001.

[118] S A Mcdonald, M Preuss, E Maire, J Y Buffiere, P M Mummery and P J Withers, "X-ray tomographic imaging of Ti/SiC composites," *J Micros – Oxford,* vol. 209 (Part 2), pp. 102–112, 2003.

[119] P M Mummery, B Derby, P Anderson, G R. Davis and J C Elliot, "X-ray mictrotomographic studies of metal–matrix composites using laboratory X-ray sources," *J Micros,* vol. 177, pp. 399–406, 1995.

[120] A Borbély, H Biermann, O Hartmann and J Y Buffiere, "The influence of the free surface on the fracture of alumina particles in an Al–Al2O3 metal–matrix composite "*Comp Mater Sci,* vol. 26, pp. 183-188, 2003.

[121] L Babout, W Ludwig, E Maire and J Y Buffiere, "Damage assessment in metallic structural materials using high resolution synchrotron X-ray tomography," *NuclInstrum Meth B,* vol. 200, pp. 303–307, 2003.

[122] I Justice, P Anderson, G Davis, B Derby and J Elliot, "Damage nucleation and growth in particle rein-forced aluminium matrix composites," *Key Eng Mat,* vol. 127–131, pp. 945–952, 1997.

[123] G Geandier, A Hazotte, S Denis, A. Mocellin and E Maire, "Microstructural analysis of alumina chromium composites by X-ray tomography and 3-D finite element simulation of thermal stresses," *Scripta Mater,* vol. 48, pp. 1219–1224, 2003.

[124] O Coban O, M. Bora, T Sinmazçelik, I Cürgül, V Günay, "Fracture morphology and deformation characteristics of repeatedly impacted thermoplastic matrix composites " *Materials &Design,* vol. 30, pp. 628-634, 2009.

[125] D D Symons, "Characterisation of indentation damage in 0/90 lay-up T300/914 CFRP " *ComposSciTechnol2000,* vol. 60, pp. 391–401, 2000.

[126] J P Dunkers, D P Sanders, D L Hunston, M J Everett and W H Green, "Comparison of optical coherence tomography, X-ray computed tomography, and confocal microscopy results from an impact damaged epoxy/E-glass composite," *J Adhesion,* vol. 78, pp. 129–154, 2002.

[127] R H Bossi and G E Georgeson, "R H Bossi and G E Georgeson, Composite structure development decisions using X-ray CT measurements, *Mater Eval*, 1995, pp. 1198–1203." *Mater Eval,* vol. 53, pp. 1198–1203, 1995.

[128] Daudeville L., Allix O., Ladeveze P, "Delamination analysis by damage mechanics: some applications," *Compos. Eng,* vol. 5, pp. 17-24, 1995.

[129] Turon A., Davila C. G., Camanho P. P., Costa J, "An engineering solution for mesh size effects in the simulation of delamination using cohesive zone models," *Eng Fracture Mech,* vol. 74, pp. 1665-82, 2007.

[130] Mehdi Barikani,Hossein Saidpour, Mutlu Sezen, "Mode-I Interlaminar Fracture Toughness in Unidirectional Carbon-fibre/Epoxy Composites," *Iranian Polymer Journal,* vol. 11, pp. 414-423, 2002.

[131] Hossein Saidpour, Mehdi Barikani and Mutlu Sezen, "Mode-II Interlaminar Fracture Toughness of Carbon/Epoxy Laminates," *Iranian Polymer Journal,* vol. 12, pp. 389-400, 2003.

[132] W.J Cantwell and J.Morton, "The impact resistance of composite materials-a review",*Journal of Composites*, vol. 22, pp.347-362, 22, 1991.

[133] B. Gözlüklü and D. Coker, "Modeling of the dynamic delamination of L-shaped unidirectional laminated composites," *Composite Structures,* vol. 94, pp. 1430-1442, 3, 2012.

[134] D. Coker, A. J. Rosakis and A. Needleman, "Dynamic crack growth along a polymer composite–Homalite interface," *J. Mech. Phys. Solids,* vol. 51, pp. 425-460, 3, 2003.

[135] C. Yu, A. Pandolfi, M. Ortiz, D. Coker and A. J. Rosakis, "Three-dimensional modeling of intersonic shear-crack growth in asymmetrically loaded unidirectional composite plates," *Int. J. Solids Structures,* vol. 39, pp. 6135-6157, 12, 2002.

[136] C. Soutis,"Fibre reinforced composites in aircraft construction", *Progress in Aerospace Sciences*, vol.41, pp. 143–151, 2005.

[137] D.S. Saunders, S.C Galea and G.K. Deirmendjian, "The development of fatigue damage around fastener holes in thick graphite/epoxycomposite laminates" *Journal of composites*, vol. 4, pp. 309-321, 1992.

138] S. Kellas, J. Morton and P.T. Curtis, "A characteristic fatigue parameter for notched composites", *Int J Fatigue*, vol. 13, pp. 35-43, 1991.

[139] C.M Wang, C.S.Shin,"Residual properties of notched [0/90]4s AS4/PEEK composites laminates after fatigue and re-consolidation", *Composites Part B*, vol.33, pp.67–76, 2002

[140] Ming-HwaR.Jen,Yu-ChungTseng,Wei-HwangLin,"Thermo-mechanical fatigue ofcentrally notched and unnotched AS-4/PEEKAPC-2 composite laminates", *International Journal of Fatigue*, vol. 28, pp. 901–909, 2006.

[141] Wayne W. Stinchcomb, "Non-destructive evaluation of damage accumulation processes in composite laminates", *Composites Science and Technology*, vol.25, pp.103-118, 1986.

[142] R.M. O'Higgins, M.A. McCarthy, C.T. McCarthy, "Comparison of open-hole tension characteristics of high strength glass and carbon fibre-reinforced composite materials", *Composites Science and Technology*, doi:10.1016/j.compscitech.2008.06.003

[143] Akbar Afaghi-Khatibi, Yiu-Wing Mai, "Characterisation of fibre/matrix interfacial degradation undercyclic fatigue loading using dynamic mechanical analysis", *Composites:Part A*, vol. 33, pp.1585-1592, 2002.

[144] AkbarAfaghi-Khatibi, LinYe,Yiu-WingMai, "An experimental study of the influence of fibre–matrix interface on fatigue tensile strength of notched composite laminates", *Composites:Part B*, vol. 32, pp.371-377, 2001.

[145] Pinho S, Iannucci L, Robinson P, "Formulation and implementation of decohesion elements in an explicit finite element code", Composites *Part A: Applied Science and Manufacturing*, vol. 37(5), pp.778-89, 2006.

[146] Camanho PP, Davila CG, De Moura MF, "Numerical simulation of mixed-mode progressive delamination in composite materials", Journal *of Composite Materials*, vol. 37(16), pp. 1415, 2003..

[147] Turon A, Camanho PP, Costa J, Renart J, "Accurate simulation of delamination growth under mixed-mode loading using cohesive elements: definition of interlaminar strengths and elastic stiffness", *Composite Structures*, vol. 92(8), pp.1857-64, 2010.

[148] R. Wisnom M, Chang FK, "Modelling of splitting and delamination in notched cross-ply laminates", *Composites Science and Technology*, vol. 60(15), pp.2849-56, 2000.

[149] Van der Meer F, Sluys L, Hallett S, Wisnom M, "Computational modeling of complex failure mechanisms in laminates", *Journal of Composite Materials*, vol. 46(5), pp.603-23, 2012.

[150] Allix O, Blanchard L, “Mesomodeling of delamination: towards industrial applications”, *Composites Science and Technology*, vol. 66(6), pp.731-44, 2006.

[151] Menna C, Asprone D, Caprino G, Lopresto V, Prota A, “Numerical simulation of impact tests on GFRP composite laminates”, *International Journal of Impact Engineering*, vol.38(8–9), pp.677-85, 2011.

[152] Aymerich F, Dore F, Priolo P, “ Simulation of multiple delaminations in impacted cross-ply laminates using a finite element model based on cohesive interface elements”, *Composites Science and Technology*, vol.69(11-12), pp.1699-709, 2009.

[153] González EV, Maimí P, Camanho PP, Turon A, Mayugo JA, “Simulation of drop-weight impact and compression after impact tests on composite laminates” *Composite Structures*, vol.94(11), pp.3364-78, 2012.

[154] Shi Y, Swait T, Soutis C, “Modelling damage evolution in composite laminates subjected to low velocity impact”, *Composite Structures*, vol. 94(9), pp. 2902-13, 2012.

[155] A. M. Amaro, P. N. B. Reis, M. F. S. F. de Moura and M. A. Neto, "Influence of open holes on composites delamination induced by low velocity impact loads," Composite Structures, vol. 97, pp. 239-244, 3, 2013.

[156] Wisnom MR, “Modelling discrete failures in composites with interface elements”, *Composites Part A: Applied Science and Manufacturing*, pp. 41(7), pp. 795-805, 2010.

[157] Fang XJ, Zhou ZQ, Cox BN, Yang QD “High-fidelity simulations of multiple fracture processes in a laminated composite in tension”, *Journal of the Mechanics and Physics of Solids*, vol. 59(7), pp.1355-73, 2011.

[158] Hallett SR, Jiang WG, Khan B, Wisnom MR, “Modelling the interaction between matrix cracks and delamination damage in scaled quasi-isotropic specimens”, *Composites Science and Technology,* vol.68(1), pp.80-89, 2008.

[159] Hallett SR, Green BG, Jiang WG, Wisnom MR, “An experimental and numerical investigation into the damage mechanisms in notched composites”, *Composites Part A*, vol.40(5), pp.613-24, 2009.

[160] Okabe T, Nishikawa M, Takeda N, “Numerical modeling of progressive damage in fiber reinforced plastic cross-ply laminates”, *Composites Science and Technology*, vol. 68(10-11), pp.2282-9, 2008.

[161] Olsson R. “Mass criterion for wave controlled impact response of composite plates”, *Composites Part A*, vol.31, pp.879-87, 2000.

[162] Cantwell W, Morton J, “*The impact resistance of composite materials - a review*”, *Composites*, vol. 22, pp.347 – 62, 1991.